Universidade de Brasília
Instituto de Geociências
Programa de Pós-Graduação em Geologia

TESE DE DOUTORADO

Nº 128

A proveniência dos sedimentos e cinzas vulcânicas dos sedimentos Permianos da Bacia do Paraná: implicações para a história geológica do sul-sudoeste de Gondwana

Lindaray Sousa da Costa

TESE DE DOUTORADO DE N° 128,
APRESENTADA AO INSTITUTO DE
GEOCIÊNCIAS DA UNIVERSIDADE
DE BRASÍLIA PARA OBTENÇÃO DO
TÍTULO DE DOUTOR EM GEOLOGIA

A proveniência dos sedimentos e cinzas vulcânicas dos sedimentos Permianos da Bacia do Paraná: implicações para a história geológica do sul-sudoeste de Gondwana

Lindaray Sousa da Costa

Orientador: Prof. Dr. Roberto Ventura Santos (IG/UnB)

Comissão Examinadora:

Prof. Dr. Roberto Ventura Santos (ORIENTADOR - IG/UnB)
Profª. Drª. Edi Mendes Guimarães (IG/UnB)
Profª. Drª. Natália Hauser (IG/UnB)
Prof. Dr. Claudio de Morison Valeriano (UERJ)
Prof. Dr. Peter Christian Hackspacher (UNESP)
Prof. Dr. Massimo Matteini (IG/UnB - SUPLENTE)

Brasília, Janeiro de 2016

Índice Geral

Lista de Figuras

Capítulo IV

Capítulo V

Lista de Tabelas e Appendix

Agradecimentos

Agradeço ao CNPq pelo financiamento – bolsa de doutorado, a Universidade de Brasília (UnB) e ao Laboratório de Geocronologia pelo suporte.

Sou grata aos Professores Roberto Ventura Santos (Orientador) e Elton Dantas pelo apoio e oportunidade de estagiar no Laboratório de Geocronologia.

Não poderia deixar de agradecer a toda equipe do Laboratório de Geocronologia (Bárbara, Carol, Érico, Gilvan, Jaqueline, Kamila, Kátia, Marcelo, dentre outros não menos importantes) que me acolheu e repassou muito conhecimento.

À todos que me acompanharam nesse processo e me ajudaram de uma maneira ou de outra, gostaria de deixar aqui registrado o meu muito obrigada, em especial a Deus, minha mãe Maria do Socorro, meu saudoso pai Francisco, meus irmãos Monalisa e Júnior, meu marido Rogério Franco e aos meus amigos Fátima, Fatinha, Giana, Luciana, Margarida, Mássimo, Natália e Nilda.

Ao Professor Elói, muito obrigada pelo enorme ato de generosidade, que me ajudou a continuar sem maiores dificuldades.

À toda minha Família sou grata pelo apoio e pelas orações, para que eu conseguisse vencer mais essa batalha em minha vida.

Dedico este trabalho à minha filha **Dominique Sousa da Costa Franco**, luz dos meus dias, que me faz prosseguir com coragem e sabedoria.

Resumo

O período geológico Permiano marca grandes mudanças climáticas e tectônicas na superfície da Terra. Duas áreas na porção sudeste da Bacia do Paraná registram relação entre os eventos climáticos e tectônicos, bem como variação na proveniência de sedimentos durante a evolução da bacia. A primeira área refere-se ao pacote de rochas sedimentares que ocorre na Serra do Rio do Rastro, Santa Catarina, Brasil, também conhecido como Coluna White. Este conjunto de rochas está associado à Permo-Carbonífera Supersequencia Gondwana I. Os resultados U-Pb em zircão detrítico e dados isotópicos Sm-Nd em rocha total dos sedimentos da Coluna White demonstram que na base (Formação Rio Bonito-Grupo Guatá) existe a predominância de uma população Paleoprotorezóica (2.5 a 1.7 Ga), seguida por populações com idades Mesoproterozóica (1.5 a 1.0 Ga) e Neoproterozóica-Cambriana (992-490 Ma). Em contraste, as rochas da Formação Rio do Rasto (Grupo Passa Dois) apresentaram zircões detríticos com idade dominantemente Neoproterozoica (935 a 543 Ma) e subordinadamente Permo-Triássica (297-216 Ma). Os resultados Lu-Hf apontaram para fontes dominantemente crustal com valores negativos de ε_{Hf} (-42 e -1) e idades modelo Hf (T_{DM}) Paleoproterozoicas na base e Meosoproterozóicas e Neopreoterozóicas no topo. Os resultados Sm-Nd em rocha total mostraram valores negativos de $\varepsilon_{Nd(T)}$ variando entre -15 e -6, corroborando os resultados ε_{Hf} em zircão. As idades modelo Nd (T_{DM}) entre 1.9 e 1.0 Ga confirmaram a contribuição das fontes Paleo a Mesoproterozóica envolvidas na sedimentação da bacia. A variação de fontes mais antigas para fontes mais jovens sugere que no Permiano médio a Bacia do Paraná passou de um comportamento intracratônico para um contexto com influência tectônica, induzido pela orogenia na porção sul e sudoeste de Gondwana. A segunda área refere-se a camadas de cinzas vulcânicas que ocorrem ao longo da Formação Irati (Base do Grupo Passa Dois), localizada no Município de São Mateus do Sul, Estado do Paraná (PR). Os resultados U-Pb em zircão ígneo revelaram a predominância de uma população permiana, com idades que variam entre 287 e 267 Ma. Os dados Lu-Hf sugerem que essa população de idade permiana deriva de uma fonte com assinatura crustal, com valores negativos de ε_{Hf} variando entre -7 e -3. As idades modelo Hf (T_{DM})

sugerem que essa fonte teria se diferenciado no final do Mesoproterozóico (1.2 Ga) e inicio do Neoproterozóico (0.8 Ga). Os dados Sm-Nd em rocha total registraram valores negativos de ε_{Nd} (-11.6 a -3.3) para uma fonte que teria se diferenciado a 1.6 Ga (Mesoproterozóico). Os resultados indicam um intervalo de mais de 15 Ma de anos durante o qual o vulcanismo esteve ativo, sendo que o pico principal deste evento ocorreu em 278 Ma. Demonstrou ainda a forte compatibilidade em idade e geoquímica com as rochas vulcânicas Choiyoi.

Abstract

The Permian geological period imprinted major climatic and tectonic changes on Earth's surface. We have studied two areas in the southeastern portion of the Paraná basin that shed light on relationship between the climatic and tectonics events and the variation of sediment provenance during the basin evolution. The first area refers to a package of sedimentary rocks across the Serra do Rio do Rastro, Santa Catarina, Brazil, that is also known as Coluna White. It includes a succession of the Gondwana I Supersequence, in which outcrop a set of rocks permo-carboniferou from the base to the top.. We present U-Pb and Lu-Hf detrital zircon data and whole rock Sm-Nd isotope data for samples across the profile. Zircon U-Pb data of the lower to middle part of the Permian (Rio Bonito Formation - Grupo Guatá Group) indicate a dominance of Paleoproterozoic (2.5 to 1.7 Ga) grains, followed by Mesoproterozoic (1.5 to 1.0 Ga) and Neoproterozoic-Cambrian (992-490 Ma) zircon grains. In contrast, sediments from the Rio Rasto Formation (Passa Dois Group) present a dominance of Neoproterozoic (935 to 543 Ma) followed by Paleozoic zircon grains, including Permo-Triassic ones (297-216 Ma). The Hf (T_{DM}) model ages indicate a Paleoproterozoic age for zircons at the base of the succession and Meso- to Neoproterozoic ages for zircon at the upper part of the succession. The Sm-Nd data reinforces the results of the other isotope systems, indicating a major change in sedimentary provenance between the lower and upper portion of the profile. This change suggests that in the middle Permian the Paraná basin evolved from a cratonic to orogenic influenced basin related to an orogeny in the south- and southwestern portion of Gondwana. In the second area we have studies volcanic ash interlayered with sedimentary rocks of the Permian Irati Formation. Zircon U-Pb data from these ash layers indicate ages ranging between 287 and 267 Ma, with a main peak at 278 Ma. Lu-Hf data of these zircons indicate crustal signature (ε_{Hf} ranging between -7 and -3) and Mesoproterozoic (1.2 Ga) and Neoproterozoic (0.8 Ga) Hf (T_{DM}) model ages. The Nd isotope data reinforce the zircon data, indicating a main crustal component in the source area of these rocks (ε_{Nd} = -11.6 to -3.3). The data further

indicate the close relationship of the Irati ash layers and the Choiyoi volcanism, which was the main source of the ash beds.

Capítulo I

1.1. Introdução

O período Permo-Triássico foi marcado por grandes mudanças climáticas que levaram a um dos eventos de extinção em massa mais importante durante o Fanerozóico. Estima-se que cerca de 90% das espécies vivas desapareceram (Sepkoski, 1984; Erwin, 2001; Mundil *et al*., 2004). Além do marcante evento de extinção em massa, no Eopermiano e Mesopermiano a atividade ígnea foi intensa ao longo da margem sul do paleocontinente Gondwana (Milani, 1997; López-Gamundí, 2006). O registro desta atividade se reflete como intrusões graníticas na Bacia de Sauce Grande (Formação Tunas, Argentina) ou como camadas de cinzas nas bacias do Paraná (Brasil, Uruguai e Paraguai) e Karoo (África do Sul, Namibia, Ilhas Falkland/Malvinas) (López-Gamudí, 2006).

Durante o Carbonífero a subducção de crosta oceânica sob o continente Gondwana levou ao desenvolvimento de um arco magmático (Ramos, 1984; Milani e Ramos, 1998a; Turner, 1999; Ramos, 2008). Este evento orogênico colisional foi responsável pela instalação de batólitos já no final do Paleozóico, inicio do Mesozóico, provavelmente relacionados a uma zona de acresção ao longo da margem sul do Gondwana (Turner, 1999). Alguns autores argumentam que o mencionado evento colisional levou às bacias do Paraná e Karoo assumirem um comportamento no contexto *foreland*, onde a subsidência foi fortemente controlada pelo regime tectônico (Milani e Ramos, 1998b; Turner, 1999). Posterior ao evento de colisão, entre o Permiano Médio e Superior, a porção ocidental da América do Sul foi soerguida em resposta a atuação da Orogênese San Rafaélica, transformando tal região em uma importante fonte de sedimentos. A orogênese em questão foi acompanhada por eventos vulcânicos, explosivos, de natureza félsica, que espalhou cinzas por vários milhares de quilômetros, registradas inclusive na Bacia do Paraná (Santos *et al*, 2006; López-Gamundí, 2006; Rocha-Campos *et al*, 2011).

O presente trabalho visa definir as áreas-fonte que contribuíram para a sedimentação da Bacia do Paraná durante o Permiano. Neste caso, um estudo de proveniência a partir de diferentes sistemas isótopicos integrados pode ser realizado. Análises U-Pb e Lu-Hf combinadas em grãos de zircão (Veevers *et al*., 2005; Gerdes e Zeh, 2006; Augustsson *et al*., 2006; Matteini *et al*., 2010; Yao *et al*., 2011), utilizando a técnica *Laser Ablation Multi-Collector Inductively Coupled Plasma Mass Spectrometer* (LA-MC-ICP-MS), permitem determinar a fonte de cristalização do mineral, bem como eventos magmáticos e metamórficos ocorridos na área-fonte. Imagens obtidas a partir de Microscopio Eletrônico de Varredura (MEV) ou de Catodoluminescencia favorecem na escolha da região do grão a ser analisada e com isto evitar *spots* nas interfaces núcleo/borda, em inclusões, ou em áreas heterogêneas. O estudo de proveniência pode ainda incluir dados isotópicos Sm-Nd em rocha total, que permitem obter informações a respeito da fonte magmática do protólito, por exemplo, se de origem mantélica ou crustal

1.2. Localização

No âmbito das técnicas isotópicas supracitadas duas áreas foram estudadas. A primeira aflora na Serra do Rio do Rastro (resultados discutidos no capítulo IV). Denominada de Coluna White, a sequência de rochas, engloba um conjunto de afloramentos integrantes da borda sudeste da Bacia do Paraná e está localizada no estado de Santa Catarina (SC), próxima a cidade de Lauro Müller. O acesso pode ser feito pela rodovia SC-438, partindo da cidade de Tubarão, próximo ao litoral de Santa Catarina (Figura 1).

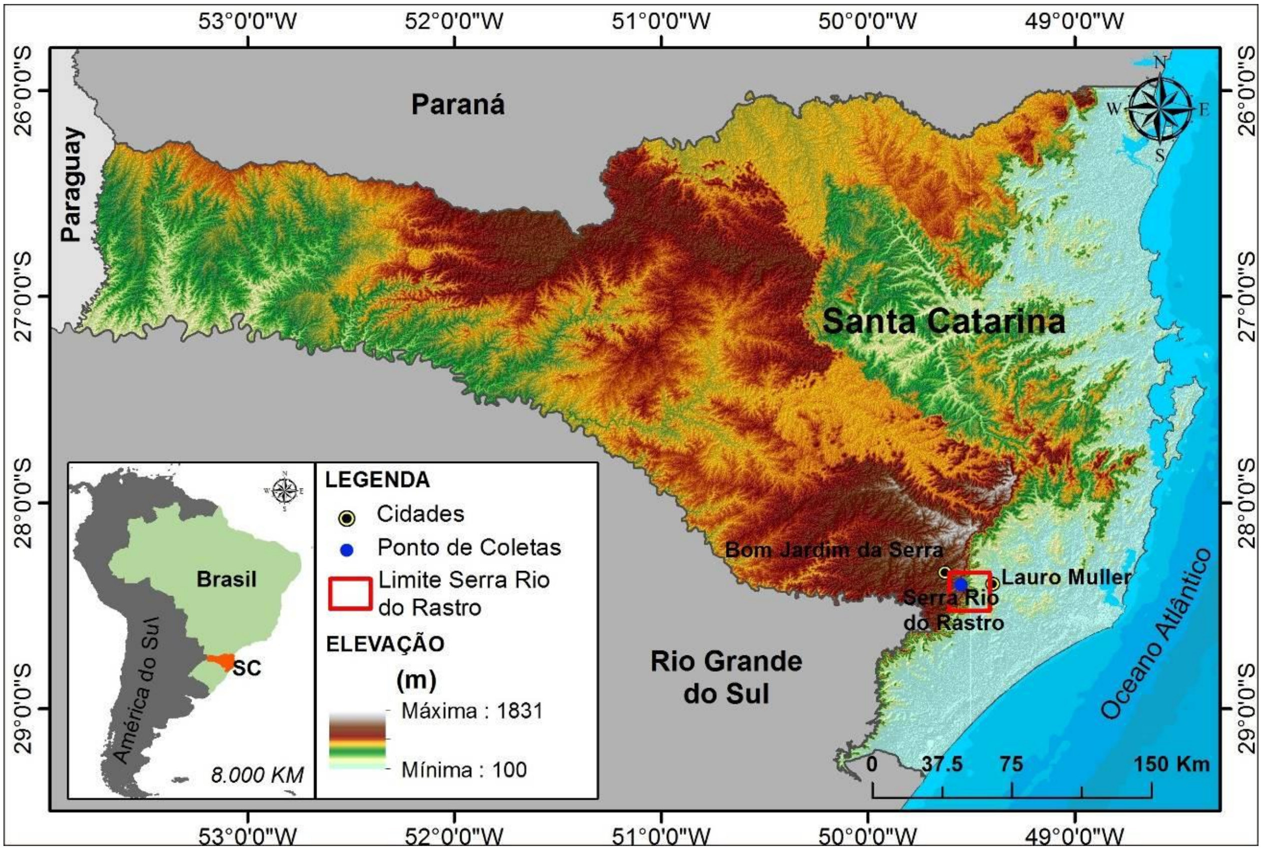

Figura 1: Mapa de localização da da Serra do Rio do Rastro, Estado de Santa Catarina (SC).

A segunda área (pedreira PETROBRAS-Six) é referente às camadas de cinzas que ocorrem ao longo da Formação Irati, próximo ao Município de São Mateus do Sul (Figura 2), Estado do Paraná (PR) (resultados discutidos no capítulo V). A Formação Irati, unidade basal do Grupo Passa Dois, representa uma espessa sequencia de folhelhos negros intercalados com calcários, que se destaca pelo seu conteúdo petrolífero e fossilífero (Mac Gregor 1908; White, 1908). O pacote, inicialmente descrito por White (1908), foi posteriormente subdividido da base para o topo nos membros Taquaral e Assistência (Barbosa e Gomes, 1958). Em escala regional, diversos autores definiram um contato superior concordante do Membro Assistência com as Formações Serra Alta, na porção centro-sul da bacia e Corumbataí, na porção norte da bacia (Mendes *et al.* 1966; Santos Neto, 1993; Milani *et al*. 1994; Araújo 2001).

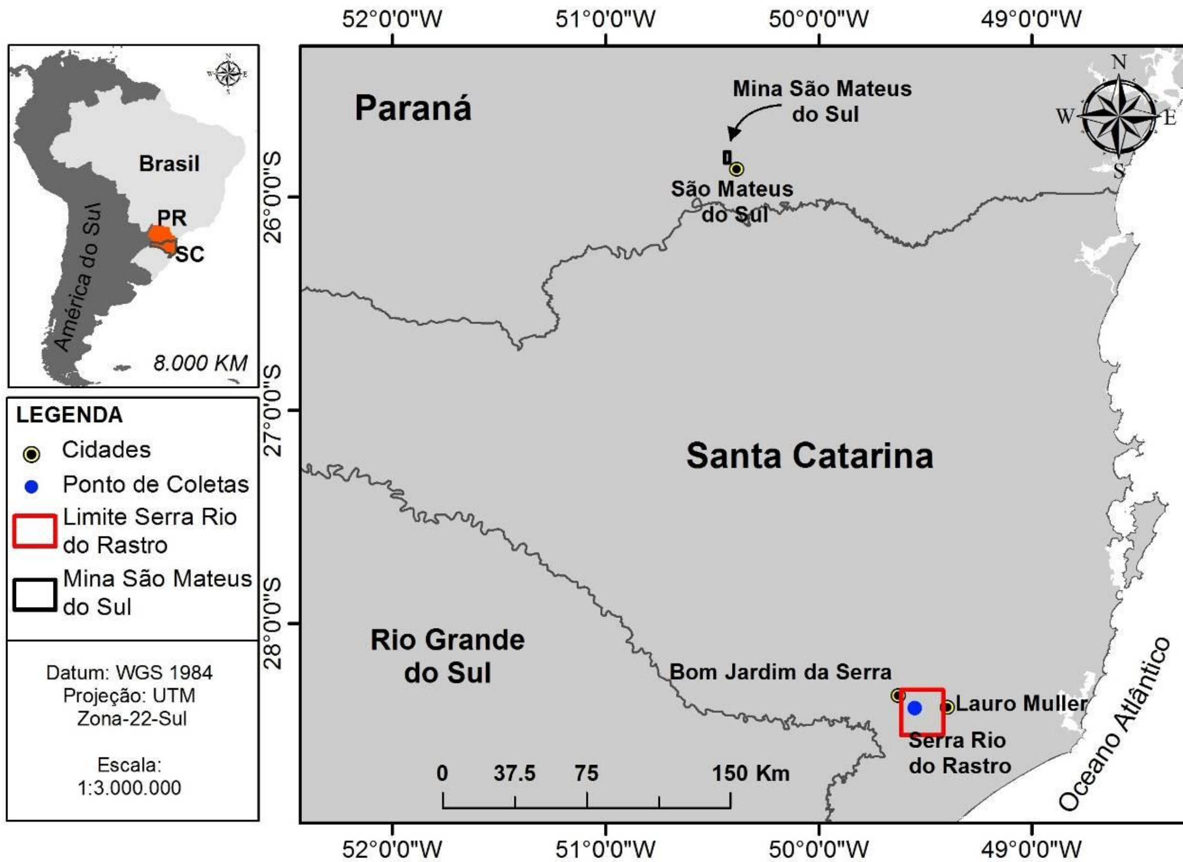

Figura 2: Mapa de localização da área de estudo referente às camadas de cinzas vulcânicas que ocorrem na Formação Irati, Município de São Mateus do Sul, Estado do Paraná (PR).

1.3. Objetivos

O presente trabalho tem como objetivo central fazer um estudo de proveniência das unidades permianas localizadas na porção sul da Bacia do Paraná, utilizando as técnicas isotópicas U-Pb e Lu-Hf combinadas em grãos de zircão e Sm-Nd em rocha total. O foco principal da pesquisa foi:

- ✓ Definir as várias populações existentes nas unidades sedimentares da Coluna White a partir da datação U-Pb em grãos de zircão detrítico; datar os grãos de zircão ígneo através do método U-Pb, para investigar qual a idade do magmatismo responsável pela geração das cinzas que estão distribuídas ao longo da Formação Irati.

- ✓ Aplicar as técnicas isotópicas U-Pb e Lu-Hf combinadas nos grãos de zircão previamente datados pelo método U-Pb para caracterizar as fontes magmáticas dos sedimentos em questão, bem como das cinzas.
- ✓ Com a técnica Sm-Nd em rocha total confirmar o tipo de fonte magmática dos protólitos dos sedimentos da Coluna White, se é de origem crustal ou matélica, assim como das cinzas vulcânicas que ocorrem na Formação Irati.

Nesse contexto, para a tese em questão são tratados os seguintes pontos:

- ✓ Capítulo I: Introdução
- ✓ Capítulo II: Metodologia;
- ✓ Capítulo III: Contexto Geológico;
- ✓ Capítulo IV: PROVENANCE OF PERMIAN SEDIMENTS AND TECTONIC EVOLUTION OF THE SOUTHEASTERN SOUTH AMERICA
- ✓ Capítulo V: PANGEA BREAK-UP AND SIGNIFICANCE OF RECURRENCE CYCLES OF ASH LAYERS PERMIAN FROM IRATI FORMATION, BRAZIL
- ✓ Capítulo VI: Considerações Finais e Conclusões
- ✓ Capítulo VII: Referências Bibliográficas.

CAPÍTULO II

2.1. Metodologia

O presente trabalho de tese doutoral foi realizado em três etapas distintas: etapa de gabinete, etapa de campo e etapa de laboratório. As atividades de preparação, datação e tratamento analítico foram conduzidas no Laboratório de Geocronologia da Universidade de Brasília (UnB).

2.1.1. Etapa de gabinete

Nesta etapa foi realizada uma revisão bibliográfica a respeito da geologia da Bacia de Paraná e das técnicas isotópicas a serem empregadas. Os métodos isotópicos selecionados foram U-Pb e Lu-Hf combinados em zircão, com utilização do equipamento *Laser Ablation Multi-Collector Inductively Coupled Plasma Mass Spectrometer* (LA-MC-ICP-MS) modelo Neptune da Thermo Finnigan, além de Sm-Nd em rocha total no *Isotope Dilution* T*hermal Ionization Mass spectromet*er (ID-TIMS) marca Finnigan MAT 262.

2.1.2. Etapa de campo

Esta etapa envolveu o reconhecimento e amostragem das rochas aflorantes na porção sul da bacia do Paraná, mais especificamente na Serra do Rio do Rastro, em Santa Catarina (SC). Os trabalhos ocorreram do dia 27 a 29 de Abril de 2012, onde foram amostrados, da base para o topo da Coluna White, um total de 16 amostras, envolvendo siltitos, folhelhos, arenitos e carbonatos, destinadas a aplicação dos métodos Sm-Nd, U-Pb e Lu-Hf.

2.1.3. Etapa de laboratório

Nesta etapa foi feito o tratamento das amostras coletadas ao longo da Serra do Rio do Rastro em Santa Catarina-SC. Desesseis exemplares de rocha foram preparados e analisados segundo o método Sm-Nd no ID-TIMS. As técnicas U-Pb e Lu-Hf no LA-MC-ICP-MS foram realizadas em 9 das 16 amostras coletadas, tendo em vista que 7 exemplares não apresentaram grãos de zircão.

Na fase laboratorial também foi realizada a análise Lu-Hf e o tratamento analítico U-Pb/Lu-Hf das cinco amostras representativas das camadas de cinzas que ocorrem na Formação Irati, coletadas e tratadas para análise U-Pb em outra etapa da pesquisa. A seguir estão descritos os métodos e o tratamento aplicado às amostras mencionadas.

2.2. Métodos geocronológicos

A rotina de datações radiométricas de rochas e minerais (*e.g.* datação em zircão) tem sido uma ferramenta muito utilizada no estudo de proveniência. Os vários métodos geocronológicos, aplicados em conjunto, reforçam o entendimento sobre as características da fonte de cristalização dos minerais analisados, bem como estima a idade máxima de deposição dos sedimentos em uma bacia e defini áreas-fonte.

Os métodos isotópicos Sm-Nd em rocha total e U-Pb e Lu-Hf em zircão detrítico foram utilizados nesta pesquisa para o entendimento da origem dos sedimentos permianos da Bacia do Paraná, em especial da Coluna White. A mesma metodologia, como algumas diferenças (vide método U-b) foi aplicada em zircões ígneos, para identificar a origem do magmatismo das camadas de cinzas mencionadas anteriormente.

2.2.1. Método Sm-Nd

O Samário é um elemento constituinte do grupo dos terras-raras leves pertencente aos lantanídeos, que ocorre naturalmente na forma de sete isótopos, dos quais três são radiogênicos e apenas um (^{147}Sm) é usado em datação de rocha. O processo de desintegração do ^{147}Sm ocorre por emissão de partícula α para o isótopo estável ^{143}Nd (Faure, 2005). Embora o ^{147}Sm apresente meia-vida longa ($T_{1/2}$ = 1.06 x 10^{11} anos; $\lambda = 6.54 \times 10^{-12}$ anos^{-1}), existem pequenas diferenças na abundância do isótopo filho ^{143}Nd que podem ser medidas, o que torna possível a datação pelo método Sm-Nd (Dickin, 2005). No processo de fusão parcial do manto o Sm tende a permanecer no *solidus* retido na estrutura cristalinas dos minerais, ao passo que o Nd, por ser mais incompatível que o Sm, tende a se concentrar no *liquidus* e ascender às porções mais rasas da litosfera. O aumento da quantidade de isótopo radiogênico ^{147}Sm no manto resulta na elevação das razões $^{143}Nd/^{144}Nd$ com relação a crosta. Consequentemente, a crosta se enriquece em Nd e as razões $^{143}Nd/^{144}Nd$ permanecem baixas.

O fracionamento isotópico do sistema Sm-Nd na Terra é reproduzido a partir de curvas evolutivas (DePaolo e Wasserburg, 1976 e DePaolo, 1981). A curva evolutiva *chondritic uniform reservoir* (CHUR) representa um sistema isotópico ideal, construída a partir da análise de meteoritos condríticos e estima a composição inicial do sistema solar. Adicionalmente, a evolução do manto é reproduzida por uma curva denominada *depleted mantle* (DM), que reflete o processo de diferenciação magmática do manto e pode ser calculado a partir da seguinte equação:

$$T_{DM} = \frac{1}{\lambda} ln \left[\frac{\left(\frac{^{143}Nd}{^{144}Nd}\right)_{Amostra} - \left(\frac{^{143}Nd}{^{144}Nd}\right)_{DM}}{\left(\frac{^{147}Sm}{^{144}Nd}\right)_{Amostra} - \left(\frac{^{147}Sm}{^{144}Nd}\right)_{DM}} + 1 \right]$$

A variação do Nd radiogênico com relação ao CHUR de uma determinada amostra é representada pela notação ε_{Nd} (DePaolo e Wasserburg, 1976). O cálculo do

ε_{Nd} estima se a fonte de um magma é de origem crustal, no caso de valores negativos, ou matélica para valores positivos e pode ser feito a partir da equação a seguir:

$$\varepsilon_{Nd}(t) = \left[\frac{\left(\frac{^{143}Nd}{^{144}Nd} \right)_{Amostra}}{\left(\frac{^{143}Nd}{^{144}Nd} \right)_{CHUR}} - 1 \right] \times 10^4$$

O método Sm/Nd tem como premissa o aumento da razão radiogênica $^{143}Nd/^{144}Nd$ em função do tempo devido ao decaimento do ^{147}Sm. Os resultados obtidos a partir dos cálculos são plotados em um diagrama binário de T (tempo) *versus* a razão $^{143}Nd/^{144}Nd$ ou ε_{Nd} (Figuras 3a e 3b).

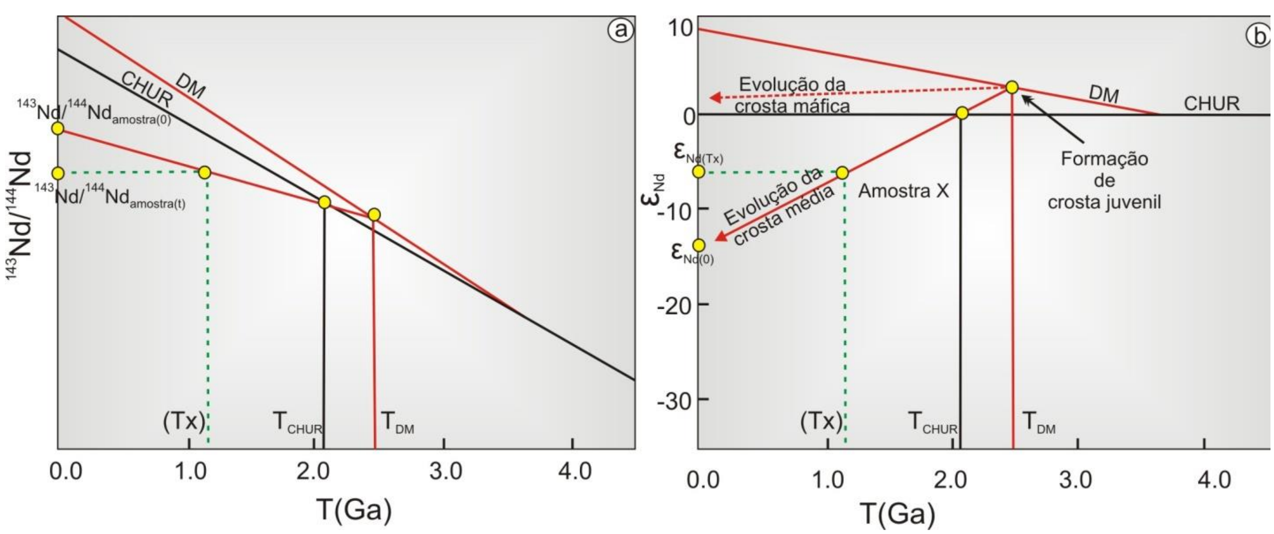

Figura 3: a) Representação gráfica da evolução isotópica do Nd *versus* T (tempo). b) Representação gráfica do sistema Sm-Nd e os parâmetros de idade modelo T_{DM}, T_{CHUR} e ε_{Nd} (modificado de DePaolo, 1988).

Análise isotópica

A fase de preparação das amostras para aplicação do método Sm-Nd foi composta pelas etapas de moagem, para redução da granulometria, de separação dos elementos Sm e Nd, segundo a metodologia proposta por Gioia e Pimentel (2000), e de análises no *Thermal Ionization Mass Spectrometer* (TIMS).

O procedimento para obtenção dos dados isotópicos Sm e Nd foi desenvolvido nas seguintes etapas: Inicialmente, alíquotas de aproximadamente 100 mg de amostra pulverizada foram separas em potes de Teflon (Savilex) e a estas adicionada uma mistura de ^{149}Sm-^{150}Nd, utilizada como padrão de referência; em seguida as amostras foram dissolvidas em 3 ml de HF e 250 μml de HNO_3, ambos concentrados e aquecidos; após a dissolução das amostras foi feita a evaporação em chapa elétrica aquecida (*Clean Box*); na sequencia foi adicionado 1 ml de HCL concentrado para dissolução da matéria orgânica e posterior evaporação; por fim as amostras repousaram durante 24 horas em 6N HCL para normalização e posterior evaporação.

A etapa de cromatografia catiônica (separação dos elementos Sm e Nd) foi realizada em dois processos. No primeiro, concentrados de cada amostra obtidos na dissolução foram passados em colunas de quartzo, empacotadas com resina seca Bio-Rad AG 50W-X8 de 200-400 *mesh*, para eluição de elementos terras-raras. No segundo, a fração contendo terras-raras foi novamente passada em uma coluna de Teflon, empacotada com resina líquida LN-Spec (HDEHP - ácido di-ethylhexil fosfórico) de 150-270 *mesh*, para separação do Sm e Nd. Samário e Neodímio coletados separadamente foram depositados em filamentos de Rênio (Re) para análise no TIMS.

2.2.2. Método U-Pb

O método de datação U-Pb é fundamentado no decaimento do Urânio (U, Z = 92), por emissão de partículas α e β, para isótopos estáveis de Chumbo (Pb, Z = 82). O Urânio tem três isótopos radioativos (^{238}U, ^{235}U e ^{234}U), dos quais dois (^{238}U e ^{235}U) são utilizados no emprego desta metodologia. O isótopo radiogênico ^{238}U se decompõe para o isótopo estável ^{206}Pb com meia-vida de 4.468 Ga e constante de decaimento (λ) de 1.55125 x 10^{-10}; o isótopo radiogênico ^{235}U se decompõe para o isótopo estável ^{207}Pb com meia-vida de 0.704 Ga e λ = 9.84485 x 10^{-10} (Faure, 2005). O cálculo das idades U-Pb pode ser feito a partir das seguintes equações:

$$\frac{^{207}Pb}{^{235}U} = (e^{\lambda 235t} - 1)$$

$$\frac{^{206}Pb}{^{238}U} = (e^{\lambda 238t} - 1)$$

O chumbo ocorre na forma de quatro isótopos estáveis (^{206}Pb, ^{207}Pb, ^{208}Pb e ^{204}Pb). Três destes isótopos são radiogênicos, onde ^{206}Pb e ^{207}Pb decaem do U e o ^{208}Pb decai do Th. O isótopo estável ^{204}Pb é o único não radiogênico (chumbo comum), que ocorre naturalmente distribuído na Terra e pode ser incorporado na estrutura cristalina de alguns minerais (*e.g*. zircão) no momento da cristalização (Faure, 2005). O chumbo comum também pode estar presente em inclusões (*e.g*. minerais inclusos em outros minerais), como contaminante na superfície dos grãos analisados, ou introduzido por processos químicos (Bowring & Schmitz, 2003). A presença do ^{204}Pb na estrutura cristalina do zircão altera as medições dos isótopos radiogênicos ^{206}Pb e ^{207}Pb produzidas pelo ^{238}U e ^{235}U, respectivamente. As alterações provocadas pela presença de chumbo comum podem ser reparadas com procedimentos de correção (Bowring & Schmitz, 2003; Dickin, 2005; Bühn *et al*. 2009; Kooijman *et al*. 2011).

O zircão ($ZrSiO_4$) é frequentemente usado como gecronômetro no sistema isotópico U-Pb por incorporar na sua rede cristalina átomos de U, bem como a natureza resistente deste mineral a processos metamórficos e intempéricos e ampla distribuição como acessório em rochas ígneas, sedimentares e metamórficas. A datação U-Pb em zircão permite a obtenção de dados referentes à idade de cristalização da rocha, assim como à idade de eventos metamórficos; em grãos detríticos (Košler *et al*., 2002; Fedo *et al*., 2003; Andersen, 2005) permite a identificação das várias populações de zircão existentes em rochas de uma determinada bacia, e quando aliado ao sistema isotópico Lu-Hf (Veevers *et al*., 2005; Gerdes e Zeh, 2006; Augustsson *et al*., 2006; Yao *et al*., 2011), permitem também caracterizar as prováveis fontes destes sedimentos.

A representação gráfica do sistema U-Pb, no caso de rochas cristalinas (e.g. ígnea e metamórfica) é feita em diagrama de eixos coordenados, onde são plotadas as razões isotópicas $^{206}Pb/^{238}U$ e $^{207}Pb/^{235}U$ em função do tempo, usando uma curva de referência denominada concórdia (Wetherill, 1956) como apresentado na figura 4a. Um diagrama alternativo (Tera & Wasserburg, 1972) pode ser usado para representar rochas cristalinas mais jovens que 1.0 Ga, no qual são usadas as razões $^{238}U/^{206}Pb$, plotadas no eixo X e as razões $^{207}Pb/^{206}Pb$ no eixo Y, caso em que a concórdia é dita inversa (Figura 4b).

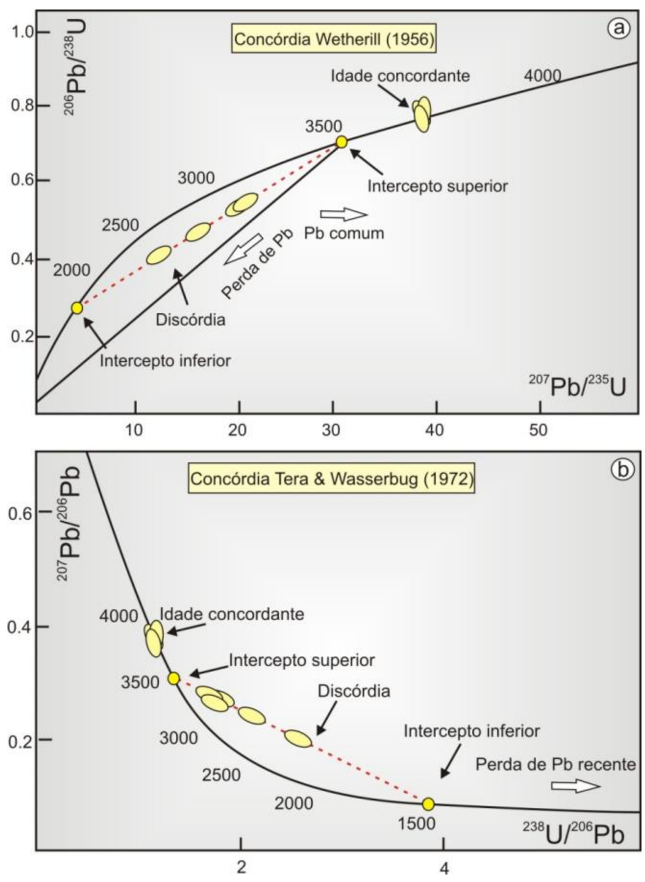

Figura 4: a) Diagrama de Concórdia de Wetherill (1956) utilizado para representação gráfica do sistema isotópico U-Pb. b) Representação gráfica alternativa para os isótopos U-Pb (Concórdia Tera & Wasserburg), comumente utilizada para rochas mais jovens que 1.0 Ga.

Contudo, no estudo de proveniência em zircão detritico, a representação gráfica é feita em diagrama com curva de densidade (histograma), que expressa a distribuição das populações de zircão no sedimento (Andersen, 2005).Grãos com idades maiores que 1 Ga, o diagrama é construído utilizando a razão$^{207}Pb/^{235}U$ e grãos com idade abaixo de 1 Ga, se utiliza a razão $^{206}Pb/^{238}U$.

Os zircões detríticos presentes em uma bacia são provenientes de vários tipos de rochas que sofreram intemperismo e posterior transporte (e.g. fluvial, marinho, glacial e eólico). Para avaliar a distribuição das diversas áreas-fonte envolvidas na sedimentação de uma bacia, um grande número de grãos (em torno de 60-100) deve ser analisado (Dodson *et al*., 1988; Sircombe, 2000; Vermeesch, 2004; Andersen, 2005; Condie *et al*., 2009), assim como a morfologia dos mesmos (*e.g.* grãos ígneos ou metamórficos) pode ser usada para determinar eventos magmáticos nas regiões de origem (Condie *et al*., 2009).

No caso da análise U-Pb em zircão ígneo, cerca de trinta grãos são suficientes para representar a rocha, tendo em vista que fazem parte da mesma unidade, embora possa haver a presença de minerais herdados de outras fontes (e.g. grãos de zircão da rocha encaixante) no momento do alojamento do corpo ígneo.

A técnica de datação U-Pb por LA-MC-ICP-MS consiste na extração dos íons da superfície da amostra, por meio de um feixe de *laser* de alta energia com diâmetro de ~30 µm (Bühn *et al*., 2009). Adicionalmente imagens de catodoluminescencia ou MEV são utilizadas para escolha da área do grão a ser analisada.

Análise Isotópica

O procedimento analítico seguiu de acordo com a rotina do Laboratório de Gocronologia da UnB descrita por Bühn *et al*. (2009). As etapas de preparação das amostras envolveram moagem, bateamento e separação por susceptibilidade magnética no equipamento isodinâmico Franz. A partir da fração não magnética foram extraídos zircões com o auxilio de uma lupa binocular (NIKON-SMZ800). A seleção dos cristais, no caso dos exemplares de rocha sedimentar, procedeu de maneira aleatória, onde cerca de 60 grãos foram separados de 9 amostras da Coluna White, com o objetivo de representar o maior número de populações existentes (Andersen, 2005). No caso das amostras das camadas de cinzas, foram priorizados, durante a seleção, cristaís ígneos prismáticos e aciculares, típicos de rochas vulcânicas. Cerca de trinta zircões foram extraídos. Os concentrados de zircão de cada amostra foram embutidos em *mounts* de epóxi, os quais foram polidos para aplainamento e exposição da superfície do mineral a ser analisado.

Imagens de catodoluminescência realizadas nos zircões previamente polidos, foram obtidas em um Microscópio Eletrônico de Varredura (MEV), para observação da estrutura interna do mineral e posterior análise no equipamento LA-MC-ICP-MS. A análise constou da ablação a *laser* da superfície dos grãos, onde foram feitos *spots* com diâmetro de ~30 µm durante 40 segundos. Um padrão de referência GJ-1 foi utilizado para estabilização da leitura.

Os resultados obtidos a aprtir da análise no LA-MC-ICP-MS foram tratados e calculados com auxílio de planilha Excel 2003 (programa Isoplot/Ex, Ludwig, 2001). O tratamento analítico consiste em fazer a redução dos dados que apresentem pontos fora da reta de regressão, muito Pb comum e erro grande. Após a redução destes dados, considerados ruins, foram gerados diagramas com curvas de densidade para os sedimentos e gráficos de concórdia para as camadas de cinzas.

2.2.3. Método Lu-Hf

O Lutécio (Lu, Z = 71) e o Háfnio (Hf, Z = 72) são elementos do grupo terras-raras cujo sistema isotópico vem sendo bastante utilizado em geocronologia. Lu tem dois isótopos que ocorrem naturalmente (^{175}Lu e ^{176}Lu). Apenas o ^{176}Lu é radioativo, com meia vida de 37.2 Ga e constante de decaimento de 1.94 ± 0.07 x 10^{-11} anos^{-1} (por emissão de partícula β para o isótopo estável ^{176}Hf , Faure 2005).

O sistema isotópico Lu/Hf é muito similar ao Sm/Nd. Assim como o Nd, o Hf tem forte tendência a se concentrar em líquidos silicáticos formados a partir de fusão parcial (Faure, 2005). Isto implica que magmas basálticos derivados do manto têm razão Lu/Hf mais baixa que sua fonte geradora, ao passo que o resíduo, por empobrecimento de Hf, tende a ter concentrações mais elevadas de Lu/Hf.

Os isótopos de Hf são importantes traçadores de processos petrogenéticos (Patchett *et al.*, 1981). Sua forte afinidade pelo zircônio (Zr) permite que zircões retenham altas concentrações deste elemento e mantenham sua razão Lu/Hf baixa (Andersen *et al.*, 2002). Isto ocorre porque o zircão, ao se cristalizar, não admite Lu em sua estrutura cristalina, diferentemente do Hf, que possui forte afinidade com este mineral. Assim, zircão é um importante mineral para determinação da composição isotópica inicial do Hf em rochas.

Análises *in situ* de isótopos de Hf em zircão por LA-MC-ICPMS, aliadas ao método de datação U-Pb, podem prover informações sobre a evolução de reservatórios crustais através do tempo e sobre a extração do magma do manto empobrecido (Nebel *et al*., 2007), sobre estudos de proveniência de sedimentos (Griffin *et al*., 2004; Condie *et al*., 2005; Kemp *et al*., 2006) e sobre processos magmáticos (Kemp *et al*., 2005; Yang *et al*., 2007).

A análise Lu-Hf é realizada zircão datado previamente pelo método U-Pb. Os *spots* devem ser próximo ou no mesmo local da perfuração produzida na obtenção dos dados U-Pb, com intuito de analisar partes do grão com as mesmas características isotópicas (Matteini *et al*., 2010).

A representação gráfica do método Lu-Hf é feita através de um diagrama binário, que reflete a variação isotópica do Hf através do tempo com relação ao CHUR (Patchett e Tatsumoto *et al*. 1980; Patchett e Tatsumoto *et al*., 1981; Patchett, 1983). O cálculo se baseia na abundância do ^{176}Hf, expressa pela razão ^{176}Hf/^{177}Hf, que aumenta com o tempo em função da razão ^{176}Lu/^{177}Hf de rochas e minerais (Faure, 2005). A idade, no método Lu-Hf, pode ser calculada com base na seguinte equação:

$$\left(\frac{^{176}\mathrm{Hf}}{^{177}\mathrm{Hf}}\right)_t = \left(\frac{^{176}\mathrm{Hf}}{^{177}\mathrm{Hf}}\right)_0 + \left(\frac{^{176}\mathrm{Hf}}{^{177}\mathrm{Hf}}\right)_t * \left(e^{\lambda t}-1\right)$$

Onde t representa o tempo e λ a constante de decaimento do ^{177}Lu (Patchett and Tatsumoto, 1980; Sguigna *et al.*, 1982).

Assim como no método Sm-Nd, a variação do Hf radiogênico em uma determinada amostra com relação ao CHUR é calculada através do ε_{Hf} , obtido a partir da equação a seguir.

$$\varepsilon_{Hf} = \left[\frac{\left(\frac{^{176}Hf}{^{177}Hf}\right)_{amostra}}{\left(\frac{^{176}Hf}{^{177}Hf}\right)_{CHUR}} - 1 \right] \text{ x } 10$$

A notação ε representa a variação da razão isotópica $^{176}Hf/^{177}Hf$ de uma determinada amostra com relação a razão isotópica $^{176}Hf/^{177}Hf$ do CHUR ou do DM (Figura 5). Assim como no sistema Sm-Nd, valores negativos de $\varepsilon_{Hf(T)}$ indicam fontes crustais e valores positivos de $\varepsilon_{Hf(T)}$ remetem a fontes mantélicas.

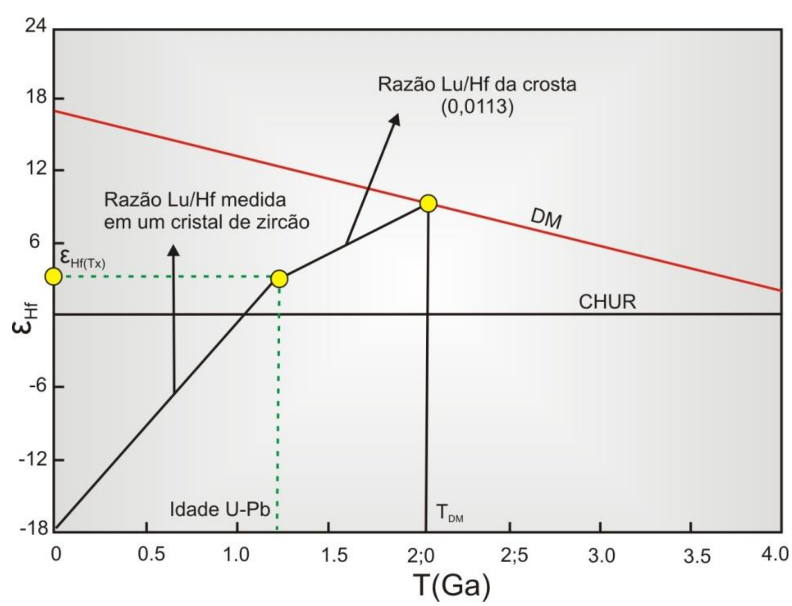

Figura 5: Diagrama de variação da razão isotópica $^{176}Hf/^{177}Hf$ de uma determinada amostra com relação a razão isotópica $^{176}Hf/^{177}Hf$ relativa ao CHUR ou ao DM.

Análise Isotópica

Os grãos de zircão foram selecionados com base no fator de concordância das idades U-Pb (Conc. ≥ 90% e ≤ 110%). Ao todo foram analisados cerca de 154 grãos de 9 amostras da Coluna White e 50 dos 5 exemplares das camadas de cinzas. A análise isotópica Lu-Hf, realizada no equipamento LA-MC-ICPMS, consistiu na técnica de ablação pontual na superfície do grão, onde é produzido um *spot* com diâmetro entre 40 e 50 µm, durante 40-50 segundos (Matteini *et al*., 2010). Um padrão de referência (GJ-1) foi analisado durante o procedimento analítico para estabilização da leitura dos dados. Os valores de $\varepsilon_{Hf(t)}$ aliados às idades U-Pb foram calculados. No caso de zircões com idade acima de 1 Ga utilizou-se as razões $^{207}Pb/^{206}Pb$ e aqueles com idade abaixo de 1 Ga, as razões $^{206}Pb/^{238}U$.

CAPÍTULO III: CONTEXTO GEOLÓGICO

3.1 – Bacia do Paraná

A Bacia do Paraná é uma vasta região sedimentar localizada na América do Sul, constituída de megassequencias com registro estratigráfico temporalmente posicionado entre Neo-Ordoviciano e o Neo-Cretáceo (Milani & Ramos, 1998). Geograficamente, abrange uma área superior a 1.500.000 km^2 e engloba as porções territoriais do Brasil meridional, Paraguai oriental, nordeste da Argentina e norte do Uruguai (Figura 6) (Milani *et al*. 1994). Em território brasileiro, compreende os estados do Mato Grosso (MT) e Goiás (GO) na porção norte, estendendo-se até o Rio Grande do Sul (RS). Trata-se de uma bacia intracratônica de registro policíclico, marcada por sucessivos episódios de subsidencia durante o Fanerozóico.

O desenvolvimento da Bacia do Paraná ocorreu em um contexto tectônico de convergência entre o paleocontinente Gondwana e o assoalho oceânico do Panthalassa. A subducção do assoalho oceânico sob o continente culminou no desenvolvimento de ativos cinturões colisionais denominados de Gondwanides (Figura 7) (Keidel, 1916 *apud* Milani *et.al*., 2007b) na margem sudoeste do Gondwana (Milani *et al*., 2007b). Os vários episódios de colisão e acresção de terrenos alóctones decorrentes da evolução desses cinturões são o reflexo dos ciclos orogênicos Famatiniano (orogenia Oclóyica e Precordilheriana – Ordoviciano a Devoniano) e Gondwaniano (orogenias Chanica e Sanrafaélica – Carbonífero a Triássico) (Ramos, 1988). A geodinâmica da borda ativa do Gondwana influenciou diretamente na história evolutiva da Bacia do Paraná, onde os episódios de subsidência aliados aos grandes eventos orogênicos favoreceram a criação de espaço deposicional na área intracratônica (Milani, 2007).

A margem ativa do Gondwana sofreu forte influência da atividade ígnea permiana, devido ao desenvolvimento do arco magmático Choiyoi (Milani, 1997). O intenso vulcanismo atuante na província foi caracterizado como explosivo, de composição cálci-alcalina e relacionado ao desenvolvimento da orogênese Sanrafaélica, de regime compressivo (López-Gamundi, 2006; Kleiman and Japas, 2009).

Figura 6: Mapa de localização da Bacia do Paraná, onde também está marcado (círculos em vermelho) as duas áreas estudadas na presente pesquisa. I) Serra do Rio do Rastro, Santa Catarina (SC) e II) Mina São Mateus do Sul, Paraná (PR).

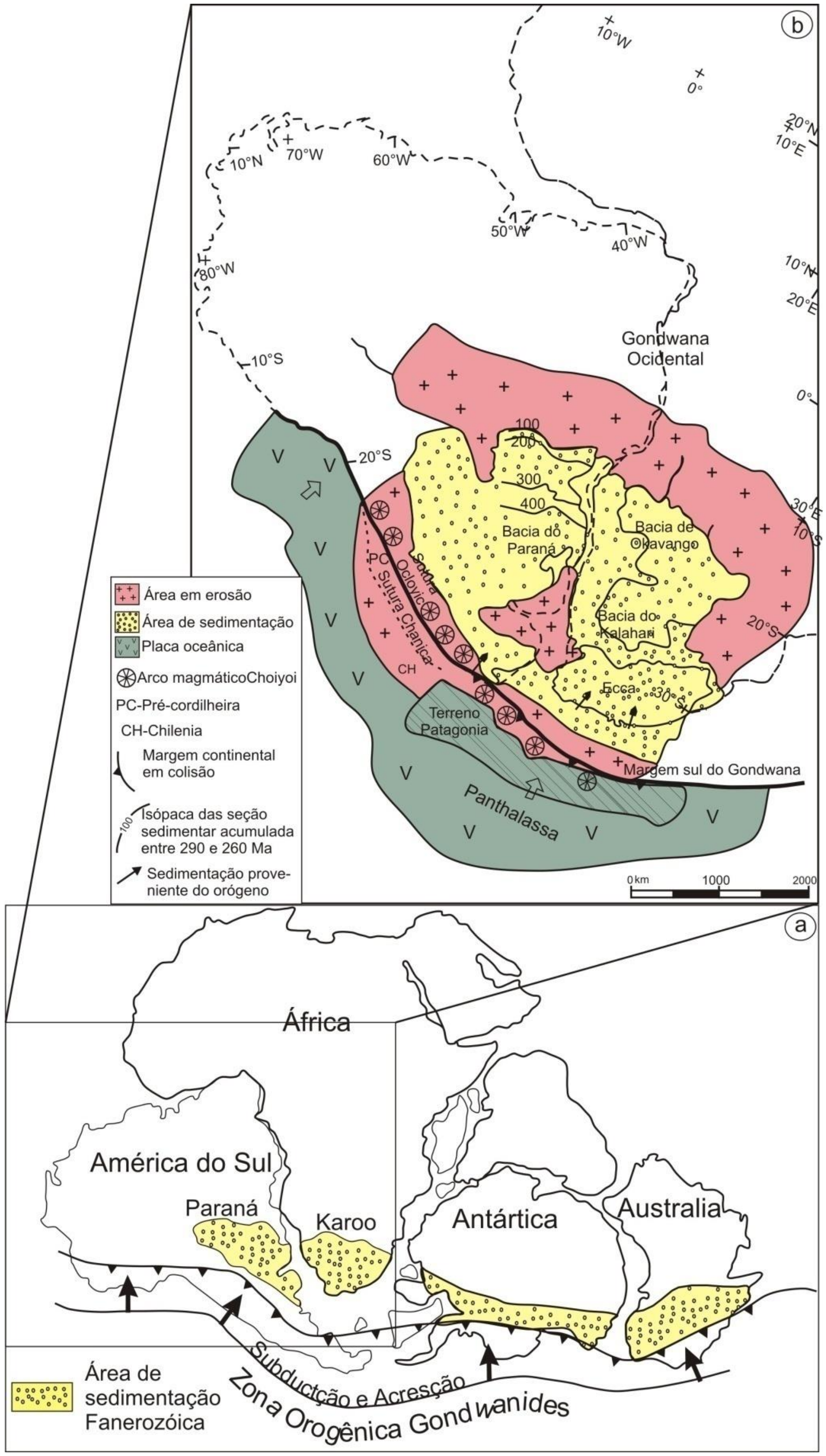

Figura 7: a) Mapa ilustrativo da zona orgência Gondwanides (modificado de De Toit (1937), *apud* Powell & Veervers (1994). b) Contextualização tectono-sedimentar do Gondwana sul-ocidental no limite Eopermiano/Neopermiano, quando a região era submetida aos efeitos da Oregenia Sanrafélica (modificado de Milani, 1997)

A atividade vulcânica decorrente da orogênese Sanrafaélica, ocorreu em pulsos magmáticos que atuaram em um período de 30 Ma, durante o Paleozóico (Rocha-Campos *et al*., 2011). Rocha-Campos *et al*. (2011), com base em dados isotópicos de U-Pb, identificaram três pulsos de atividade vulcânica (respectivamente 281, 264 e 251 Ma) para o arco magmático em desenvolvimento. Esse evento orogênico e a implantação do arco magmático foram eventos geológicos expressivos que atuaram no Permiano (Milani, 1997). O reflexo da referida atividade ígnea foi documentado nos estratos da Bacia do Paraná (Coutinho *et al*. 1991), em especial nas Formações Rio Bonito (Formoso *et al*., 1997) e Irati (Maynard *et al*. 1996; Santos *et a.* 2006; Rocha-Campos *et al*. 2011), como camadas de cinzas distribuídas ao longo dos depósitos paleozoicos. O registro de leitos vulcanoclásticos também foi reconhecido nas Bacias de Sauce Grande (Formação Tunas) e Calingasta-Uspallata (sequência equivalente), bem como nos Grupos Ecca e Beaufort da Bacia do Karoo (Johnson, 1991).

Milani (1997) estabeleceu para o arcabouço estratigráfico da Bacia do Paraná seis unidades de ampla escala ou supersequencias (Vail *et al.,* 1977) que refletem as sucessivas fases de acumulação sedimentar distribuídas entre 450 e 65 Ma. As unidades Rio Ivaí (Caradociano-Llandoveriano), Paraná (Lochkoviano-Frasniano) e Gondwana I (Westphaliano-Scythiano) evoluíram no contexto dos ciclos transgressivos-regressivos. As unidades Gondwana II (Neoanisiano-Eonoriano), Gondwana III (Neojurássico-Berriasiano) e Bauru (Aptiano-Maestrichtiano) correspondem a pacotes sedimentares continentais com vulcânicas associadas (Figura 8 e 9a).

O foco deste estudo se insere no contexto estatigráfico da Supersequência Gondwana I (Figura 9b), embora aqui também sejam apresentados dados sobre a Formação Batucatu (Grupo São Bento - Supersequencia Gondwana III), como complemento à pesquisa.

A Supersequencia Gondwana I corresponde a uma área bastante expressiva da Bacia do Paraná, com espessura máxima da ordem de 2.500 m (Milani *et al*., 1994). A porção basal é representada pelos depósitos sedimentares do Grupo Itararé e seu equivalente estratigráfico (França e Potter, 1988), a Formação Aquidauana, ligados à fase de degelo da grande glaciação gondwânica (Schneider *et al.*, 1974).

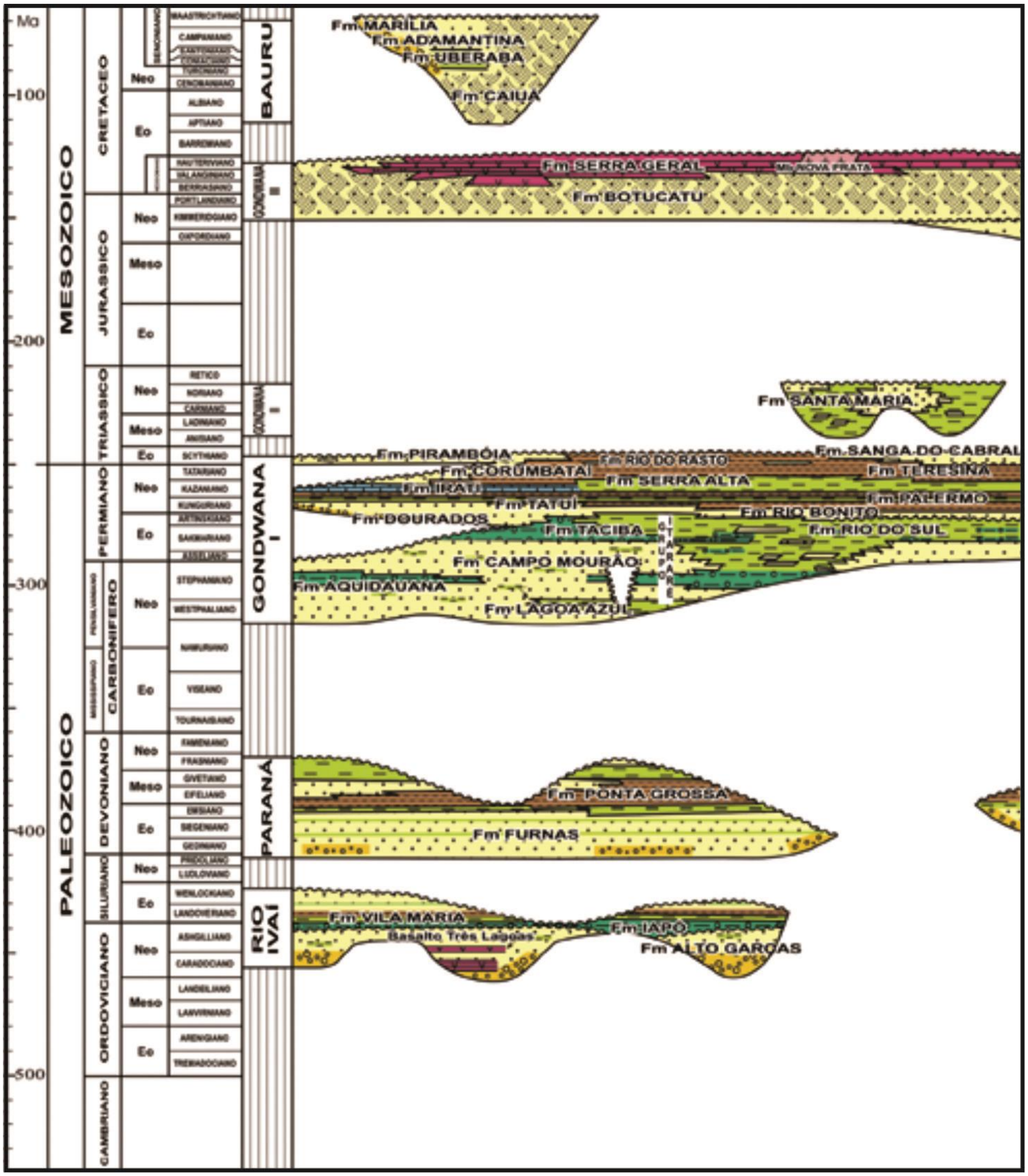

Figura 8: Carta crono-estratigráfico da Bacia do Paraná, baseada em informações de subsuperfície (compilado de Milani, 1997).

Sucedendo o registro glaciogênico, em um contexto marinho trangressivo (Permiano), desenvolveram-se os depósitos sedimentares do Grupo Guatá, porção sul da bacia, no centro-norte as formações Tietê (Fulfaro, *et al*. 1991) e Tatuí, equivalentes à Formação Três Islas no Urugaui (Milani et al., 2007b). O pacote Permo-Triássico do Grupo Passa Dois depositou-se na seqüência em condições regressivas, seguido por depósitos eólicos (Eotriássico) das Formações Sanga do Cabral e Pirambóia, culminando no encerramento da Supersequência Gondwana I (Milani, 1997; Milani & Ramos, 1998; Milani *et al*. 2007).

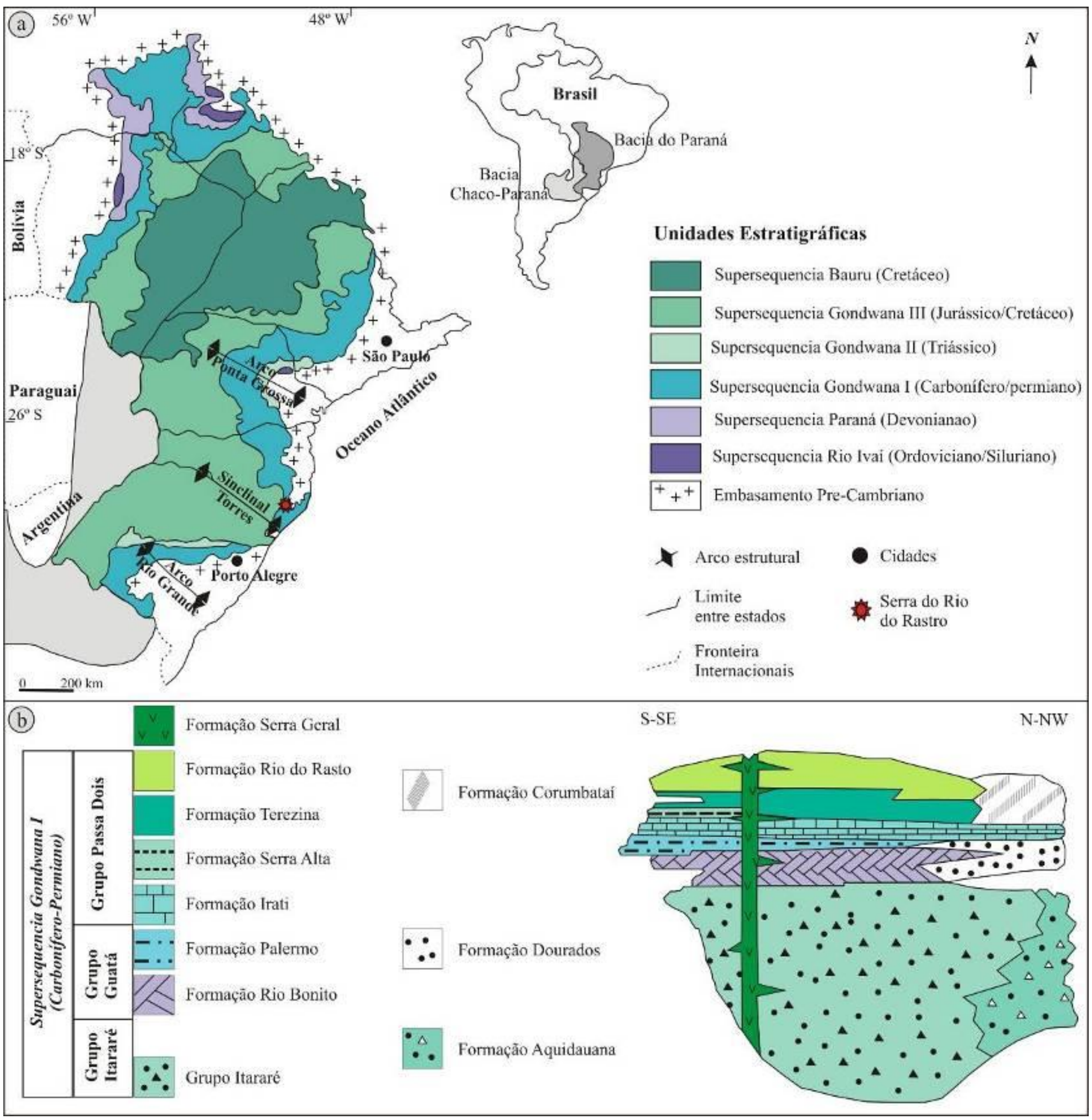

Figura 9: a) Mapa geológico mostrando a distribuição das unidades estratigráficas da Bacia do Paraná. b) Coluna estratigráfica da Supersequencia Gondwana I (modificado de Mori *et al*., 2012).

O Grupo Itararé se desenvolveu em um ambiente deposicional marinho periglacial, associado a fase final da deglaciação Mississipiana (Moscoviano). A unidade ocorre sobreposta aos estratos devonianos da Supersequencia Paraná (Formação Furnas e Ponta Grossa) e é composta por um pacote arenoso na porção inferior, sobreposto por folhelhos e diamictitos representativos da Formação Lagoa Azul (França & Potter, 1988), que aflora apenas em algumas regiões dos estados de São Paulo, Paraná e Mato Grosso do Sul. Acima da seção de base, ocorre a Formação Campo Mourão (França & Potter, 1988) formada por rochas arenosas de ampla distribuição na Bacia do Paraná, com ocorrência de diamictitos em algumas regiões. Essa formação equivale às formações Mafra e Campo do Tenente de Schneider *et al.* (1974). O topo do grupo em questão é representado pela Formação Taciba (França e Potter, 1988), que inclui a Formação Rio do Sul de Schneider *et al.* (1974), constituída de folhelhos com intercalações de arenitos (parte sul da Bacia do Paraná) e diamictitos (Membro Chapéu do Sol) na parte centro e norte da bacia. Segundo França e Potter (1988), com base em dados de subsuperfície, a Formação Aquidauana corresponde estratigraficamente ao Grupo Itararé, se diferenciando deste pelas suas rochas oxidadas e de coloração vermelha e com ocorrencia restrita à porção setentrional da bacia.

O contexto de deposição do Grupo Itararé remete a processos de sedimentação distintos, que envolve fluxos gravitacionais e progradação deltaica a máxima inundação (Eyles *et al*. 1993). Eyles *et al*. (1993) com base em dados de poços, registraram a presença de diamictitos, conglomerados e depósitos arenosos gradando a pacotes argilosos. O primeiro tipo de rocha foi associado ao transporte por geleira e o segundo tipo a processos turbidíticos. Os depósitos que iniciam em sedimentos grossos com afinamento para cima foram atribuídos ao contexto deposicional de progradação deltaica (mar baixo), culminando em afogamento devido a progressiva subida do nível relativo do mar (degelo). As caracteríticas dos depósitos sedimentares, no topo do Grupo Irararé (sedimentos argilosos), refletem um sistema deposicional trangressivo. Contudo, a tendência trangressiva foi interrompida por uma queda do nível relativo do mar (Milani 1997), que culminou na entrada de cunhas arenosas da Formação Rio Bonito (Grupo Guatá) no Artinskiano/Kunguriano. Este contexto, onde a trangressão temporareamente foi quebrada, insere o pacote da Formação Rio bonito em um trato de sistema de mar baixo. Neste contexto o contato entre o Grupo Itararé e o Grupo Guatá ocorre discordante, embora tenha sido descrito como concordante/transicional em alguns setores da bacia (Castro, 1991 *apud* Milani, 1997).

Sobre o pacote glacial Itararé desenvolveu-se o **Grupo Guatá** em um contexto marinho trangressivo. Os lobos deltaicos (Formação Rio Bonito), posicionados na base do referido grupo, envolve um conjunto de rochas areníticas associadas a pelitos e camadas de carvão. Diante da alternância entre os depósitos arenosos e pelíticos, Schneider *et al.* (1974) subdividiram a Formação Rio Bonito em três membros: o Triunfo posiciona-se na porção basal e é formado por um pacote arenoso, o Paraguaçu trata-se de um pacote pelítico que ocupa a posição intermediária e o Siderópolis refere-se a um pacote arenoso com presença de leitos de carvão e ocorre no topo da formação.

A retomada das condições trangressivas culminou em um contexto deposicional de plataforma marinho rasa em que se desenvolveu a Formação Palermo (Schneider *et al.*, 1974), sobre os depósitos deltáicos da Formação Rio Bonito. A sedimentação envolveu a deposição de de siltitos arenosos, que apresentam evidências de bioturbações em todos os domínios de ocorrência da formação em questão (Milani, 1997).

A Formação Palermo reflete o contexto de máxima inundação da Supersequencia Gondwana I (Milani, 1997). A partir desse ponto, onde a transgressão atingiu seu máximo, tem inicio a deposição do **Grupo Passa Dois** sob condições regressivas. A base desse grupo é representada por siltitos e folhelhos da Formação Irati, subdividida por Schneider *et al*. (1974) em dois membros: Taquaral representado por siltitos e folhelhos pobres em matéria orgânica, depositados abaixo do nível de ondas; Assistência,formada por folhelhos pirobetuminosos, associados a horizontes de calcários dolomíticos com presença de fósseis (*Mesosaurus Brasiliensis e Stereosternum Tumidum*, restos de vegetais, peixes e crustáceos, além de palinomorfos). A evolução do ciclo regressivo culminou no afogamento do golfo Irati e deu lugar a um ambiente deposicional marinho de águas calmas que resultou no pacote pelítico da Formação Serra Alta.

As condições de sedimentação marinha foram substituídas por um contexto de progressiva continentalização, no qual a Bacia do Paraná foi submetida. Assim, acima do pacote pelítico Serra Alta, sob ação de ondas e marés, depositou-se a Formação Teresina. Sequencialmente, o ocorre a Formação Rio do Rasto, constituída de arenitos finos intercalados com siltitos e argilitos. Gordon Jr. (1947) subdividiu esta formação em dois membros: o Membro Serrinha (porção inferior), depositado em condições marinho-transgressivas, constituído por siltitos e argilitos com lentes locais de calcário margoso; e o Membro Morro Pelado (porção superior), formado por siltitos e argilitos. Para Schneider *et al.* (1974) a deposição deste membro se deu em condições estritamente continentais, ao passo que para Aborrage & Lopes (1986), as condições de deposição se deram em ambiente flúvio-deltáico.

O equivalente estratigráfico dos depósitos Teresina e Rio do Rasto ocorre na porção nordeste da Bacia do Paraná (Milani, 1997), denominada de Formação Corumbataí. Na porção gaúcha, o segundo deposito foi interpretado como cronoequivalente à Formação Sanga do Cabral (Lavina, 1988). A Formação Rio do Rasto encerra o ciclo trangressivo-regressivo referente a Supersequência Gondwana I.

A progressiva continentalização dos sistemas deposicionais na Bacia do Paraná, culminou na deposição de sedimentos arenosos durante o Neojurássico (Milani *et al*., 1998). O extenso campo de dunas, que cobriu a referida bacia e regiões adjacentes, consitui a Formação Botucatu. No Eocretáceo, diante dos primeiros estágios de ruptura do paleocontinente Gondwana, um volumoso derrame de lavas (Milani *et al*., 1998) intrudiu os depósitos sedimentares espalhando-se sobre os mesmos (Formação Serra Geral). O conjunto de rohcas eólicas e os derrames básicos das unidades mencionadas constiutem o **Grupo São Bento,** referente a Supersequencia jurássica-eocretácea Gondwana III.

Na Serra do Rio do Rastro, o Grupo São Bento (Formações Botucatu e Serra Geral) ocorre diretamente sobre os estratos permianos da Formação Rio do Rasto (Supersequencia Gondwana I). Embora a presente pesquisa tenha como objetivo definir a proveniencia dos sedimentos referentes ao pacote permo-carbonífero, achou-se necessário acrescentar dados da Formação Botucatu, para complementar o estudo referente à todos os depósitos sedimentares que ocorrem ao londo da Coluna White.

3.2 – Coluna White

Na borda sudeste da Bacia do Paraná, em particular na Serra do Rio do Rastro, sul do Estado de Santa Catarina (Figura 1), aflora um conjunto de rochas que representa classicamente o contexto estratigráfico desenvolvido durante os períodos Permo-Carbonífero (Supesequencia Gondwana I) e Juro-Cretáceo (Supersequencia Gondwana III) (Figura 10). White (1908) foi quem primeiro reuniu essas rochas em um grupo que deminou Sistema de Santa Catarina, formado da base para o topo pelas séries Tubarão, Passa Dois e de São Bento .

Posteriormente, as unidades sedimentares da Bacia do Paraná foram reagrupadas e subdivididas em termos de fácies, descontinuidades e correlações regionais. Na coluna estratigráfica de Schneider *et. al.* (1974) as seções Gondwana I e Gondwana III (Milani, 1997) são constituídas da base para o topo pelos Grupos Itararé, Guatá, Passa Dois (Supersequencia Gondwana I) e São Bento (Supersequencia Gondwana III).

Pontos de amostragem

O conjunto de afloramentos na Serra do Rio do Rastro é representado pela coluna estratigráfica denominada de Coluna White, em homenagem ao pesquisador pioneiro nesta área Israel Charles White. Ao todo foram amostrados 16 afloramentos entre a base e o topo da seção geológica (Tabela 1), localizada ao longo da rodovia SC-438 (Figura 11).

Próximo a entrada da cidade de Lauro Müller localiza-se o primeiro exemplar representativo da base da Coluna White. O afloramento constitui-se na porção inferior de folhelhos siltíticos da Formação Rio do Sul, que integra o Grupo Itararé, sobrepostos por arenitos referente ao Membro Triunfo da Formação Rio Bonito (Grupo Guatá).

Na sequencia, aflora um pacote arenoso associado ao Membro Paraguaçu (Formação Rio Bonito – Grupo Guatá) formado por siltitos argilosos de cor cinza que gradam para o topo à arenitos finos, com grãos bem selecionados, de cor cinza claro apresentando estraificação plano-paralela. Sobrepostos, através de superfície erosiva, está o pacote arenoso do Membro Siderópolis formado por arenitos argilosos, com estratificação tangencial e níveis de folhelhos negros. A Formação Palermo (Grupo Guatá) ocorre sob a forma de siltitos e flolhelhos de cor amarelada.

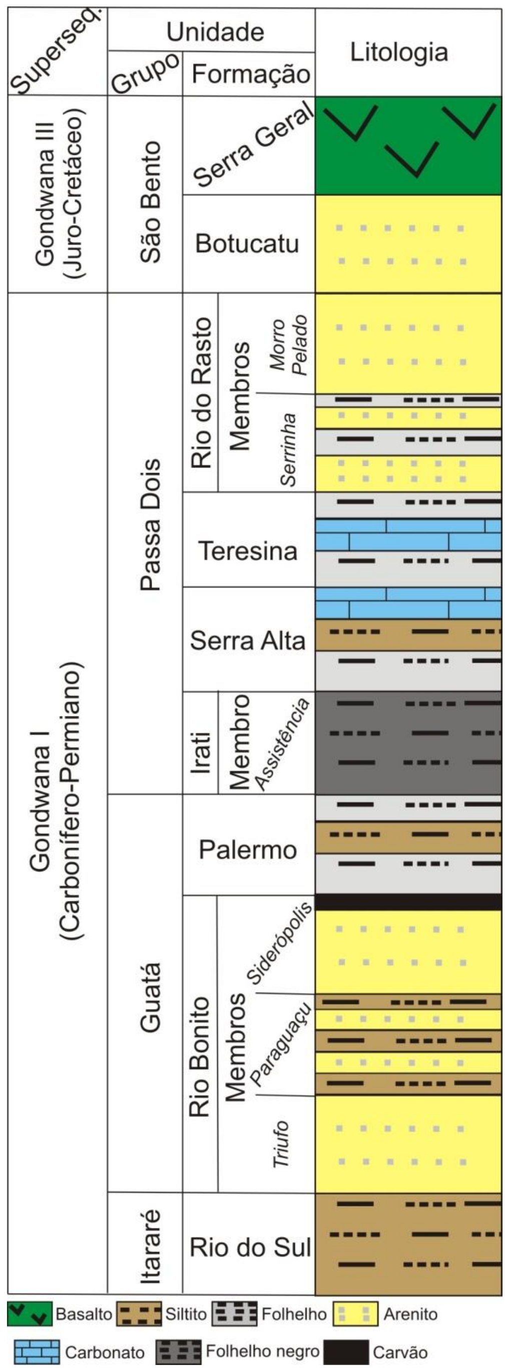

Figura 10: Coluna estratigráfica esquemática mostrando as unidades que ocorrem ao longo da Serra do Rio do Rastro (SC).

Tabela 1: Resumo dos pontos de amostragem ao longo da Coluna White e das análises realizadas em cada amostra.

Unidade	*Idade	Ambiente	Litologia/Amostras	Tipo de análise
Grupo Itararé: Fm Rio do Sul	Sakmariano (295.0 ± 0.18 a 290.1 ± 0.26 Ma)	Marinho peri-glacial	Folhelho/CW-01A	Sm-Nd
Grupo Guatá: Fm Rio Bonito (Mb Triunfo)	Sakmariano (295.0 ± 0.18 a 290.1 ± 0.26 Ma)	Marinho costeiro	Arenito/CW-01B	Sm-Nd, U-Pb e Lu-Hf
Grupo Guatá: Fm Rio Bonito (Mb Paraguaçu)	Sakmariano (295.0 ± 0.18 a 290.1 ± 0.26 Ma)	Marinho costeiro	Siltito/CW-02A	Sm-Nd, U-Pb e Lu-Hf
			Arenito fino/CW-02B	Sm-Nd
Grupo Guatá: Fm Rio Bonito (Mb Paraguaçu)	Sakmariano (295.0 ± 0.18 a 290.1 ± 0.26 Ma)	Marinho costeiro	Arenito fino/CW-03	Sm-Nd, U-Pb e Lu-Hf
Grupo Guatá: Fm Rio Bonito (Mb Siderópolis)	Artinskiano (290.1 ± 0.26 a 283.5 ± 0.6)	Marinho plataformal	Folhelho negro/ CW-04A	Sm-Nd
			Arenito argiloso/ CW-04B	Sm-Nd, U-Pb e Lu-Hf
			Argila/CW-05	Sm-Nd, U-Pb e Lu-Hf
Grupo Guatá: Fm Palermo	Artinskiano (290.1 ± 0.26 a 283.5 ± 0.6)	Marinho plataformal	Siltito/CW-06	Sm-Nd
Grupo Passa Dois: Fm Irati (Mb Assistência)	Kunguriano (283.5 ± 0.6 a 272.3 ± 0.5)	Marinho restrito	Siltito/CW-07	Sm-Nd
Grupo Passa Dois: Fm Serra Alta	Kunguriano (283.5 ± 0.6 a 272.3 ± 0.5)	Marinho plataformal	Folhelho/CW-09G	Sm-Nd
			Carbonato/CW-09A, CW-09BCO, CW-09C, CW-09DCO, CW-09ECO, CW-09F, CW-09BASE, CW-09SUL_PIR, CW-09FRAN e CW-09NÌVEL	Sm-Nd
Grupo Passa Dois: Fm Teresina	Wordiano (268.8 ± 0.5 a 265.1 ± 0.4) ao Capitaniano (265.1 ± 0.4 a 259.8 ± 0.4)	Continental lagos rasos	Carbonato/CW-10BCO	Sm-Nd
Grupo Passa Dois: Fm Rio do Rasto (Mb Serrinha)	Capitaniano (265.1 ± 0.4 a 259.8 ± 0.4) ao Wchiapiniano (259.8 ± 0.4 a 254.14 ± 0.07)	Continental fluvial	Arenito/CW-10A, CW-11B e CW-11C	Sm-Nd, U-Pb e Lu-Hf
Grupo Passa Dois: Fm Rio do Rasto (Mb Morro Pelado)	Changhsingiano (254.14 ± 0.07 a 252.17 ± 0.06)	Continental fluvial	Arenito/CW-13 e CW-14	Sm-Nd
Grupo São Bento: Fm Botucatu	Tithoniano (152.1 ± 0.9 a ~145.0) ao Valangiano (~139.8 a ~132.9)	Continental eólico	Arenito/CW-16A e CW-16B	Sm-Nd, U-Pb e Lu-Hf

*Fonte Milani *et al*. (2007)

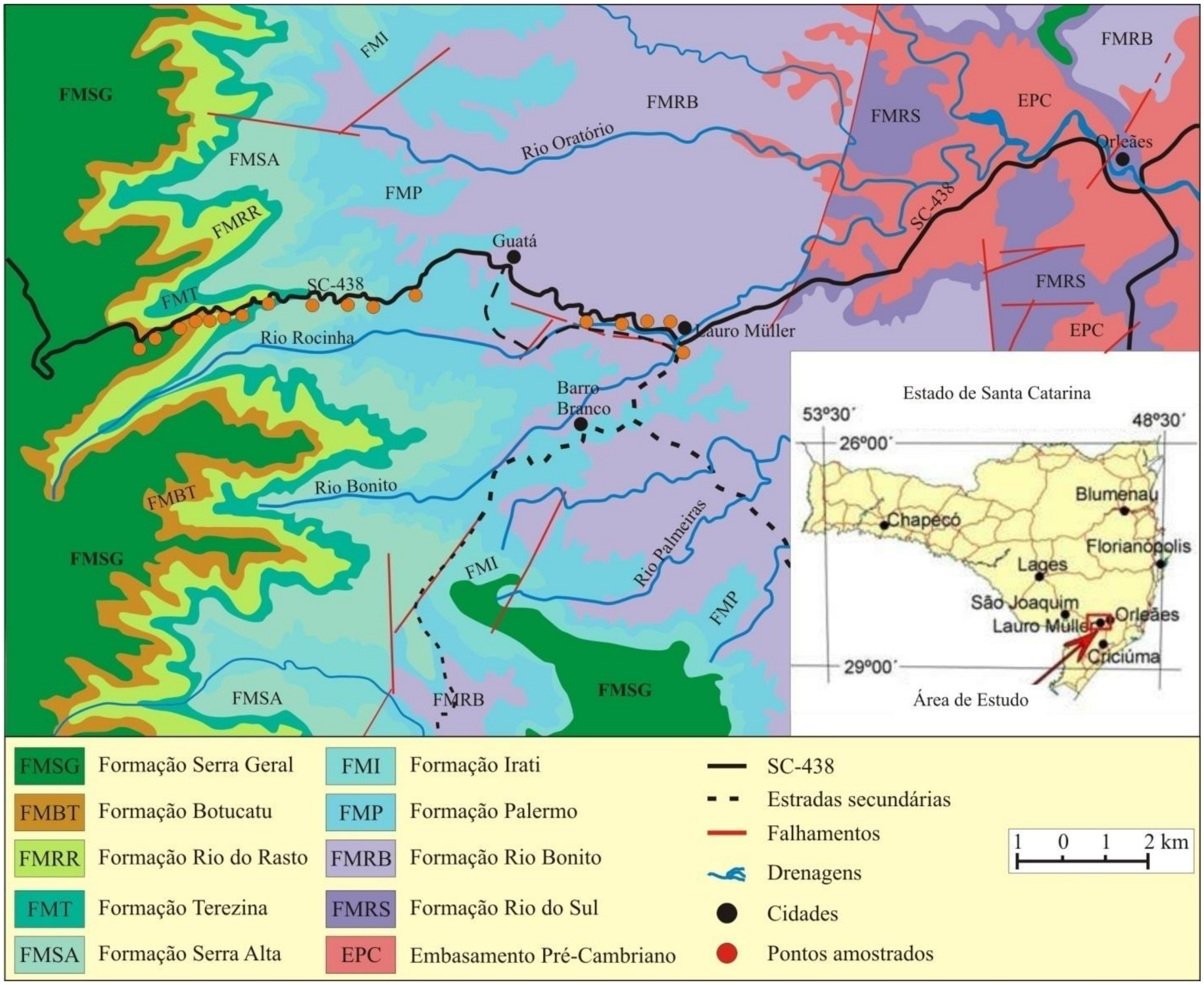

Figura 11: Mapa geológico da Serra do Rio do Rastro (modificado de Orlandi Filho *et al*., 2006).

O pacote referente ao Grupo Passa Dois acha-se representado na base pelos folhelhos betuminosos de cor escura, referente ao Membro Assistência, Formação Irati. O espesso pacote Serra Alta (Grupo Passa Dois), ocorre sob a forma de folhelhos e siltitos de cor cinza-escuro, por vezes com concreções calcáreas, exibindo laminação plano-paralela.

A continuada ocorrência do Grupo Passa Dois se manifesta nos folhelhos e siltitos com concreções calcáreas da Formação Teresina, bem como nos pacotes arenosos da Formação Rio do Rasto. Esta última formação está representada por folhelhos cinza-escuro intercalados a arenitos (Membro Serrinha) e por arenitos de cor avermelhada do Membro Morro Pelado.

Sobrepondo aos arenitos do Membro Morro Pelado ocorrem os sedimentos eólicos da Formação Botucatu (Grupo São Bento). Este último pacote apresenta-se com estratificação cruzada acanalada de grande porte, coberto pelas rochas vulcâncias básicas da Formação Serra Geral, juntos formando o Grupo São Bento.

CAPÍTULO IV

PROVENANCE OF PERMIAN SEDIMENTS AND TECTONIC EVOLUTION OF SOUTHEASTERN GONDWANA

Lindaray Sousa da Costa[1, 2], Roberto Ventura Santos[1], Elton Luiz Dantas[1], Lucieth Cruz Vieira[1]

[1]Universidade de Brasília, Instituto de Geociencias, Laboratorio de Geocronologia 70910-900 Brasília-DF, Brazil

[2]Corresponding author lindaraygeo@gmail.com

ABSTRACT

The southwestern margin of Gondwana was marked by major tectonic and environmental changes during the Permian, such as the development of a major subduction and accretion zone along the Southern Panthalassan margin. This event may have affected drainage pattern and sediment source areas in southwestern Gondwana intracratonic basins, such as the Paraná basin. The Serra do Rio do Rastro, southeastern Brazil, features outcrops of a Permian succession of sedimentary rocks that may have recorded these tectonic changes that affected southwestern Gondwana. We present U-Pb and Lu-Hf detrital zircon data and whole rock Sm-Nd isotope data from samples across this succession, known as the White Column after an American geologist that studied these rocks in the last century. The zircon U-Pb data from the lower to middle part of the Permian (Rio Bonito Formation - Grupo Guatá Group) indicate a dominance of Palaeoproterozoic (2.5 to 1.7 Ga) grains, followed by Mesoproterozoic (1.5 to 1.0 Ga) and Neoproterozoic (992 to 550 Ma) grains. In contrast, the sediments from the Rio Rasto Formation (Passa Dois Group) present a dominance of Neoproterozoic (935 to 545 Ma) grains, followed by Palaeozoic, including Permo-

Triassic (297-216 Ma), grains. The Hf (T_{DM}) model ages indicate a Palaeoproterozoic age for the zircons at the base of the succession and Meso- to Neoproterozoic ages for zircon in the upper part of the succession. The Sm-Nd data reinforce the results of the other isotope systems and indicate a major change in sedimentary provenance between the lower and upper portions of the profile. These changes suggest that, during the mid-Permian, the Paraná basin was affected by the orogeny that developed along the southern and southwestern margins of Gondwana.

Keywords: Permian, Serra do Rio do Rastro, Coluna White, U-Pb, Lu-Hf.

1. Introduction

Southeastern South America experienced major tectonic changes during the assembly of West Gondwana between the end of Neoproterozoic and the Palaeozoic, in particular, during the Permian. The region was strongly affected by convergence related to the collision of South America and Africa, which led to the development of a sequence of mountain chains on the South American side that is known today as the Don Feliciano, Ribeira, and Araçuaí Belts (Basei et al., 2005; Heilbron et al., 2008; Schmitt et al., 2008; Frimmel et al., 2011). Later, during the Carboniferous, the Patagonian continent began to collide with the southwestern part of Gondwana, developing a magmatic arc related to the subduction of oceanic crust beneath Gondwana (Ramos, 1984; Milani and Ramos, 1998a; Turner, 1999; Ramos, 2008). This orogeny was responsible for upper Palaeozoic-lower Mesozoic batholiths, such as those that occur in north-central Chile (Hervé et al., 2014), and was likely related to a subduction and accretion zone along Southern Panthalassan Margin of Gondwana (Turner, 1999). The presence of this collision event has led some authors to argue that the Paraná and Karoo basins may have behaved as a foreland basin, in which subsidence was strongly controlled by the tectonic regime (Milani and Ramos, 1998b; Turner, 1999). The later stages of this collision in the middle to late Permian is related to the San Raphael Orogeny that uplifted the western part of South America and transformed this region into an important source region of sediment. This orogeny was also accompanied by explosive felsic volcanism that spread ash across a very large area (Santos et al., 2006; López-Gamundí, 2006a; Rocha-Campos et al., 2011).

In addition to the regional tectonic, southeastern South America also underwent major changes induced by global climatic events. For instance, in the early Permian, a trangressive-regressive cycle (Gondwana I Sequence, Milani 1997) related to a global sea level rise initiated due to the Mississippian deglaciation. Variations in subsidence rate and even local uplift during this cycle have been attributed to tectonic activity at the margins (Milani, França and Schneider, 1994a; Milani and Ramos, 1998b). The Permo-Triassic boundary marks one of the most important mass extinction events in the Phanerozoic, during which approximately 90% of the living species are estimated to have disappeared (Sepkoski, 1984; Sepkoski, 1996; Erwin, 2001). Initially believed to be the result a single extinction event, it was later shown that there were in fact two events, one in the Middle Permian (Guadalupian) and another at the Permo-Triassic boundary (Stanley and Yang, 1994; Isozaki, 2003; Isozaki et al., 2006; Isozaki et al., 2007). The Middle Permian event was associated with the Kamura cooling event, which was likely related to a major increase in global felsic volcanism (Isozaki et al., 2007).

Provenance studies based on geochronology and isotope geochemistry have contributed significantly to our understanding of sedimentary basin evolution. For instance, U-Pb and Lu-Hf data from zircons (Veevers et al., 2005; Gerdes e Zeh, 2006; Augustsson et al., 2006; Yao et al., 2011), as well as Nd isotope data from sediments, have been commonly used to identify changes in sediment source regions during the filling of sedimentary basins. These changes in provenance can be induced either by climatic events, which expose and cover large areas via fluctuations in sea level, or by tectonic activity, which uplift large areas surrounding the basin. Geochronologic and isotope geochemical approaches may shed light on the relationship between tectonic and sediment provenance during the filling of the Permian Paraná basin.

In South Brazil, the whole Permian sequence is well exposed along the Rio do Rastro Road, which is located on the eastern border of the Paraná basin. The sequence is situated near the city of Lauro Müller and can be accessed via the SC-438 highway, starting from the city of Tubarão, near the coast of Santa Catarina in South Brazil. This section is also known as the “White Column” after White (1908) and has a total vertical displacement of 780 m. The outcropping sediments belongs to the Itararé (Upper Carboniferous), Guatá (Permian), Passa Dois (Permian), and São Bento Groups (Jurassic/Cretaceous). In the present study, we have sampled sediments from the base to the top of the succession to understand the variations in sediment provenance across the profile. This study focuses on U-Pb and Lu-Hf analyses of zircon grains and whole rock Nd isotope geochemistry.

2. Geological framework

The Paraná basin is a large intracratonic basin, located in the central-eastern part of the South-American Platform. It comprises a thick (ca. 5,000 m) and extensive sedimentary-magmatic sequence, which covers an area of approximately 1,500,000 km^2 of Brazil, Uruguay, Argentina and Paraguay. According to Milani et al. (1994) and Milani and Zalán (1999), six supersequences are represented in this basin, ranging from Upper Ordovician to Upper Cretaceous: the Rio Ivaí (Caradociano-Llandoverian), Paraná (Lochkoviano-Frasnian) and Gondwana I (Westphalian-Scythian) are associated with transgressive-regressive cycles, and the Gondwana II (Neoanisian-Eonorian), Gondwana III (Neojurassic-Berriasian) and Bauru (Aptian-Maestrichtian) are associated with continental sedimentation and coeval volcanism.

The Permian development of the Paraná Basin occurred at the same time as the convergence between the Gondwana palaeocontinent and the Panthalassa ocean. The subduction of the ocean floor beneath the continent led to the development of an active collisional belt known as the Gondwanides (Fig. 1) along the southwestern margin of Gondwana (Milani et al., 2007b). The episodes of collision and accretion associated with the allochthonous domain are the reflection of the Famatinian (Ocloyic and Precordilherian Orogenies – Ordovician to Devonian) and Gondwanic (Chanic and San Rafael Orogenies – Carboniferous to Triassic) orogenic cycles (Ramos, 1988). The geodynamics of the active border of Gondwana directly influenced the evolutionary history of the Paraná Basin, during which episodes of subsidence associated with major orogenic events favoured the creation of depositional space in the intracratonic area (Milani, 2007).

The Serra do Rio do Rastro is located on the southeastern margin of the Paraná basin (Fig. 2a). It includes a set of rocks that is typical of the stratigraphic framework that developed during the Permo-Carboniferous (Supesequence Gondwana I) and Juro-Cretaceous (Supersequence Gondwana III) periods (Fig. 2b). The supersequence Gondwana I has an area of approximately 2.500 m^2 (Milani et al., 1994) and is characterized at its base by sediments of the Itararé Group and Rio Bonito Formation, which are related to the Gondwanic deglaciation (Schneider et al., 1974). Above these rocks, transgressive marine sediments of the lower Permian Palermo Formation (Guatá Group) were deposited, marking the maximum inundation of this cycle (Schneider et al., 1974). The Permo-Triassic succession includes the Passa Dois Group, deposited under regressive conditions, and the Neojurassic eolian sediments of the Botucatu Formation (São Bento Group-Gondwana III) (Milani, 1997).

The Itararé Group was deposited in a marine periglacial environment under a transgressive systems tract (Milani, 1997) associated with the end stage of the Mississippian deglaciation. At the base of the succession, Upper Carboniferous sediments were deposited in a fluvio-lacustrian environment that developed after the glacial event (Schneider et al. 1974). The lower formation of this unit (Campo do Tenente Fm.) is composed of fluvio-glacial pelites, rhythmites, and diamictites that grade into marine-continental sandstones, diamictites, and subordinated argillites of the Mafra Fm. The Upper Itararé Group is characterized by black shales, turbidites, diamictites and sandstones deposited in a marine-deltaic environment (Rio Sul Fm.). These rocks grade into sandstones of the Guará Group (Rio Bonito Formation), which are located at the base of the Permian sequence.

The Guatá Group is the lower Permian unit that crops out across the Serra do Rio do Rastro section. This unit in divided into the lower Rio Bonito and the upper Palermo Formations, which marks the highest inundation level of the Permian according to Schneider et al. (1974). The base of the Guatá Grupo is characterized by siltites, claystones, carbonaceous siltites and rare layers of coal (Triunfo Mb.), which grade upward into sandstones, siltites and claystones (Paraguaçu Mb.). At the top of the Rio Bonito Fm., sandstones are intercalated with siltstones, black shales and coal (Siderópolis Mb.), and this formation represents the main coal horizon in the Paraná

Basin. The upper Guatá Group is composed of bioturbated siltstones with lenses of fine-grained to microconglomeratic sandstone.

The middle to upper Permian is marked by the deposition of the **Passa Dois Group**, which represents a regressive sequence that is covered by aeolian sandstone of the Juro-Cretaceous **São Bento Group** (Botucatu Formation). The base of the Passa Dois Group is made of siltites and black shales of the Irati Formation, which are believed to have been deposited in a low-energy marine environment. Towards the top, the sedimentary deposition becomes increasingly controlled by shallower water conditions, ending with the sandstone and siltites of the Rio do Rastro Formation, which were deposited under transitional (Scheider et al. 1974) or fully continental conditions (Alboarrage e Lopes, 1986). The units of the Passa Dois Group are very rich in fossils such as Mesosaurus Brasiliensis and Stereosternum Tumidum in the Irati Formation and plants, palynomorphs, and lamelibranquios in the Teresina Formation.

The Column White profile

The first representative sample of the base of the White Column is located at the entrance of the town of Lauro Müller. The lower portion of the outcrop consists of shales and siltstones of the Rio do Sul Formation, part of the Itararé Group, which are overlain by sandstones of the Triunfo Member of the Rio Bonito Formation, Guatá Group (Fig. 2b).

The upper portion of the succession includes sandstones of the Paraguaçu Member (Rio Bonito Formation - Guatá Group), which consists of grey clayey siltstone horizons that grade upwards into fine sandstones, with well-sorted grains, a light grey colour and plane-parallel stratification. These sediments are overlain by an erosion surface and the sandy layers of the Siderópolis Member, composed of clayey sandstone with cross stratification and black shale layers. The Palermo Formation (Guatá Group) occurs as siltstone and shales.

The Passa Dois Group is represented at the base by dark shales of the Assistência Member (Irati Formation). The Serra Alta Formation (Passa Dois Group) occurs in the form of shales and siltstones, sometimes with calcareous concretions, with parallel lamination.

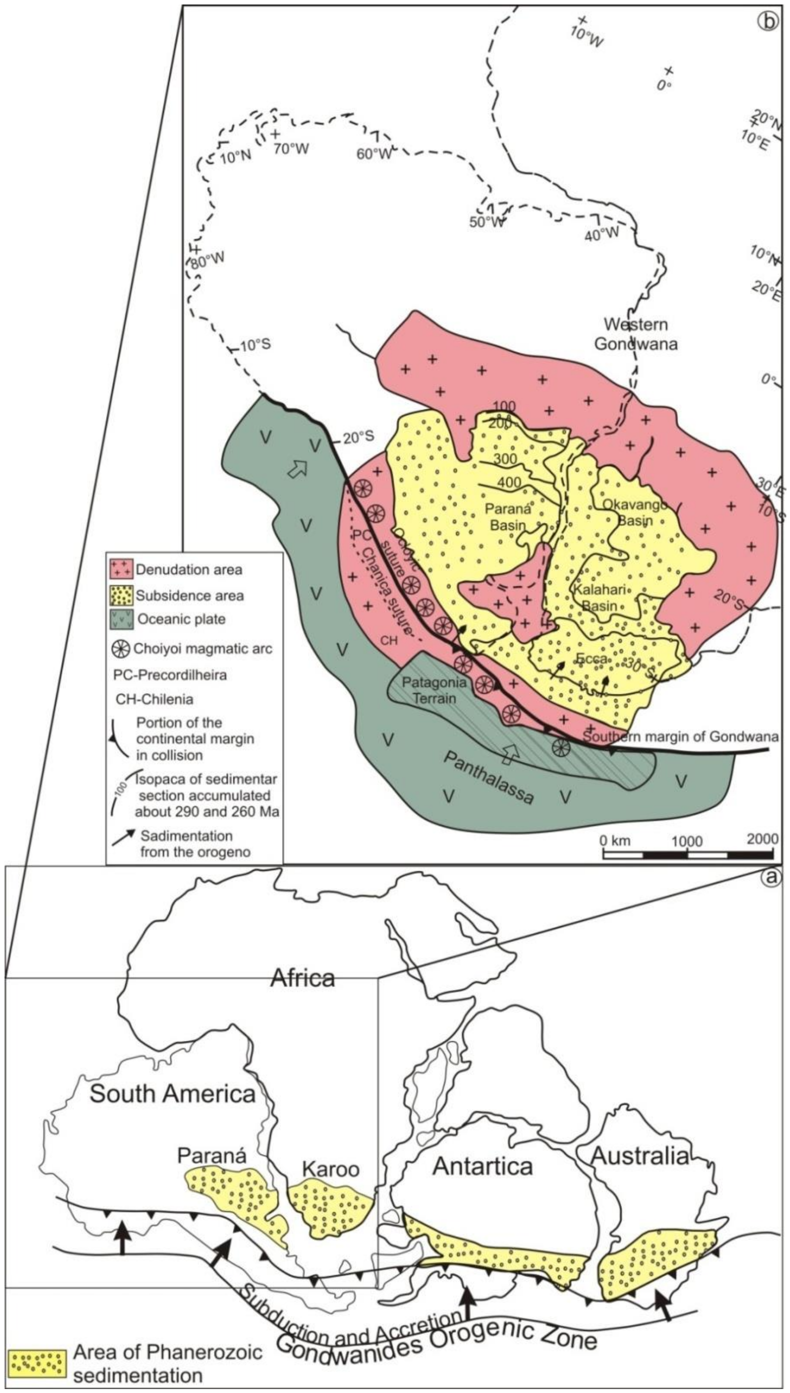

Fig. 1. a) Illustrative map of Gondwanides orogenic zone (modified de De Toit, 1937, *apud* Powell & Veervers, 1994). b) Tectono-sedimentary context of south-western Gondwana in the limit Early Permian/Late Permian, when the region was subjected to the effect of San Rafael Orogeny.

The upper portion of the Passa Dois Group is composed of in shales and siltstones with carbonate concretions in the Teresina Formation and sandy layers in the Rio do Rasto Formation. The Rio do Rasto Formation features sandstones intercalated with dark grey shales in the Serrinha Member and reddish sandstones associated with the Morro Pelado Member.

The aeolian sediments of the Botucatu Formation (São Bento Group) occur above the sandstones of the Morro Pelado Member. This formation presents cross-fluted stratification covered by basic volcanic rocks of the Serra Geral Formation (São Bento Group).

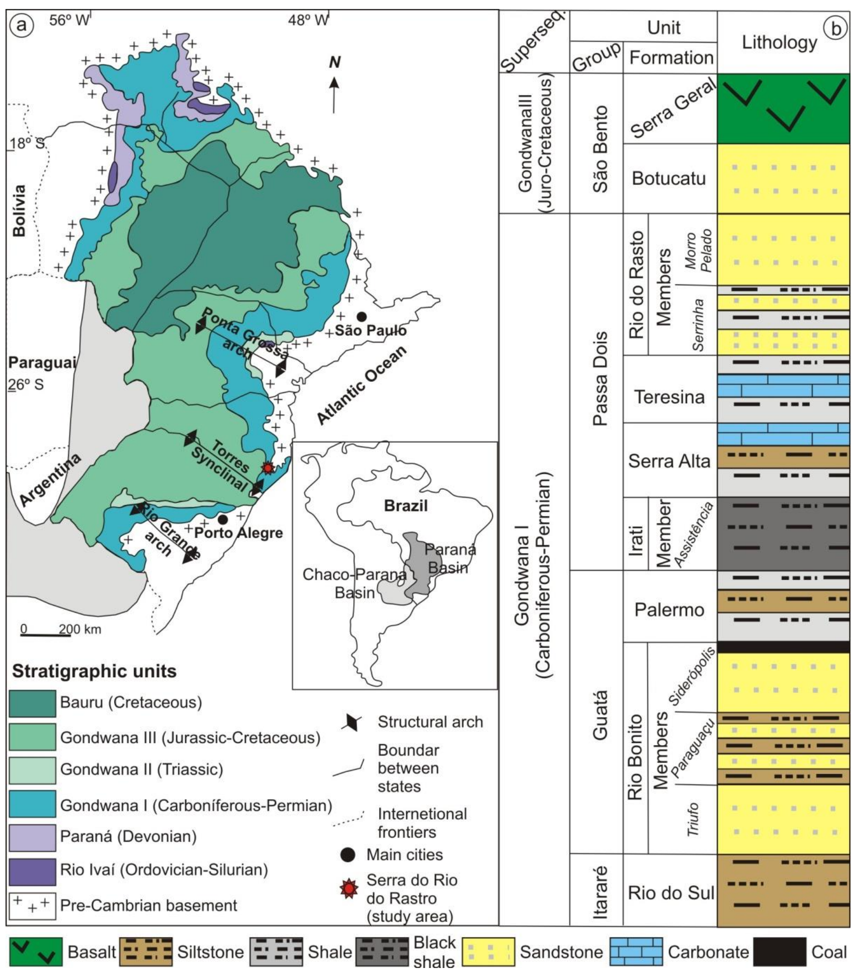

Fig. 2: a) Geological map showing the distribution of stratigraphic units of the Paraná Basin (modified of Mori *et al.*, 2012). b) Schematic stratigraphic column showing the units that outcrop across the Serra do Rio do Rastro.

3. Sampling and analytical procedures

Sixteen samples were collected along the Serra do Rio do Rastro section, following the field guide of the Brazilian Geological Survey that describes the main outcrops of the units along the road. The samples include sandstone, claystone, siltstone and limestone, and all were analysed for whole rock Sm-Nd. Among the 16 samples, only 9 had a sufficient number of recovered zircon grains to perform U-Pb and Lu-Hf geochronological and geochemical analyses: samples CW-01B, CW-02A, CW-03, CW-04B e CW-05 of the Guatá Group; samples CW-11B and CW-11C of the Passa Dois Group; and samples CW-16A e CW-16B of the Botucatu Formation (São Bento Group). All sample preparation and analyses were performed at the Geochronos Lab of the University of Brasília following the routines of Gioia and Pimentel (2000) for Sm-Nd, Bühn et al. (2009) for U-Pb zircon and Matteini el al. (2010) for Lu-Hf analytical procedures. The Sm-Nd analyses were performed using a thermal ionization mass spectrometer (TIMS), and the U-Pb and Lu-Hf analyses were performed using a laser ablation multi-collector inductively coupled plasma mass spectrometer (LA-MC-ICP-MS).

For provenance studies, the number of analysed zircons is very important, and a total of 60 to 100 grains is considered statistically significant (Dodson et al., 1988; Sircombe, 2000; Vermeesch, 2004, Andersen, 2005). The steps of sample preparation involved grinding, sandblasting and separation via magnetic susceptibility via isodynamic Franz equipment. In this study, approximately 60 zircon grains from each concentrate were then picked under a binocular microscope and mounted in epoxy, together with GJ-1 reference zircons. Later, the mounts were polished and observed under cathodoluminescence to observe their internal structure.

Zircon ages were obtained using an LA-MC-ICP-MS by moving the ~30-µm-diameter laser spot across the grain for 40 seconds. All data were processed using Isoplot/Ex (Ludwig, 2001) and a software developed at the Geochronos Lab of the University of Brasilia. The analytical processing consisted of reducing the data by removing points outside the regression line, with high common Pb or with high error. Then, density curve diagrams were generated.

The measurement of Lu-Hf isotopes was performed on zircons previously analysed using the laser ablation U-Pb method to determine the relationship among Hf isotope ratios and age. The two spots analyses must be as close as possible in order to analyse portions of the zircon grain with the same isotopic characteristics (Matteini et al., 2010).

Zircons for Lu-Hf measurements were selected based on the agreement factor of their U-Pb ages (Conc. ≥ 90% e ≤ 110%) among the one hundred and fifty-four grains from 9 samples of the Coluna White. Lu-Hf isotopic analyses were performed via the spot ablation technique at the grain surface using a spot diameter of 40-50 µm and a measurement duration of 40-50 seconds. The reference zircon GJ-1 was analysed during the procedure to calibrate the data. The $\varepsilon_{Hf(t)}$ values and the U-Pb ages were calculated and plotted in binary diagrams,] that related the Hf isotopic variation to CHUR (Patchett e Tatsumoto et al. 1980; Patchett e Tatsumoto et al.1981; Patchett 1983). For zircons older than 1 Ga, we used $^{207}Pb/^{206}Pb$ ratios, and for zircons younger than 1 Ga, we used $^{206}Pb/^{238}U$ ratios.

Sample dissolution for Sm and Nd isotope analyses was carried out in Teflon Savillex beakers or Parr-type Teflon bombs. Approximately 100 mg of each sample was spiked (^{149}Sm-^{150}Nd) and attacked with a heated mixture of concentrated HF and HNO_3. After evaporation, 6 N HCl was added to each beaker to prepare a chromatographic separation. Sm and Nd extraction followed the technique of Richard et al. (1976) and Gioia and Pimentel (2000); the separation of the rare earth elements (REEs) as a group using cation-exchange columns precedes reversed-phase chromatography for the separation of Sm and Nd using columns loaded with HDEHP (di-2-ethylhexeyl phosphoric acid) supported on Teflon powder. We used the REE-Spec and Ln-Spec resins for REE and Sm-Nd separation. A mixed ^{149}Sm-^{150}Nd spike was used. Sm and Nd samples were loaded onto Re evaporation filaments in a double-filament assembly. The Sm and Nd isotopic analyses were carried out using a Finningan MAT-262 mass spectrometer. The uncertainties in the Sm/Nd and $^{143}Nd/^{144}Nd$ ratios are considered to be less than ±0.1% (1σ) and 0.000001 (1σ), respectively, based on repeated analyses of the international rock standards BCR-1 and BHVO-1. The $^{143}Nd/^{144}Nd$ ratios were normalized to a $^{146}Nd/^{144}Nd$ ratio of 0.7129. The Nd procedure blanks were less than 100 pg.

4. Results

Most zircon grains (approximately 60%) are euhedral to subhedral as revealed by the cathodoluminescence images (Fig. 3). The exceptions are grains from samples of the eolian sandstone of the Botucatu Formation (CW-16A and CW-16B), in which approximately 80% of the grains exhibits rounded to oval shapes. The euhedral and subhedral shapes of most grains are indicative of a proximal source area and a transport process that was not very abrasive. All samples, however, also contain rounded to subrounded grains, indicating more than one source of zircon grains.

A total of 540 zircon grains were dated via U-Pb analysis (Appendix A), if all analysed samples are considered. Zircons from the early Permian Rio Bonito Formation samples (CW-01B, CW-02A, CW- 03, CW-04B and CW-05) present three main groups of age intervals (Figs. 4a, 4b, 4c, 4d and 4e): Palaeoproterozoic (2.5 to 1.7 Ga), comprising 42 to 66%; Mesoproterozoic (1.5 to 1.0 Ga), comprising 16 to 24%; and Neoproterozoic and Cambrian (992 to 490 Ma), comprising 8 to 22% and 2 to 18%, respectively. Among these age intervals, the Palaeoproterozoic is present in all samples. Therefore, this is a main source of sediments for these rocks. In contrast, the other age intervals display a more variable pattern; for example, Neoproterozoic zircons are absent in sample CW-05 and Mesoproterozoic zircons are almost absent in samples CW-01B and CW-04B. Except for sample CW-01B, most samples also present a minor population of Archean (2.9 to 2.6 Ga) zircon grains, comprising 5 to 13%, as well as younger grains, such as Devonian (CW-01B, comprising 2%) and Ordovician (CW-02A and CW04B, comprising 2% and 3%, respectively).

In contrast to the Rio Bonito Formation, the zircon population of the Rio do Rasto Formation (Figs. 5f and 5g) is dominated by Neoproterozoic (approximately 31 to 41%) and younger zircons with ages that are as young as Permo-Triassic. These samples exhibit Palaeozoic zircon grains that have Cambrian (10-20%), Ordovician (2-10%), Silurian (3%), Devonian (3%), Carboniferous (2-3%), Permian (2-3%) and Triassic (2-10%) U-Pb ages (Appendix A). Neoproterozoic zircons comprise the main population of the Rio do Rastro samples and have a wide age range (935 to 545 Ma). Mesoproterozoic and Palaeoproterozoic grains are almost absent in these samples. Thus, source regions of these rocks are quite different from those of the lower unit.

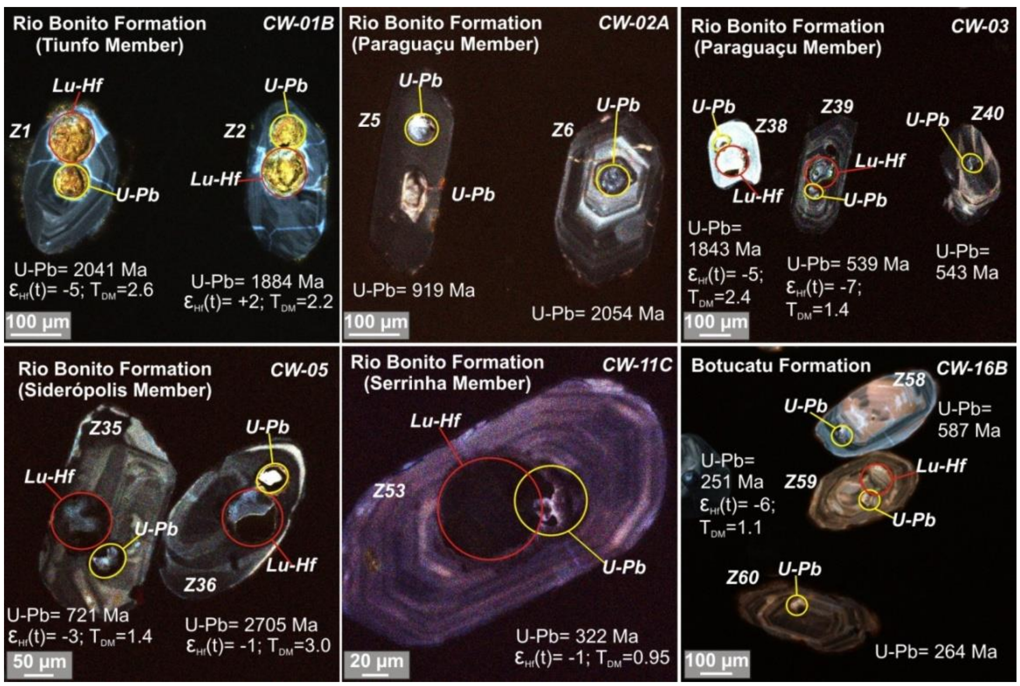

Fig. 3: Cathodoluminescence image of the zircons showing analysis spots with U-Pb ages and Lu-Hf isotopic results calculated.

The sandstone from the Botucatu Formation, samples CW-16A (Fig. 5h) and CW-16B (Fig. 5i), exhibit a major concentration of Neoproterozoic (924 to 543 Ma) zircons grains, comprising 41 to 42%, followed by a smaller proportion of Palaeoproterozoic grains (2216 and 1690 Ma), comprising 18 to 20%, Mesoproterozoic grains (1507 and 1011 Ma), comprising 5 to 11% and Archean grains (2837 and 2713 Ma), comprising 2 to 3%. In addition to the main Neoproterozoic age peak at 613 to 551 Ma, these samples also present various populations of Palaeozoic zircons, as shown in figs. 5h and 5i.

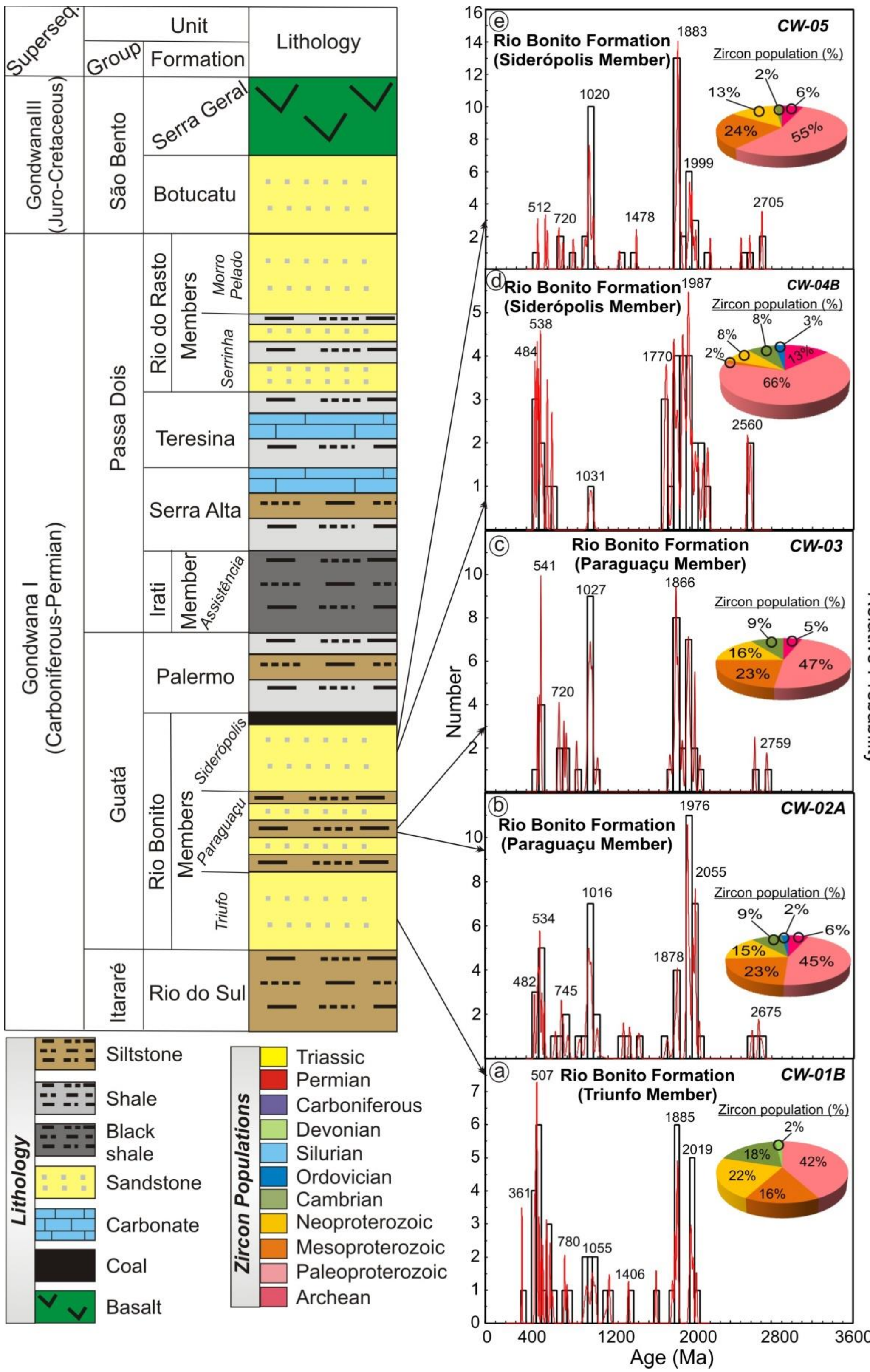

Fig. 4: Relative probability *versus* age diagrams showing results obtained from samples across of the Serra do Rio do Rastro (schematic stratigraphic column). The zircon populations identified in samples CW-01B, CW-02A, CW- 03, CW-04B and CW-05 are represented in percentage graphs.

The Lu-Hf results for all the samples (Appendix B) are plotted according to zircon age in figs. 6a, 6b, 6c, 6d and 6e: five samples from the Rio Bonito Formation (CW-01B, CW-02A, CW- 03, CW-04B and CW-05), one sample from the Rio do Rasto Formation (CW-11C; Fig. 6f) and two samples from the Botucatu Formation (CW-16A e CW-16B; Figs. 6g and 6h). Sample CW-11B did not have enough zircon grains to perform the Lu-Hf analyses. The $\varepsilon_{Hf(t)}$ versus Age (Ma) diagram of the Rio Bonito samples clearly shows the three main zircon populations described above. Except for sample CW-04B, all other samples have Palaeoproterozoic grains with $\varepsilon_{Hf(t)}$ values near +5, which indicates that the magma source areas have variable amounts of crustal and mantle components. The Mesoproterozoic zircons, on the other hand, have a clear crustal component because the majority of grains have $\varepsilon_{Hf(t)}$ values below -15. The Hf (T_{DM}) values of the Palaeoproterozoic and Mesoproterozoic grains were extracted from the mantle between the Archean (2.7 Ga) and the late Palaeoproterozoic (1.6 Ga). Most Neoproterozoic grains have Mesoproterozoic model ages and $\varepsilon_{Hf(t)}$ values that are close to zero, indicating a mantle component in the sediment source region. The few Palaeozoic zircon grains that have been analysed in these samples indicate a wide range of $\varepsilon_{Hf(T)}$ values and model ages that are comparable to those of the Neoproterozoic grains.

The only sample of the Rio do Rasto Formation (CW-11C) that was analysed is similar to those described above, except for the minor Mesoproterozoic zircon population. These grains have $\varepsilon_{Hf(t)}$ values close to zero, indicating an input of mantle component relative to those of the Rio Bonito Formation (Figs. 6a, 6b, 6c, 6d and 6e). This Mesoproterozoic zircon pattern is also observed in zircons from the Aquidauna Formation, suggesting a major change in sediment source across the Rio Bonito – Rio do Rasto transition. Zircon grains from the Botucatu Formation have negative $\varepsilon_{Hf(t)}$ values (9 to -37) and Hf (T_{DM}) model ages ranging between 3.0 e 1.0 Ga (Figs. 6g and 6h).

The Epsilon Nd versus T(Ga) plot for all samples also shows two main Nd (T_{DM}) intervals in the model ages (Fig. 7). At the base of the sequence (the Rio Bonito Formation – Guatá Group), the T_{DM} model ages range between 1.4 to 1.7 Ga and the $\varepsilon_{Nd(t)}$ values average approximately -12 (Appendix C). Above the contact with the sediments of the Palermo Formation, most T_{DM} model ages range between 1.0 and 1.2

Ga and the $\varepsilon_{Nd(t)}$ values average approximately -8, except for two samples of sandstones from the aeolian Botucatu Formation that present model ages of 1.53 and 1.75 Ga.

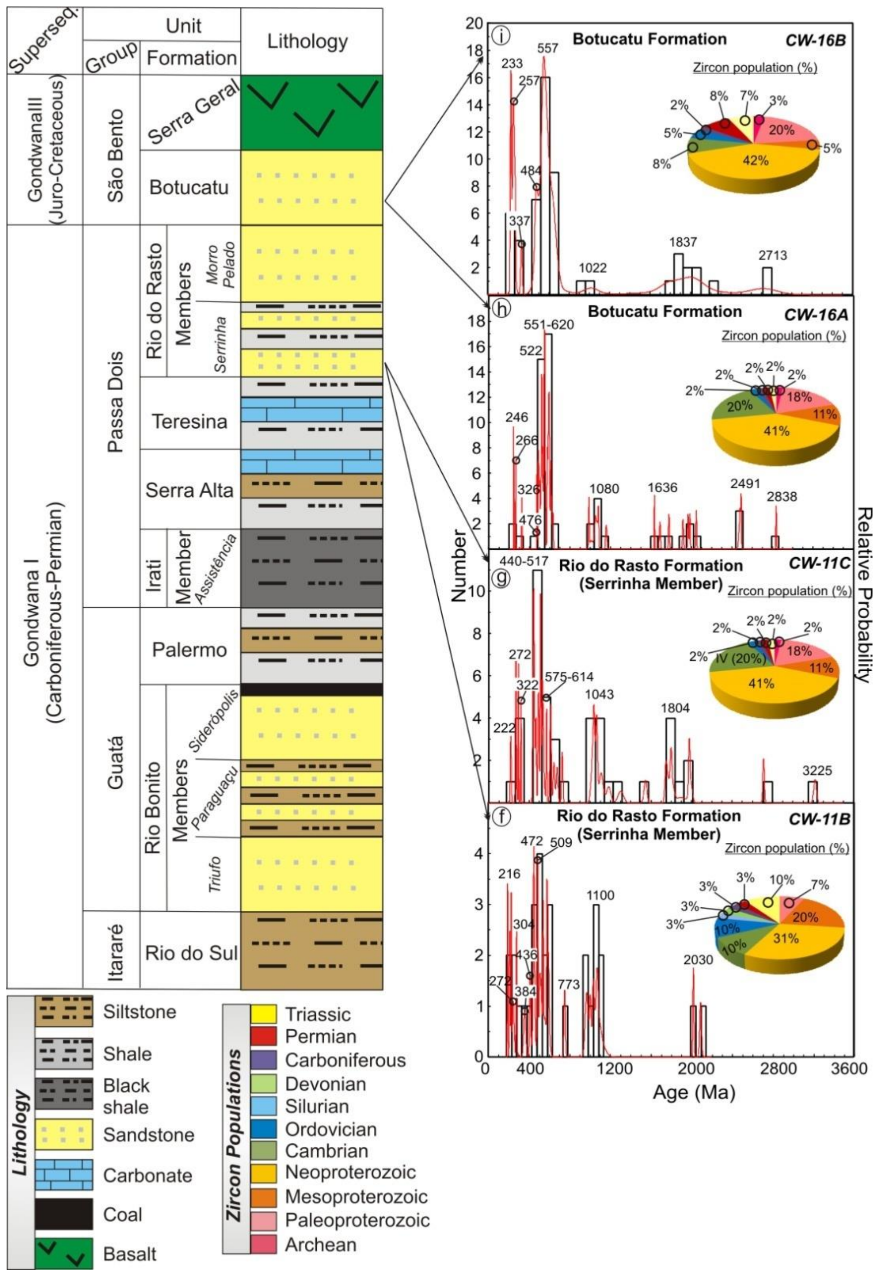

Fig. 5: Relative probability versus age diagrams showing results obtained from samples across of the Serra do Rio do Rastro (schematic stratigraphic column). The zircon populations identified in samples CW-11B, CW-11C, CW-16A and CW-16B are represented in percentage graphs.

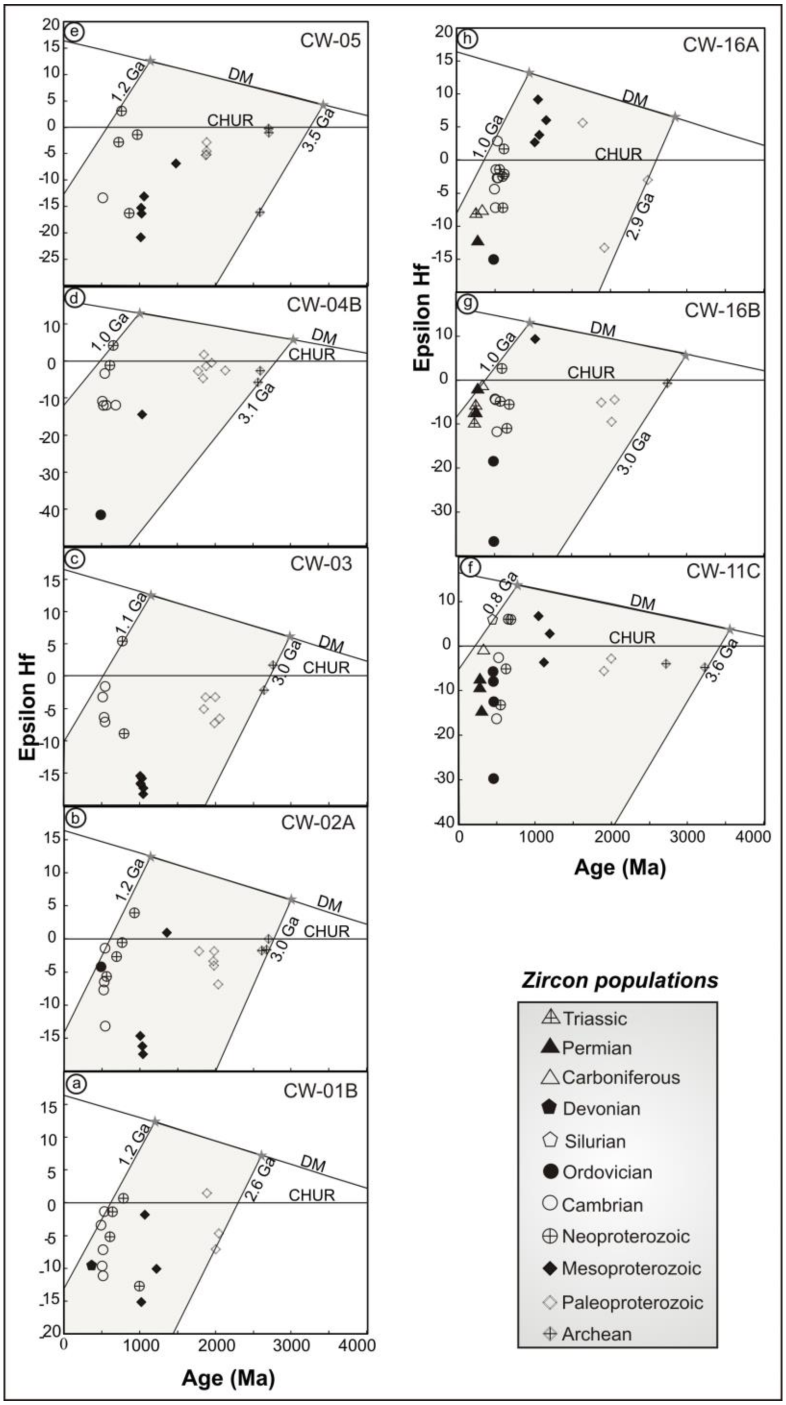

Fig. 6: Lu-Hf diagram showing ε_{Hf} composition *versus* T(Ga) for the zircons of Serra do Rio do Rastro. The diagrams a, b, c, d and e present Rio Bonito Formation results, f Rio do Rasto Formation results and g and h Botucatu Formation results.

Appendix C shows that samples of the Serrinha Member of the Passa Dois Formation present Nd concentrations of up to 200 ppm, suggesting the presence of alkaline igneous rocks in the source region of these sediments. Similar behaviour was observed in the Karoo Basin (Veevers and Saeed, 2007).

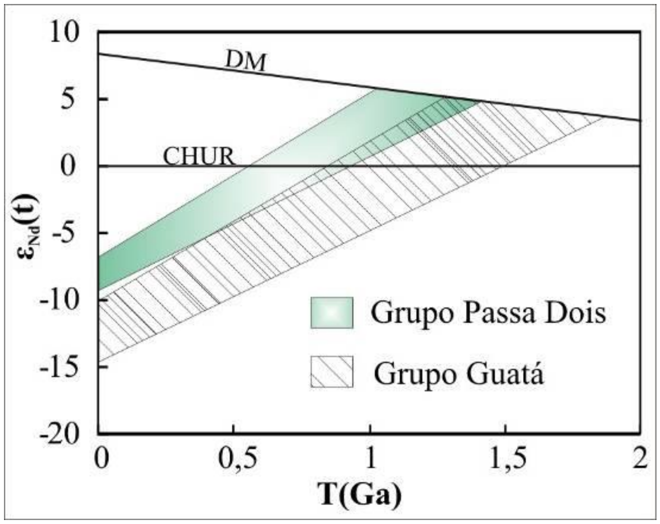

Fig. 7: Evolution $\varepsilon_{Nd(t)}$ *versus* time (T) for the samples of Guatá and Passa Dois Groups.

5. Discussion

During the Permian, western Gondwana was affected by the Terra Australi Orogen, one of the longest known accretionary systems in the Palaeozoic (Cawood, 2005). This orogen extended for more than 18.000 km and is recorded today in rocks of the western margin of South America, Africa, Antarctica, and Australia. The establishment of this orogen and its subsequent exhumation strongly affected the evolution of the sedimentary basins located on the continental side of the mountain belt, including the Paraná and Karoo basins. The geochronologic and isotope geochemical data across the Permian of the Rio do Rastro section show that this orogeny was the main driver of the changes in provenance of the Paraná Basin.

The data presented here indicate that sedimentary rocks across the Serra do Rio do Rastro record major changes in sediment provenance between the lower Permian units (Rio Bonito Fm.) and the upper Permian units (Rio do Rasto Fm.). For instance, the majority of zircons in the lower units are derived from Palaeoproterozoic terrains and, secondarily, by Neoproterozoic and Mesoproterozoic terrains. In contrast, zircons from upper Permian units are mostly Neoproterozoic and younger, with ages as young as Permo-Triassic. The exact position of this major change in sediment provenance is not clear but seems to have happened in the upper part of the Rio Bonito Formation as shown by the histogram of U-Pb ages for sample CW-05 (Fig. 4e). In addition to the differences in age intervals, the $\varepsilon_{Hf(t)}$ values of the Mesoproterozoic zircons from the lower units reveal the contribution of a strong fraction of crustal evolved rocks, which contrasts with the juvenile provenance of zircons of this same age in the upper units. Finally, the Nd isotope data also reveal a major change in provenance because the analysed samples display two distinct intervals of Nd (T_{DM}) model ages (Fig. 7). These observations raise the following points concerning the sedimentary evolution of the eastern Paraná Basin during the Permian. What are the possible source areas of these sediments? Was this change in provenance driven by climatic or tectonic processes? Are the young zircons found in upper part of the succession a record of the global explosive felsic volcanism that affected the global Permian climate?

One of the main characteristics of the Rio Bonito sediments is the presence of Palaeoproterozoic zircons in all the analysed samples. Based on histograms of fig. 4, these zircons have two main age intervals (Figs. 4a, 4b, 4c, 4d and 4e): 1988-1866 Ma is the main population and is present in all samples (CW-01B, CW-02A, CW-03, CW-04B and CW-05) and 2054-2019 Ma is present in samples CW-01B and CW-02A.

Possible source area for the populations of Palaeoproterozoic zircons may include regions located northeast of the Serra do Rio do Rastro, e.g. the Port Nolloth Zone, east of the Gariep Belt, in which rocks feature ages of 2.0-1.8 Ga (Basei et al., 2005). Zircons ranging in age from 2054-2019 Ma can also be found in the Florianópolis and Camboriú region, which is less than a 100 km to the northeast but was likely not exposed in the Permian. This area presents three main zircon populations that are associated with the Águas Mornas complex (2018 Ma), the Camboriú complex amphibolite xenolith (2016 Ma) and the Camboriú complex orthogneiss (2000 Ma) (da Silva et al., 2000). Palaeoproterozoic zircons with U-Pb ages of 2.07 Ga, which could account for the older zircon grains found in the Palaeoproterozoic interval, have been reported in granitic rocks of the Rio de La Plata Craton (Hartmann et al., 2000), Uruguay, which is located to the southeast to the Serra do Rio do Rastro. Based on the age range of our samples and the available zircon ages of Palaeoproterozoic terrains in the Serra do Rio do Rastro surroundings, we argue that most sediments of the Rio Bonito Formation were derived from northern or northeastern Gondwana.

Mesoproterozoic zircon grains with ages varying between 1031 and 1016 Ma are present in samples CW-02A, CW-03, CW-04B and CW-05. Zircons with this age interval have been reported in sedimentary rocks from different regions, such as in sandstone and arkose samples from the West Congolian Group (Frimmel et al., 2006), in quartzites and siliciclastic phyllites from the Gariep Belt (Basei et al., 2005), in a paragneiss from the Ribeira Belt (Schmitt et al., 2004) and in quartzites from the Neoproterozoic Vazantes Group in Brazil (Rodrigues et al., 2012). The primary source area of these zircons has not been clearly identified (Neves et al., 2014) because extension associations of granitic rocks of these age are restricted to batholiths from the Mayo Kebi domain, Cameroon, and from the Alto Pajeú domain, NE Brazil (De Wit et al., 2008). Less extensive occurrences of granitic rocks of these ages crop out in Eastern Namaqualand and Lesotho and are believed to be related to granulitization of pre-existing Archean and Palaeoproterozoic lower crust (Eglington et al., 2003; Schmitz and Bowring, 2004). The origin of these zircons are probably related to a “hidden” Grenvillian-age area located west of the Congo Craton (Frimmel et al., 2011) or to an African source without specifying its source region (Anon, 2008). We argue that the source of these zircons, which have a strong crustal component as revealed by the $\varepsilon_{Hf(t)}$ values, are also derived from the north of the Serra do Rio do Rastro and likely includes both Brazilian and Africa terrains.

The origin of the Neoproterozoic zircons is more difficult to constrain because the main assembly of Gondwana took place during the Brazilian. Available data indicate that this assembly had four main pulses that cover all intervals of the Neoproterozoic zircon ages observed in the lower Permian rocks: i) ca. 800-740 Ma; ii) ca. 660-610; iii) 590-560 Ma; and 520-500 Ma (Neves et al., 2014). Hence, these Neoproterozoic zircon grains are not good indicators of sediment provenance areas.

In addition to detrital zircon U-Pb ages, provenance studies can be strongly supported by palaeocurrent data. Unfortunately, only limited palaeocurrent data are available for the Rio Bonito Formation sediments. In general, most of these studies were conducted on the Tatuí Formation, which crops out to the north of the Serra do Rio do Rastro and has been correlated to the Rio Bonito and Palermo Formations. These studies identify primarily southward- and southwestward-directed sedimentary flow (Assine et al., 2003). Fulfaro et al. (1984) suggest that, in the early Permian, the sedimentary flow was northeastwards following the end of the glaciation and later shifted to the south-southeast after the establishment of the Permian gulf in the area. Based on palaeocurrent measurements of the Tatuí Formation in the Rio Claro region, approximately 500 km to the north, Assine et al. (2003) concluded that the main flow was directed to the south and that the palaeobeach line had an E-W orientation. In spite of the limited available palaeocurrent data, the main sedimentary flow during the lower Permian was southwards. This interpretation is further reinforced by the Permian palaeogeographic map of the Artinskian (Ziegler, 1997), which shows that most of the elevated areas during that time were located to the north and northeast of the Serra do Rio do Rastro area.

The geochronology and isotope geochemistry across the Serra do Rio do Rastro reveals a major change in sediment provenance in the transition between the Guatá and Passa Dois Groups. The two major differences are the decrease in Mesoproterozoic and Palaeoproterozoic zircon grains towards the top of the succession and the appearance of a large population of Palaeozoic zircons. Stratigraphic studies indicate that the highest flooding surface across the Permian of the Paraná basin is placed in Palermo Formation and that the upper Permian (Passa Dois Group) constitutes a regressive sequence (Milani, França and Schneider, 1994a; Milani et al., 1998). The mechanisms responsible for the swallowing of the basin and fluctuations in its subsidence have been related to tectonic events (Schneider and Castro 1975, Milani 1997). The latter author compared the depositional evolution of the basin with the geotectonic evolution of southwestern Gondwana and showed a strong correlation between the tectonic activity and subsidence rates during the lower Permian (Milani 1997). The tectonic activity was related to the Sanrafaélica Orogeny (270-250 Ma), which affected the southwestern and southern portions of Gondwana (Milani 1997; Turner, 1999; López-Gamundí, 2006b; Fanning et al., 2011). We argue that the appearance of young zircon grains is related to the tectonic inversion of the basin induced by the Terra Australi Orogen, which affected the eastern margin of the Paraná Basin. Similar conclusion was reached for the Sierra de Ventania System in the southern Rio de la Plata Craton, where (Ramos et al., 2014) reported a change in sedimentary provenance induced by the tectonic evolution of the western sector of the Gondwanides mountain belt.

The decrease in Palaeoproterozoic zircons and the appearance of Palaeozoic zircons in the upper Permian of the Rio do Rasto succession is related to the rise of the orogen in southern and southwestern Gondwana. Palaeogeographic maps from that time interval reveal higher elevations along the Gondwana border, which significantly modified the sedimentary source and transport across the whole region (Ziegler, 1997). Previous studies have already noted the effects of this orogeny on the southwestern Gondwana palaeogeography (Ramos et al., 2014).

In addition to the decrease in the number of Palaeoproterozoic and Mesoproterozoic zircons across the lower Permian (Rio Bonito Fm.) – upper Permian (Passa Dois Fm.) transition, the isotope record shows a significant change in the nature of the Mesoproterozoic grains. Based on Lu-Hf isotopes, the Mesoproterozoic zircons of the Rio Bonito Fm. exhibit a strong crustal component, whereas those of the Passa Dois Fm. exhibit a juvenile component. A possible source of these juvenile zircons can be found in the allochthonous terrains located in western Gondwana, such as Arequipa, Pampia and Patagônia (Casquet et al., 2008, 2010, 2012; Ramos et al, 2010). Juvenile Mesoproterozoic crust has been described in all these segments, which would account for the source of these zircons. The available U-Pb geochronologic and Lu-Hf geochemical data show that detrital zircons in metasediments from the Arequipa, Peru, and Maz Domains in Argentina range in age between 1.0 and 1.5 Ga and have zircon populations similar to those found in this study (Ramos, 2010).

Based on structural heights and zones with higher subsidence rates, Almeida (1980) was the first to suggest that the evolution of the Paraná basin was controlled by its basement tectonics. Later, two main hypotheses evolved concerning the evolution of this basin. One argues in favour of a rigid intracratonic basin, and the other argues in favour of a basin affected by compressive events related to the continental margin (Milani, 1997; Milani e Ramos, 1998). The Paraná is not considered a classical foreland basin and its subsidence mechanism remains poorly understood (De Wit, 2008). Nevertheless, the coincidence between the subsidence and tectonic records strongly favours the second interpretation and also argues in favour of a common origin for the Karoo basin.

6. Conclusions

Zircon U-Pb data of the lower to middle part of the Permian (Rio Bonito Formation - Grupo Guatá Group) indicate a dominance of Palaeoproterozoic (2.5 to 1.7 Ga) grains, followed by Mesoproterozoic (1.5 to 1.0 Ga) and Neoproterozoic (992 to 490 Ma) grains. In contrast, sediments from the Rio Rastro Formation (Passa Dois Group) present a dominance of Neoproterozoic (935 to 543 Ma) grains, followed by Palaeozoic, including Permo-Triassic (297-216 Ma), grains. The Hf (T_{DM}) model ages indicate a Palaeoproterozoic age for zircons at the base of the succession and Meso- to Neoproterozoic ages for zircons in the upper portion of the succession. The Sm-Nd data reinforce the results of the other isotope systems, indicating a major change in sedimentary provenance between the lower and upper portions of the profile. This shift in sediment provenance was related to the Gondwanides mountain belt and was also affected the subsidence rate of the Paraná basin (Milani, 1997). The data further suggest that, in the mid-Permian, the Paraná basin evolved from a cratonic to a foreland-like environment due to the orogeny along the southern and southwestern margins of Gondwana.

Appendix A: Summary U-Pb detrital zircon results for samples of Serra do Rio do Rastro by LA-MC-ICP-MS

Sample/grain	7/6 ratio	1σ(%)	7/5 ratio	1σ(%)	6/8 ratio	1σ(%)	rho	7/6 age	1σ(Ma)	7/5 age	1σ(Ma)	6/8 age	1σ(Ma)	Conc (%)
CW-01B: Rio Bonito Formation (Triunfo Member)														
Z26	0.0534	0.66	0.4240	0.96	0.0576	0.71	0.69	346	15	359	3	361	2	104
Z29	0.0580	0.44	0.6246	0.77	0.0781	0.63	0.78	530	10	493	3	485	3	91
Z21	0.0582	0.67	0.6340	1.16	0.0791	0.95	0.80	536	15	499	5	490	4	92
Z49	0.0593	0.69	0.6548	1.04	0.0801	0.78	0.72	578	15	511	4	497	4	86
Z25	0.0578	0.66	0.6413	1.16	0.0805	0.95	0.81	521	14	503	5	499	5	96
Z46	0.0585	0.90	0.6572	1.15	0.0815	0.72	0.80	548	20	513	5	505	3	92
Z42	0.0584	0.66	0.6574	1.00	0.0816	0.75	0.88	545	14	513	4	506	4	93
Z48	0.0581	0.55	0.6616	0.92	0.0825	0.73	0.77	535	12	516	4	511	4	96
Z41	0.0580	0.56	0.6600	0.98	0.0826	0.81	0.80	528	12	515	4	512	4	97
Z28	0.0584	0.47	0.6883	0.71	0.0855	0.53	0.68	544	10	532	3	529	3	97
Z34	0.0597	0.62	0.7324	0.89	0.0890	0.64	0.84	591	14	558	4	550	3	93
Z19	0.0611	1.12	0.7748	1.31	0.0920	0.67	0.71	643	24	583	6	567	4	88
Z53	0.0628	0.77	0.8460	1.42	0.0978	1.19	0.83	700	16	622	7	601	7	86
Z08	0.0599	0.43	0.8104	0.90	0.0981	0.79	0.86	601	9	603	4	603	5	100
Z24	0.0610	0.39	0.8729	0.72	0.1037	0.60	0.80	641	8	637	3	636	4	99
Z30	0.0647	1.16	0.9583	1.84	0.1075	1.43	0.77	764	25	682	9	658	9	86
Z18	0.0651	0.28	1.1558	0.64	0.1287	0.57	0.87	779	6	780	3	780	4	100
Z37	0.0674	0.58	1.2327	1.14	0.1327	0.98	0.85	850	12	816	6	803	7	95
Z58	0.0722	0.86	1.5685	1.17	0.1575	0.80	0.85	992	17	958	7	943	7	95
Z39	0.0755	0.46	1.6908	0.98	0.1624	0.87	0.87	1082	9	1005	6	970	8	90
Z50	0.0743	0.43	1.6748	0.67	0.1636	0.51	0.83	1048	9	999	4	977	5	93
Z03	0.0724	1.05	1.6605	1.28	0.1664	0.74	0.77	997	21	994	8	992	7	99
Z17	0.0748	0.51	1.8023	0.79	0.1748	0.60	0.71	1063	10	1046	5	1038	6	98
Z07	0.0731	1.22	1.7707	1.48	0.1757	0.84	0.77	1017	25	1035	10	1043	8	103
Z36	0.0799	1.03	2.0672	1.65	0.1876	1.29	0.77	1195	20	1138	11	1108	13	93
Z13	0.0891	0.36	2.5109	0.67	0.2044	0.56	0.79	1406	7	1275	5	1199	6	85
Z06	0.0808	0.36	2.2946	0.72	0.2059	0.62	0.83	1218	7	1211	5	1207	7	99
Z14	0.1029	0.29	3.6968	0.58	0.2606	0.50	0.80	1677	5	1571	5	1493	7	89
Z11	0.1155	0.56	4.3119	0.81	0.2707	0.59	0.83	1888	10	1696	7	1544	8	82
Z16	0.1156	0.39	4.5663	0.65	0.2866	0.52	0.73	1889	7	1743	5	1625	8	86
Z20	0.1139	0.60	4.6420	1.26	0.2956	1.10	0.87	1862	11	1757	10	1669	16	90
Z54	0.1122	0.38	4.6317	0.76	0.2993	0.65	0.90	1836	7	1755	6	1688	10	92
Z23	0.1151	0.34	4.7566	0.75	0.2997	0.67	0.92	1881	6	1777	6	1690	10	90
Z12	0.1138	0.24	4.9713	0.60	0.3169	0.55	0.88	1861	4	1814	5	1775	9	95
Z44	0.1238	0.30	5.5566	0.66	0.3254	0.59	0.86	2012	5	1909	6	1816	9	90
Z35	0.1243	0.28	5.7071	0.58	0.3329	0.51	0.82	2019	5	1932	5	1853	8	92
Z40	0.1280	0.32	5.9491	0.77	0.3370	0.70	0.89	2071	6	1968	7	1872	11	90
Z02	0.1152	0.28	5.3944	0.61	0.3395	0.55	0.85	1884	5	1884	5	1884	9	100
Z47	0.1250	0.39	5.9478	0.85	0.3450	0.76	0.87	2029	7	1968	7	1911	13	94
Z61	0.1230	0.38	6.0374	0.68	0.3560	0.57	0.78	2000	7	1981	6	1963	10	98
Z01	0.1259	0.30	6.3614	0.69	0.3666	0.63	0.87	2041	5	2027	6	2013	11	99
CW-02A: Rio Bonito Formation (Paraguaçu Member)														
Z27	0.0574	1.50	0.6149	1.78	0.0776	0.96	0.76	509	33	487	7	482	4	95
Z50	0.0563	2.29	0.6380	2.70	0.0823	1.42	0.77	462	51	501	11	510	7	110
Z35	0.0580	1.21	0.6671	1.88	0.0835	1.44	0.76	528	26	519	8	517	7	98

Appendix A (*Continued*)

Sample/grain	7/6 ratio	1σ(%)	7/5 ratio	1σ(%)	6/8 ratio	1σ(%)	rho	7/6 age	1σ(Ma)	7/5 age	1σ(Ma)	6/8 age	1σ(Ma)	Conc (%)
CW-02A: Rio Bonito Formation (Paraguaçu Member)														
Z27	0.0574	1.50	0.6149	1.78	0.0776	0.96	0.76	509	33	487	7	482	4	95
Z50	0.0563	2.29	0.6380	2.70	0.0823	1.42	0.77	462	51	501	11	510	7	110
Z35	0.0580	1.21	0.6671	1.88	0.0835	1.44	0.76	528	26	519	8	517	7	98
Z15	0.0576	1.36	0.6727	1.76	0.0847	1.11	0.83	515	30	522	7	524	6	102
Z19	0.0591	1.12	0.7044	1.33	0.0865	0.71	0.74	570	24	541	6	535	4	94
Z36	0.0612	0.91	0.7337	1.61	0.0869	1.31	0.81	648	20	559	7	537	7	83
Z9	0.0593	0.57	0.7353	1.01	0.0899	0.83	0.81	578	12	560	4	555	4	96
Z7	0.0613	1.47	0.7955	1.72	0.0940	0.91	0.75	651	31	594	8	579	5	89
Z24	0.0631	1.03	0.9790	1.91	0.1125	1.61	0.84	712	22	693	10	687	10	97
Z55	0.0675	0.50	1.1405	0.90	0.1225	0.75	0.80	854	10	773	5	745	5	87
Z8	0.0638	0.80	1.1015	1.28	0.1252	1.00	0.76	736	17	754	7	760	7	103
Z37	0.0642	1.85	1.1836	2.46	0.1336	1.63	0.65	750	39	793	14	809	12	108
Z57	0.0699	0.74	1.2947	1.18	0.1344	0.93	0.76	925	15	843	7	813	7	88
Z44	0.0727	0.32	1.5074	0.64	0.1503	0.55	0.82	1006	7	933	4	903	5	90
Z5	0.0740	0.49	1.5631	1.03	0.1533	0.90	0.87	1040	10	956	6	919	8	88
Z12	0.0720	0.47	1.5304	0.97	0.1541	0.85	0.86	986	10	943	6	924	7	94
Z45	0.0731	0.66	1.6335	0.99	0.1620	0.74	0.72	1018	13	983	6	968	7	95
Z38	0.0748	2.98	1.6749	3.75	0.1624	2.27	0.83	1064	60	999	24	970	20	91
Z52	0.0725	0.65	1.6374	1.21	0.1638	1.02	0.83	1001	13	985	8	978	9	98
Z49	0.0735	0.49	1.7204	0.80	0.1697	0.63	0.74	1029	10	1016	5	1010	6	98
Z21	0.0738	0.43	1.7942	0.91	0.1763	0.80	0.86	1037	9	1043	6	1046	8	101
Z1	0.0760	0.54	1.8605	0.90	0.1775	0.71	0.76	1095	11	1067	6	1053	7	96
Z41	0.0731	0.34	1.7910	0.68	0.1777	0.59	0.83	1016	7	1042	4	1054	6	104
Z40	0.0893	0.47	2.3517	1.21	0.1909	1.11	0.91	1412	9	1228	9	1126	12	80
Z22	0.0937	0.59	2.9073	1.06	0.2250	0.88	0.81	1503	11	1384	8	1308	10	87
Z17	0.0866	0.42	2.7779	0.83	0.2325	0.71	0.84	1353	8	1350	6	1348	9	100
Z28	0.1209	0.43	4.7459	1.32	0.2846	1.25	0.94	1970	8	1775	11	1614	18	82
Z54	0.1088	0.82	4.7309	1.14	0.3155	0.80	0.85	1779	15	1773	10	1768	12	99
Z42	0.1133	0.92	4.9944	1.27	0.3197	0.88	0.86	1853	17	1818	11	1788	14	96
Z58	0.1152	0.56	5.0888	0.80	0.3204	0.57	0.82	1883	10	1834	7	1792	9	95
Z18	0.1250	0.44	5.5316	0.98	0.3209	0.88	0.88	2029	8	1906	8	1794	14	88
Z59	0.1213	0.41	5.3985	1.14	0.3228	1.06	0.93	1975	7	1885	10	1803	17	91
Z29	0.1148	0.33	5.1122	0.69	0.3230	0.60	0.85	1877	6	1838	6	1804	10	96
Z60	0.1210	0.43	5.4377	1.02	0.3258	0.93	0.90	1972	8	1891	9	1818	15	92
Z2	0.1216	0.38	5.5297	0.71	0.3299	0.60	0.80	1979	7	1905	6	1838	10	93
Z56	0.1231	0.34	5.6707	0.71	0.3340	0.62	0.84	2002	6	1927	6	1858	10	93
Z13	0.1264	0.45	5.9378	1.15	0.3406	1.06	0.92	2049	8	1967	10	1890	17	92
Z32	0.1225	0.41	5.7910	0.92	0.3429	0.83	0.88	1993	7	1945	8	1901	14	95
Z6	0.1268	0.39	6.0193	0.94	0.3442	0.86	0.90	2054	7	1979	8	1907	14	93
Z53	0.1221	0.52	5.9156	1.00	0.3513	0.85	0.84	1988	9	1964	9	1941	14	98
Z16	0.1213	0.40	5.8779	0.87	0.3514	0.77	0.87	1976	7	1958	8	1941	13	98
Z11	0.1215	0.77	5.9114	0.95	0.3529	0.57	0.75	1978	14	1963	8	1949	10	99
Z26	0.1139	0.68	5.5813	1.24	0.3553	1.03	0.82	1863	12	1913	11	1960	17	105
Z34	0.1253	0.68	6.1939	0.91	0.3586	0.61	0.82	2032	12	2004	8	1976	10	97
Z43	0.1208	0.68	6.0284	1.24	0.3620	1.04	0.83	1968	12	1980	11	1992	18	101

Appendix A (*Continued*)

Sample/grain	7/6 ratio	1σ(%)	7/5 ratio	1σ(%)	6/8 ratio	1σ(%)	rho	7/6 age	1σ(Ma)	7/5 age	1σ(Ma)	6/8 age	1σ(Ma)	Conc (%)
Z48	0.1269	0.32	6.3718	0.66	0.3643	0.57	0.83	2055	6	2028	6	2003	10	97
Z20	0.1295	0.43	6.5128	0.73	0.3647	0.59	0.76	2091	8	2048	6	2004	10	96
Z31	0.1269	0.37	6.4036	0.69	0.3659	0.58	0.80	2056	7	2033	6	2010	10	98
Z30	0.1252	0.35	6.3247	0.80	0.3664	0.72	0.88	2032	6	2022	7	2012	12	99
Z61	0.1243	1.02	6.5230	1.52	0.3806	1.12	0.72	2019	18	2049	13	2079	20	103
Z3	0.1820	0.49	12.2768	0.78	0.4891	0.61	0.87	2672	8	2626	7	2567	13	96
Z33	0.1754	0.61	11.9470	1.20	0.4941	1.04	0.85	2610	10	2600	11	2588	22	99
Z23	0.1850	0.88	12.7500	1.13	0.4997	0.71	0.80	2699	15	2661	11	2613	15	97
CW-03: Rio Bonito Formation (Paraguaçu Member)														
Z28	0.0603	0.46	0.6827	0.87	0.0821	0.74	0.83	616	10	528	4	508	4	83
Z2	0.0579	0.52	0.6802	0.89	0.0852	0.72	0.78	526	11	527	4	527	4	100
Z39	0.0582	0.52	0.7006	1.01	0.0873	0.87	0.84	538	11	539	4	539	5	100
Z44	0.0580	0.37	0.7003	0.89	0.0875	0.81	0.90	531	8	539	4	541	4	102
Z40	0.0579	0.45	0.7018	1.05	0.0879	0.95	0.89	525	10	540	4	543	5	103
Z54	0.0643	1.42	1.0366	1.80	0.1169	1.11	0.81	752	30	722	9	713	7	95
Z18	0.0651	0.53	1.0643	0.93	0.1185	0.77	0.80	778	11	736	5	722	5	93
Z35	0.0651	0.34	1.1352	0.75	0.1265	0.67	0.87	778	7	770	4	768	5	99
Z27	0.0662	0.71	1.1894	1.07	0.1304	0.79	0.87	812	15	796	6	790	6	97
Z41	0.0680	1.04	1.3914	1.32	0.1483	0.82	0.59	870	22	885	8	892	7	103
Z9	0.0728	0.73	1.6440	1.28	0.1638	1.05	0.81	1008	15	987	8	978	10	97
Z12	0.0741	0.49	1.7424	0.79	0.1704	0.63	0.74	1045	10	1024	5	1014	6	97
Z14	0.0761	0.51	1.7945	0.93	0.1711	0.78	0.81	1097	10	1043	6	1018	7	93
Z24	0.0726	0.58	1.7300	0.90	0.1727	0.69	0.73	1004	12	1020	6	1027	7	102
Z33	0.0735	0.27	1.7559	0.68	0.1734	0.62	0.90	1027	5	1029	4	1031	6	100
Z26	0.0729	0.38	1.7560	0.98	0.1746	0.90	0.92	1012	8	1029	6	1038	9	103
Z60	0.0740	0.37	1.7892	0.82	0.1753	0.73	0.87	1042	7	1042	5	1041	7	100
Z46	0.0742	0.72	1.8589	0.97	0.1816	0.65	0.79	1048	14	1067	6	1076	6	103
Z53	0.0734	0.72	1.8931	1.31	0.1870	1.09	0.82	1025	15	1079	9	1105	11	108
Z34	0.0733	0.73	1.8892	1.13	0.1871	0.86	0.89	1021	15	1077	8	1105	9	108
Z29	0.1181	0.38	4.5183	1.21	0.2775	1.14	0.95	1927	7	1734	10	1579	16	82
Z8	0.1157	0.57	4.7243	1.10	0.2960	0.93	0.84	1891	10	1772	9	1672	14	88
Z56	0.1210	0.43	4.9392	1.65	0.2962	1.57	0.96	1970	8	1809	14	1672	23	85
Z51	0.1134	0.54	5.0340	1.12	0.3220	0.98	0.87	1854	10	1825	9	1800	15	97
Z47	0.1302	0.54	5.7952	1.16	0.3228	1.03	0.88	2101	9	1946	10	1804	16	86
Z22	0.1147	0.43	5.1508	0.76	0.3257	0.62	0.78	1875	8	1845	6	1817	10	97
Z45	0.1142	0.43	5.1350	0.90	0.3261	0.79	0.86	1867	8	1842	8	1820	13	97
Z20	0.1153	0.28	5.2000	0.71	0.3272	0.65	0.90	1884	5	1853	6	1825	10	97
Z52	0.1141	0.49	5.1703	1.03	0.3286	0.90	0.86	1866	9	1848	9	1832	14	98
Z38	0.1127	0.88	5.1574	1.45	0.3320	1.15	0.78	1843	16	1846	12	1848	19	100
Z58	0.1239	0.69	5.7178	1.02	0.3346	0.75	0.86	2013	12	1934	9	1861	12	92
Z6	0.1105	0.54	5.1677	1.00	0.3393	0.85	0.83	1807	10	1847	9	1883	14	104
Z21	0.1141	0.26	5.3992	0.66	0.3432	0.60	0.90	1866	5	1885	6	1902	10	102
Z59	0.1224	0.52	5.8028	0.97	0.3438	0.82	0.83	1992	9	1947	8	1905	14	96
Z5	0.1164	0.46	5.8287	0.77	0.3633	0.62	0.76	1901	8	1951	7	1998	11	105
Z25	0.1219	0.38	6.1230	0.80	0.3643	0.71	0.86	1984	7	1994	7	2003	12	101
Z31	0.1226	0.46	6.1755	0.91	0.3654	0.78	0.84	1994	8	2001	8	2008	14	101

Appendix A (*Continued*)

Sample/grain	7/6 ratio	1σ(%)	7/5 ratio	1σ(%)	6/8 ratio	1σ(%)	rho	7/6 age	1σ(Ma)	7/5 age	1σ(Ma)	6/8 age	1σ(Ma)	Conc (%)
Z50	0.1217	0.77	6.1894	1.00	0.3687	0.64	0.78	1982	14	2003	9	2023	11	102
Z7	0.1219	1.23	6.3536	1.50	0.3780	0.86	0.77	1984	22	2026	13	2067	15	104
Z36	0.1267	0.30	6.6333	0.73	0.3798	0.66	0.89	2052	5	2064	6	2075	12	101
Z37	0.1264	0.32	6.6794	0.86	0.3832	0.79	0.92	2049	6	2070	8	2091	14	102
Z57	0.1916	0.54	13.2263	0.79	0.5005	0.57	0.66	2756	9	2696	7	2616	12	95
Z49	0.1784	0.38	12.3370	0.82	0.5015	0.73	0.87	2638	6	2630	8	2620	16	99
CW-04B: Rio Bonito Formation (Siderópolis Member)														
Z59	0.0571	0.58	0.6142	1.11	0.0780	0.94	0.84	495	13	486	4	484	4	98
Z55	0.0578	0.63	0.6506	1.04	0.0817	0.82	0.77	521	14	509	4	506	4	97
Z58	0.0580	1.45	0.6703	1.72	0.0839	0.94	0.74	529	32	521	7	519	5	98
Z40	0.0580	0.53	0.6953	0.97	0.0869	0.81	0.82	530	12	536	4	537	4	101
Z28	0.0619	0.65	0.7661	2.23	0.0898	2.13	0.96	669	14	578	10	554	11	83
Z17	0.0603	0.65	0.8182	1.08	0.0985	0.86	0.78	613	14	607	5	605	5	99
Z02	0.0644	1.05	0.9418	1.47	0.1061	1.03	0.68	755	22	674	7	650	6	86
Z19	0.0736	0.94	1.8079	1.28	0.1781	0.88	0.80	1032	19	1048	8	1056	9	102
Z45	0.1087	0.54	3.9161	1.06	0.2613	0.92	0.85	1778	10	1617	9	1497	12	84
Z06	0.1182	0.49	4.4159	1.39	0.2710	1.30	0.93	1929	9	1715	11	1546	18	80
Z13	0.1075	0.47	4.2363	0.91	0.2857	0.78	0.84	1758	9	1681	7	1620	11	92
Z54	0.1193	0.67	4.8146	1.19	0.2927	0.98	0.88	1946	12	1787	10	1655	14	85
Z26	0.1267	0.56	5.1259	1.98	0.2934	1.90	0.96	2053	10	1840	17	1659	28	81
Z41	0.1127	0.85	4.6299	1.39	0.2980	1.10	0.78	1843	15	1755	12	1681	16	91
Z18	0.1083	0.55	4.6719	0.82	0.3130	0.61	0.70	1770	10	1762	7	1755	9	99
Z35	0.1220	0.45	5.3022	1.47	0.3153	1.40	0.95	1985	8	1869	13	1766	22	89
Z07	0.1148	0.89	5.0555	1.21	0.3194	0.82	0.78	1877	16	1829	10	1787	13	95
Z15	0.1221	0.69	5.3923	1.29	0.3203	1.09	0.88	1987	12	1884	11	1791	17	90
Z56	0.1180	0.51	5.2342	1.07	0.3217	0.95	0.87	1926	9	1858	9	1798	15	93
Z12	0.1130	0.47	5.1468	0.82	0.3302	0.67	0.78	1849	9	1844	7	1839	11	99
Z21	0.1123	0.52	5.1200	1.51	0.3306	1.42	0.94	1837	9	1839	13	1841	23	100
Z20	0.1149	0.60	5.3570	0.88	0.3382	0.65	0.69	1878	11	1878	8	1878	11	100
Z49	0.1245	0.44	5.9813	0.90	0.3485	0.78	0.85	2021	8	1973	8	1927	13	95
Z08	0.1215	0.64	5.8436	1.09	0.3488	0.89	0.79	1979	11	1953	9	1929	15	97
Z57	0.1229	0.50	5.9256	0.91	0.3496	0.76	0.81	1999	9	1965	8	1933	13	97
Z61	0.1359	0.52	6.5613	1.28	0.3501	1.16	0.91	2176	9	2054	11	1935	19	89
Z11	0.1197	0.64	5.8479	1.00	0.3542	0.77	0.82	1952	11	1954	9	1955	13	100
Z38	0.1287	0.60	6.5972	1.07	0.3718	0.88	0.87	2080	11	2059	9	2038	15	98
Z30	0.1738	0.53	9.0682	1.09	0.3785	0.95	0.86	2594	9	2345	10	2069	17	80
Z39	0.1325	0.64	7.3701	0.93	0.4035	0.68	0.69	2131	11	2157	8	2185	13	103
Z51	0.1707	0.47	10.6133	0.85	0.4509	0.71	0.80	2565	8	2490	8	2399	14	94
CW-05: Rio Bonito Formation (Siderópolis Member)														
Z9	0.0578	0.39	0.6586	0.81	0.0826	0.71	0.85	524	9	514	3	512	4	98
Z55	0.0604	0.44	0.7935	0.72	0.0952	0.57	0.74	619	9	593	3	587	3	95
Z06	0.0595	0.46	0.8098	0.91	0.0987	0.79	0.84	585	10	602	4	607	5	104
Z35	0.0634	0.44	1.0336	0.77	0.1183	0.63	0.78	721	9	721	4	721	4	100
Z23	0.0645	0.99	1.1106	1.36	0.1249	0.93	0.85	758	21	758	7	759	7	100
Z61	0.0674	0.56	1.3251	0.93	0.1427	0.74	0.77	849	12	857	5	860	6	101
Z50	0.0733	2.35	1.4732	2.66	0.1458	1.24	0.71	1022	48	919	16	877	10	86

Appendix A (*Continued*)

Sample/grain	7/6 ratio	1σ(%)	7/5 ratio	1σ(%)	6/8 ratio	1σ(%)	rho	7/6 age	1σ(Ma)	7/5 age	1σ(Ma)	6/8 age	1σ(Ma)	Conc (%)
Z19	0.0742	0.93	1.5747	1.90	0.1539	1.65	0.96	1047	19	960	12	923	14	88
Z41	0.0716	0.37	1.5971	0.67	0.1617	0.56	0.79	975	8	969	4	966	5	99
Z42	0.0731	0.81	1.6488	1.02	0.1637	0.62	0.77	1016	16	989	6	977	6	96
Z57	0.0733	0.22	1.6748	0.65	0.1657	0.61	0.92	1023	4	999	4	988	6	97
Z47	0.0731	0.36	1.6801	0.68	0.1668	0.57	0.80	1016	7	1001	4	994	5	98
Z48	0.0729	0.37	1.6815	1.01	0.1672	0.94	0.92	1012	8	1002	6	997	9	98
Z46	0.0742	0.55	1.7442	0.86	0.1705	0.67	0.87	1046	11	1025	6	1015	6	97
Z58	0.0724	0.88	1.7106	1.28	0.1712	0.92	0.88	999	18	1013	8	1019	9	102
Z21	0.0731	0.30	1.7389	0.87	0.1725	0.82	0.93	1017	6	1023	6	1026	8	101
Z03	0.0728	0.49	1.7370	0.79	0.1732	0.62	0.88	1007	10	1022	5	1030	6	102
Z60	0.0745	0.30	1.7882	0.69	0.1740	0.62	0.87	1056	6	1041	4	1034	6	98
Z20	0.0848	0.50	2.1049	1.48	0.1801	1.38	0.94	1310	10	1150	10	1067	14	81
Z18	0.0925	0.23	3.2117	0.72	0.2519	0.68	0.93	1477	4	1460	6	1448	9	98
Z52	0.1174	0.29	4.6002	0.73	0.2842	0.67	0.90	1917	5	1749	6	1612	10	84
Z43	0.1160	0.25	4.5620	0.91	0.2851	0.87	0.96	1896	4	1742	8	1617	12	85
Z10	0.1157	0.29	4.6239	0.99	0.2899	0.94	0.95	1891	5	1754	8	1641	14	87
Z45	0.1166	0.27	4.8502	0.63	0.3016	0.57	0.87	1905	5	1794	5	1699	8	89
Z12	0.1142	0.36	4.9623	0.69	0.3151	0.59	0.82	1867	6	1813	6	1766	9	95
Z02	0.1153	0.28	5.1263	0.63	0.3224	0.56	0.86	1885	5	1840	5	1801	9	96
Z54	0.1233	0.79	5.5074	1.11	0.3240	0.78	0.86	2004	14	1902	10	1809	12	90
Z28	0.1136	0.26	5.1052	0.84	0.3259	0.80	0.95	1858	5	1837	7	1819	13	98
Z37	0.1146	0.31	5.2411	0.72	0.3318	0.65	0.88	1873	6	1859	6	1847	10	99
Z40	0.1151	0.32	5.2944	0.74	0.3336	0.67	0.88	1881	6	1868	6	1856	11	99
Z30	0.1144	0.30	5.3002	0.65	0.3360	0.58	0.85	1870	5	1869	6	1868	9	100
Z27	0.1151	0.44	5.3381	0.72	0.3363	0.58	0.87	1882	8	1875	6	1869	9	99
Z01	0.1151	0.25	5.3421	0.64	0.3365	0.59	0.90	1882	4	1876	5	1870	10	99
Z15	0.1215	0.43	5.6441	0.71	0.3369	0.57	0.87	1978	8	1923	6	1872	9	95
Z32	0.1151	0.24	5.3715	0.53	0.3385	0.47	0.83	1881	4	1880	5	1880	8	100
Z59	0.1230	0.40	5.8349	0.66	0.3441	0.52	0.72	2000	7	1952	6	1906	9	95
Z53	0.1245	0.22	5.9072	0.63	0.3441	0.59	0.92	2022	4	1962	6	1907	10	94
Z14	0.1230	0.29	5.8449	0.69	0.3446	0.63	0.88	2000	5	1953	6	1909	10	95
Z05	0.1152	0.26	5.4834	0.67	0.3452	0.61	0.90	1883	5	1898	6	1911	10	101
Z25	0.1243	0.35	5.9468	0.79	0.3470	0.70	0.88	2019	6	1968	7	1920	12	95
Z31	0.1225	0.29	5.9475	0.59	0.3522	0.51	0.81	1993	5	1968	5	1945	9	98
Z07	0.1158	0.38	5.6720	0.94	0.3552	0.86	0.95	1893	7	1927	8	1959	15	104
Z44	0.1271	0.26	6.2492	0.63	0.3565	0.57	0.88	2059	5	2011	5	1966	10	95
Z24	0.1256	0.32	6.4855	0.69	0.3744	0.61	0.86	2038	6	2044	6	2050	11	101
Z22	0.1378	0.33	7.3573	0.68	0.3872	0.60	0.84	2200	6	2156	6	2110	11	96
Z49	0.1643	0.33	8.9743	1.07	0.3960	1.01	0.95	2501	6	2335	10	2151	19	86
Z11	0.1729	0.31	11.5287	0.67	0.4837	0.59	0.92	2586	5	2567	6	2543	12	98
Z38	0.1852	0.52	13.0346	0.79	0.5104	0.59	0.82	2700	9	2682	7	2659	13	98
Z36	0.1858	0.26	13.1587	0.73	0.5137	0.68	0.92	2705	4	2691	7	2672	15	99
CW-11B: Rio do Rasto Formation (Serrinha Member)														
Z15	0.0515	2.81	0.2422	3.10	0.0341	1.31	0.66	264	63	220	6	216	3	82
Z33	0.0510	1.95	0.2636	2.55	0.0375	1.65	0.64	241	44	238	5	237	4	98
Z10	0.0491	1.88	0.2695	2.24	0.0398	1.21	0.53	155	44	242	5	251	3	163

Appendix A (*Continued*)

Sample/grain	7/6 ratio	1σ(%)	7/5 ratio	1σ(%)	6/8 ratio	1σ(%)	rho	7/6 age	1σ(Ma)	7/5 age	1σ(Ma)	6/8 age	1σ(Ma)	Conc (%)
Z26	0.0572	4.13	0.3391	5.27	0.0430	3.26	0.62	498	88	297	13	272	9	55
Z34	0.0540	2.43	0.3600	2.75	0.0483	1.29	0.71	371	55	312	7	304	4	82
Z17	0.0538	1.88	0.4553	3.36	0.0614	2.77	0.83	364	42	381	11	384	10	105
Z12	0.0564	1.23	0.5443	1.87	0.0699	1.40	0.74	470	27	441	7	436	6	93
Z29	0.0583	0.89	0.6103	1.31	0.0759	0.96	0.71	541	19	484	5	472	4	87
Z24	0.0584	2.10	0.6126	3.46	0.0761	2.75	0.79	544	46	485	13	473	13	87
Z21	0.0576	1.86	0.6070	2.45	0.0764	1.61	0.65	514	41	482	9	475	7	92
Z16	0.0590	1.22	0.6690	1.58	0.0822	0.99	0.61	568	26	520	6	509	5	90
Z18	0.0564	0.99	0.6397	1.40	0.0823	1.00	0.69	468	22	502	6	510	5	109
Z19	0.0593	2.28	0.7009	2.66	0.0858	1.36	0.75	577	49	539	11	531	7	92
Z39	0.0589	1.35	0.7166	2.02	0.0883	1.51	0.74	563	29	549	9	545	8	97
Z32	0.0599	0.47	0.7548	0.82	0.0914	0.67	0.79	599	10	571	4	564	4	94
Z09	0.0597	1.35	0.7719	2.67	0.0938	2.30	0.86	592	29	581	12	578	13	98
Z40	0.0610	0.38	0.8220	0.73	0.0977	0.63	0.82	640	8	609	3	601	4	94
Z38	0.0599	3.10	0.8240	3.33	0.0998	1.21	0.60	599	66	610	15	613	7	102
Z11	0.0613	4.44	0.8460	5.00	0.1001	2.29	0.71	649	93	622	23	615	13	95
Z25	0.0677	0.58	1.1892	1.15	0.1275	0.99	0.85	858	12	796	6	774	7	90
Z41	0.0721	0.78	1.4507	1.38	0.1460	1.13	0.81	988	16	910	8	878	9	89
Z07	0.0751	0.73	1.6078	0.87	0.1552	0.47	0.67	1072	15	973	5	930	4	87
Z01	0.0774	1.97	1.6929	2.34	0.1586	1.26	0.53	1132	39	1006	15	949	11	84
Z02	0.0759	0.45	1.6643	1.08	0.1591	0.98	0.90	1092	9	995	7	952	9	87
Z23	0.0721	0.70	1.6053	0.88	0.1614	0.53	0.72	989	14	972	6	965	5	97
Z04	0.0744	0.39	1.6621	0.75	0.1620	0.65	0.82	1052	8	994	5	968	6	92
Z20	0.0734	0.42	1.7600	0.80	0.1740	0.69	0.83	1024	8	1031	5	1034	7	101
Z37	0.0766	1.04	1.8807	1.30	0.1782	0.78	0.57	1110	21	1074	9	1057	8	95
Z36	0.1251	0.31	6.0722	0.67	0.3520	0.59	0.86	2030	5	1986	6	1944	10	96
Z27	0.1302	0.51	6.5263	0.78	0.3636	0.59	0.85	2100	9	2049	7	1999	10	95
CW-11C: Rio do Rasto Formation (Serrinha Member)														
Z58	0.0529	0.68	0.2560	2.31	0.0351	2.21	0.96	326	15	231	5	222	5	68
Z18	0.0499	1.16	0.2964	1.73	0.0431	1.29	0.73	188	27	264	4	272	3	145
Z11	0.0499	5.64	0.2983	6.11	0.0434	2.34	0.63	189	126	265	14	274	6	145
Z43	0.0542	0.65	0.3526	1.03	0.0472	0.76	0.73	378	15	307	3	297	2	79
Z53	0.0547	0.52	0.3866	1.12	0.0513	0.99	0.88	399	12	332	3	322	3	81
Z51	0.0558	1.01	0.5429	1.42	0.0706	1.00	0.69	444	22	440	5	440	4	99
Z56	0.0578	0.42	0.5714	0.94	0.0716	0.84	0.88	524	9	459	3	446	4	85
Z47	0.0577	1.00	0.5758	1.37	0.0723	0.94	0.66	519	22	462	5	450	4	87
Z26	0.0567	1.50	0.5683	2.49	0.0727	1.99	0.80	479	33	457	9	453	9	94
Z10	0.0581	1.86	0.5866	2.39	0.0732	1.49	0.62	534	40	469	9	455	7	85
Z35	0.0589	0.63	0.6153	1.11	0.0758	0.91	0.80	562	14	487	4	471	4	84
Z46	0.0584	1.76	0.6387	1.97	0.0793	0.90	0.69	546	38	502	8	492	4	90
Z39	0.0581	1.43	0.6437	1.70	0.0804	0.92	0.52	532	31	505	7	498	4	94
Z40	0.0606	0.44	0.6950	0.86	0.0831	0.73	0.83	626	10	536	4	515	4	82
Z23	0.0569	2.74	0.6570	3.05	0.0837	1.34	0.69	489	61	513	12	518	7	106
Z42	0.0604	1.01	0.6969	1.24	0.0837	0.72	0.77	618	22	537	5	518	4	84
Z49	0.0617	0.65	0.7335	0.97	0.0862	0.73	0.71	664	14	559	4	533	4	80
Z60	0.0591	0.65	0.7142	1.16	0.0877	0.96	0.81	570	14	547	5	542	5	95

Appendix A (*Continued*)

Sample/grain	7/6 ratio	1σ(%)	7/5 ratio	1σ(%)	6/8 ratio	1σ(%)	rho	7/6 age	1σ(Ma)	7/5 age	1σ(Ma)	6/8 age	1σ(Ma)	Conc (%)
Z15	0.0590	4.60	0.7170	5.17	0.0881	2.37	0.71	568	97	549	22	544	12	96
Z38	0.0625	1.04	0.8041	1.22	0.0934	0.63	0.71	690	22	599	6	575	3	83
Z32	0.0636	0.99	0.8740	1.55	0.0996	1.19	0.76	729	21	638	7	612	7	84
Z25	0.0619	0.42	0.8550	1.07	0.1002	0.99	0.91	670	9	627	5	616	6	92
Z05	0.0620	0.85	0.9041	1.56	0.1057	1.30	0.83	675	18	654	7	648	8	96
Z20	0.0636	1.10	0.9746	1.78	0.1111	1.40	0.78	730	23	691	9	679	9	93
Z45	0.0674	0.45	1.1125	1.02	0.1197	0.91	0.88	850	9	759	5	729	6	86
Z41	0.0735	0.78	1.4145	1.26	0.1396	0.99	0.77	1028	16	895	7	842	8	82
Z33	0.0740	0.35	1.4627	0.67	0.1434	0.58	0.81	1042	7	915	4	864	5	83
Z30	0.0749	0.48	1.5046	0.90	0.1457	0.76	0.83	1065	10	932	5	877	6	82
Z22	0.0738	0.91	1.4975	1.45	0.1472	1.14	0.77	1036	18	929	9	885	9	85
Z54	0.0766	1.51	1.6220	1.68	0.1535	0.73	0.65	1112	30	979	10	921	6	83
Z12	0.0767	0.84	1.7662	1.35	0.1671	1.05	0.77	1113	17	1033	9	996	10	89
Z24	0.0751	0.37	1.7975	0.91	0.1736	0.83	0.90	1071	7	1045	6	1032	8	96
Z09	0.0740	0.85	1.7984	1.28	0.1762	0.96	0.73	1042	17	1045	8	1046	9	100
Z06	0.0797	1.02	2.1566	1.39	0.1964	0.95	0.66	1189	20	1167	10	1156	10	97
Z52	0.0846	1.40	2.3485	1.97	0.2013	1.39	0.69	1306	27	1227	14	1183	15	91
Z01	0.0961	0.76	2.9820	1.39	0.2251	1.17	0.83	1549	14	1403	11	1309	14	84
Z48	0.1071	0.54	3.6737	0.87	0.2487	0.68	0.75	1751	10	1566	7	1432	9	82
Z27	0.1083	0.78	3.7569	1.37	0.2516	1.13	0.94	1771	14	1584	11	1447	15	82
Z55	0.1102	0.47	3.9976	0.88	0.2632	0.74	0.82	1802	9	1634	7	1506	10	84
Z59	0.1217	0.37	4.9291	0.82	0.2938	0.74	0.87	1981	7	1807	7	1661	11	84
Z07	0.1163	3.20	5.1558	3.49	0.3215	1.40	0.65	1900	58	1845	30	1797	22	95
Z16	0.1226	0.88	5.5685	1.33	0.3293	1.00	0.74	1995	16	1911	11	1835	16	92
Z08	0.1109	1.00	5.3580	1.67	0.3505	1.33	0.79	1814	18	1878	14	1937	22	107
Z50	0.1868	0.44	10.9650	0.80	0.4258	0.66	0.91	2714	7	2520	7	2287	13	84
Z02	0.2559	0.87	20.7200	1.19	0.5872	0.82	0.66	3222	14	3126	12	2978	20	92
CW-16A: Botucatu Formation														
Z27	0.0534	0.97	0.2859	1.08	0.0389	0.47	0.58	344	22	255	2	246	1	71
Z08	0.0515	0.50	0.2993	0.80	0.0422	0.63	0.74	263	11	266	2	266	2	101
Z52	0.0555	0.39	0.3974	1.00	0.0519	0.92	0.91	433	9	340	3	326	3	75
Z03	0.0575	0.31	0.6075	0.53	0.0767	0.43	0.84	509	7	482	2	476	2	94
Z39	0.0586	0.42	0.6346	0.73	0.0785	0.60	0.77	552	9	499	3	487	3	88
Z47	0.0588	0.42	0.6427	0.77	0.0793	0.64	0.80	560	9	504	3	492	3	88
Z58	0.0586	2.44	0.6465	2.78	0.0800	1.33	0.72	552	53	506	11	496	6	90
Z11	0.0574	2.13	0.6368	2.35	0.0804	1.00	0.66	507	46	500	9	499	5	98
Z14	0.0580	0.35	0.6521	0.80	0.0816	0.72	0.88	529	8	510	3	505	3	95
Z48	0.0585	0.21	0.6702	0.62	0.0830	0.59	0.93	550	5	521	3	514	3	94
Z43	0.0587	0.21	0.6809	0.49	0.0841	0.44	0.82	558	5	527	2	520	2	93
Z54	0.0584	0.88	0.6795	1.10	0.0844	0.66	0.78	545	19	526	5	522	3	96
Z33	0.0587	0.22	0.6843	0.52	0.0846	0.48	0.86	554	5	529	2	524	2	94
Z06	0.0577	0.39	0.6762	0.75	0.0849	0.64	0.82	520	9	525	3	526	3	101
Z20	0.0580	0.23	0.6862	0.48	0.0858	0.42	0.78	531	5	531	2	530	2	100
Z46	0.0596	0.55	0.7114	0.80	0.0866	0.58	0.86	589	12	546	3	535	3	91
Z25	0.0591	0.43	0.7176	0.79	0.0880	0.66	0.81	572	9	549	3	544	3	95
Z01	0.0597	0.61	0.7258	1.10	0.0881	0.92	0.82	594	13	554	5	544	5	92

Appendix A (*Continued*)

Sample/grain	7/6 ratio	1σ(%)	7/5 ratio	1σ(%)	6/8 ratio	1σ(%)	rho	7/6 age	1σ(Ma)	7/5 age	1σ(Ma)	6/8 age	1σ(Ma)	Conc (%)
Z41	0.0582	0.37	0.7090	0.58	0.0883	0.44	0.64	539	8	544	2	545	2	101
Z55	0.0592	0.44	0.7283	0.77	0.0892	0.63	0.78	575	10	556	3	551	3	96
Z51	0.0608	0.53	0.7476	0.77	0.0892	0.56	0.66	631	11	567	3	551	3	87
Z19	0.0589	0.53	0.7267	0.75	0.0895	0.53	0.84	562	12	555	3	553	3	98
Z50	0.0582	0.80	0.7186	1.25	0.0896	0.97	0.91	537	18	550	5	553	5	103
Z17	0.0598	0.38	0.7398	0.69	0.0898	0.58	0.79	595	8	562	3	554	3	93
Z45	0.0605	0.43	0.7594	0.65	0.0910	0.49	0.66	621	9	574	3	562	3	90
Z61	0.0600	0.42	0.7745	0.70	0.0936	0.57	0.75	604	9	582	3	577	3	95
Z35	0.0597	0.26	0.7753	0.55	0.0941	0.48	0.82	594	6	583	2	580	3	98
Z40	0.0603	0.41	0.7915	0.72	0.0952	0.60	0.78	614	9	592	3	586	3	96
Z13	0.0607	0.63	0.7974	0.98	0.0953	0.74	0.73	628	14	595	4	587	4	94
Z49	0.0619	0.39	0.8215	0.94	0.0963	0.86	0.90	670	8	609	4	593	5	88
Z34	0.0600	0.50	0.7968	0.73	0.0963	0.53	0.85	603	11	595	3	593	3	98
Z07	0.0605	1.12	0.8079	1.39	0.0968	0.82	0.80	622	24	601	6	596	5	96
Z60	0.0600	0.21	0.8028	0.58	0.0970	0.54	0.91	604	5	598	3	597	3	99
Z42	0.0613	0.74	0.8255	0.96	0.0977	0.61	0.81	649	16	611	4	601	4	93
Z56	0.0604	0.32	0.8274	0.73	0.0994	0.66	0.88	617	7	612	3	611	4	99
Z05	0.0604	0.24	0.8312	0.55	0.0998	0.50	0.85	618	5	614	3	613	3	99
Z59	0.0615	0.45	0.8584	0.81	0.1012	0.67	0.80	657	10	629	4	622	4	95
Z53	0.0654	0.32	0.9311	0.76	0.1033	0.69	0.89	787	7	668	4	634	4	81
Z22	0.0721	0.15	1.5321	0.46	0.1541	0.43	0.90	989	3	943	3	924	4	93
Z15	0.0729	0.87	1.6188	1.14	0.1610	0.73	0.83	1011	18	978	7	962	7	95
Z28	0.0745	0.38	1.6783	0.74	0.1635	0.64	0.83	1054	8	1000	5	976	6	93
Z18	0.0755	0.20	1.7071	0.49	0.1639	0.45	0.86	1083	4	1011	3	978	4	90
Z30	0.0744	0.57	1.7038	0.95	0.1662	0.76	0.77	1051	12	1010	6	991	7	94
Z26	0.0751	0.33	1.7346	0.62	0.1675	0.53	0.79	1071	7	1021	4	998	5	93
Z37	0.0785	0.32	2.0398	0.71	0.1884	0.63	0.87	1160	6	1129	5	1113	6	96
Z29	0.1036	0.30	3.8414	0.70	0.2688	0.63	0.88	1690	6	1601	6	1535	9	91
Z21	0.1006	0.15	3.7591	0.46	0.2709	0.43	0.90	1636	3	1584	4	1545	6	94
Z57	0.1088	0.24	4.4384	0.55	0.2959	0.50	0.86	1779	4	1720	5	1671	7	94
Z16	0.1208	0.24	5.4370	0.55	0.3265	0.50	0.85	1968	4	1891	5	1821	8	93
Z24	0.1175	0.28	5.2943	0.63	0.3269	0.56	0.86	1918	5	1868	5	1823	9	95
Z36	0.1219	0.24	5.5148	0.69	0.3280	0.64	0.92	1985	4	1903	6	1829	10	92
Z23	0.1264	0.22	6.4746	0.47	0.3714	0.41	0.89	2049	4	2042	4	2036	7	99
Z09	0.1635	0.18	8.9022	0.56	0.3949	0.52	0.92	2492	3	2328	5	2146	10	86
Z10	0.1617	0.45	9.0228	0.74	0.4047	0.59	0.75	2473	8	2340	7	2191	11	89
Z02	0.1626	0.29	10.0922	0.70	0.4501	0.63	0.89	2483	5	2443	6	2396	13	96
Z12	0.2014	0.21	13.7041	0.48	0.4935	0.43	0.82	2837	3	2729	5	2586	9	91
CW-16B: Botucatu Formation														
Z48	0.0518	0.62	0.2590	1.03	0.0363	0.82	0.77	277	14	234	2	230	2	83
Z35	0.0514	0.74	0.2617	1.42	0.0369	1.20	0.84	260	17	236	3	234	3	90
Z53	0.0525	0.63	0.2687	0.95	0.0371	0.72	0.71	306	14	242	2	235	2	77
Z59	0.0522	0.57	0.2858	1.35	0.0397	1.22	0.90	295	13	255	3	251	3	85
Z13	0.0514	1.01	0.2856	1.62	0.0403	1.26	0.77	257	23	255	4	255	3	99
Z38	0.0506	1.74	0.2837	1.96	0.0407	0.90	0.69	223	40	254	4	257	2	115
Z60	0.0545	0.71	0.3140	2.49	0.0418	2.38	0.96	390	16	277	6	264	6	68

Appendix A (*Continued*)

Sample/grain	7/6 ratio	1σ(%)	7/5 ratio	1σ(%)	6/8 ratio	1σ(%)	rho	7/6 age	1σ(Ma)	7/5 age	1σ(Ma)	6/8 age	1σ(Ma)	Conc (%)
Z14	0.0570	0.69	0.3310	1.04	0.0421	0.79	0.72	492	15	290	3	266	2	54
Z25	0.0517	0.46	0.3112	0.80	0.0436	0.66	0.79	273	10	275	2	275	2	101
Z12	0.0532	0.57	0.3942	0.91	0.0537	0.70	0.74	338	13	337	3	337	2	100
Z45	0.0574	0.30	0.6115	0.57	0.0773	0.49	0.78	506	7	485	2	480	2	95
Z11	0.0596	2.51	0.6402	2.97	0.0780	1.60	0.78	587	53	502	12	484	7	82
Z02	0.0572	0.39	0.6155	0.89	0.0781	0.80	0.88	497	9	487	3	485	4	97
Z55	0.0582	0.55	0.6478	0.94	0.0807	0.76	0.79	538	12	507	4	500	4	93
Z07	0.0580	1.46	0.6549	1.82	0.0819	1.08	0.81	529	32	511	7	508	5	96
Z06	0.0569	1.19	0.6521	1.75	0.0831	1.28	0.72	488	26	510	7	515	6	105
Z31	0.0570	0.72	0.6552	2.03	0.0834	1.89	0.93	490	16	512	8	517	9	105
Z08	0.0582	0.52	0.6813	0.84	0.0849	0.66	0.74	538	11	528	3	525	3	98
Z23	0.0585	0.54	0.7090	0.80	0.0879	0.59	0.84	549	12	544	3	543	3	99
Z41	0.0592	0.46	0.7236	0.83	0.0887	0.69	0.80	574	10	553	4	548	4	95
Z30	0.0585	0.29	0.7175	0.53	0.0890	0.45	0.74	547	6	549	2	550	2	101
Z44	0.0599	0.30	0.7410	0.60	0.0897	0.51	0.81	600	7	563	3	554	3	92
Z37	0.0579	0.32	0.7228	0.68	0.0905	0.59	0.84	528	7	552	3	558	3	106
Z56	0.0592	0.37	0.7489	0.72	0.0917	0.62	0.82	575	8	568	3	566	3	98
Z50	0.0596	0.75	0.7544	1.01	0.0919	0.68	0.83	587	16	571	4	567	4	96
Z15	0.0591	1.01	0.7507	1.18	0.0922	0.61	0.69	569	22	569	5	568	3	100
Z34	0.0586	0.80	0.7668	1.00	0.0949	0.60	0.77	553	17	578	4	584	3	106
Z09	0.0605	0.41	0.7934	0.94	0.0951	0.85	0.89	621	9	593	4	586	5	94
Z42	0.0602	0.65	0.7906	0.87	0.0952	0.57	0.80	611	14	592	4	586	3	96
Z58	0.0605	0.73	0.7953	0.98	0.0954	0.65	0.82	621	16	594	4	587	4	95
Z19	0.0596	1.21	0.7872	1.83	0.0957	1.38	0.91	590	26	590	8	589	8	100
Z61	0.0594	0.68	0.7905	1.21	0.0966	1.01	0.82	581	15	591	5	594	6	102
Z03	0.0579	2.57	0.7756	2.82	0.0971	1.17	0.66	526	56	583	13	598	7	114
Z52	0.0617	0.31	0.8495	0.67	0.0998	0.59	0.85	664	7	624	3	613	3	92
Z57	0.0622	0.85	0.8561	1.27	0.0998	0.94	0.72	681	18	628	6	613	6	90
Z01	0.0603	0.67	0.8484	1.52	0.1020	1.37	0.89	615	14	624	7	626	8	102
Z05	0.0599	0.60	0.8577	1.11	0.1038	0.94	0.83	602	13	629	5	636	6	106
Z20	0.0631	0.65	0.9155	0.92	0.1051	0.65	0.66	713	14	660	4	645	4	90
Z40	0.0618	0.29	0.9081	0.66	0.1065	0.59	0.87	669	6	656	3	652	4	98
Z29	0.0614	0.47	0.9059	0.90	0.1070	0.76	0.83	654	10	655	4	655	5	100
Z21	0.0623	0.33	0.9642	0.73	0.1122	0.65	0.87	686	7	685	4	685	4	100
Z16	0.0586	1.53	0.9194	2.47	0.1138	1.94	0.78	553	33	662	12	695	13	126
Z46	0.0707	2.22	1.4528	2.40	0.1491	0.90	0.60	948	45	911	14	896	7	94
Z10	0.0733	0.33	1.7016	0.71	0.1683	0.63	0.85	1022	7	1009	5	1003	6	98
Z18	0.1190	0.72	3.7196	1.87	0.2266	1.71	0.92	1942	13	1576	15	1317	20	68
Z54	0.1138	1.30	4.9188	1.61	0.3134	0.94	0.79	1861	24	1805	14	1757	14	94
Z39	0.1148	0.31	5.1567	0.60	0.3258	0.51	0.80	1876	6	1845	5	1818	8	97
Z36	0.1085	0.25	4.9333	0.66	0.3299	0.61	0.91	1774	5	1808	6	1838	10	104
Z27	0.1152	0.58	5.3358	0.75	0.3360	0.47	0.73	1883	10	1875	6	1867	8	99
Z49	0.1231	0.28	5.9578	0.75	0.3510	0.70	0.92	2002	5	1970	7	1939	12	97
Z26	0.1391	0.70	6.8021	0.91	0.3547	0.57	0.56	2216	12	2086	8	1957	10	88
Z51	0.1269	0.25	6.3079	0.72	0.3604	0.67	0.93	2056	4	2020	6	1984	12	97
Z24	0.1242	0.39	6.3204	0.75	0.3691	0.64	0.82	2017	7	2021	7	2025	11	100
Z43	0.1867	0.30	9.8857	0.81	0.3841	0.76	0.92	2713	5	2424	8	2095	14	77
Z33	0.1901	0.30	14.3449	0.66	0.5474	0.59	0.86	2743	5	2773	6	2814	13	103

Appendix B: Lu-Hf isotope composition of zircon for samples of Serra do Rio do Rastro by LA-MC-ICP-MS

Sample/grain	$^{176}Lu/^{177}Hf$ (±2σ)	$^{176}Hf/^{177}Hf$ (±2σ)	$^{176}Hf/^{177}Hf_{(t)}$	$\varepsilon_{Hf(t)}$ (±2σ)	T_{DM} (Ga)	Age (Ma)
CW-01B: Rio Bonito Formation (Triunfo Member)						
Z1	0.000750 ± 20	0.281379 ± 57	0.281350	-5 ± 0.13	2.57	2041
Z2	0.000593 ± 7	0.281646 ± 57	0.281625	2 ± 0.02	2.20	1884
Z3	0.001011 ± 16	0.281817 ± 113	0.281799	-13 ± 0.29	1.99	992
Z6	0.000641 ± 27	0.281744 ± 110	0.281729	-10 ± 0.48	2.07	1218
Z7	0.000437 ± 2	0.281723 ± 116	0.281714	-15 ± 0.46	2.09	1017
Z8	0.000562 ± 3	0.282266 ± 65	0.282259	-5 ± 0.07	1.36	603
Z24	0.000797 ± 5	0.282356 ± 91	0.282346	-1 ± 0.02	1.25	636
Z25	0.000266 ± 2	0.282201 ± 86	0.282199	-10 ± 0.18	1.44	499
Z26	0.000928 ± 27	0.282297 ± 165	0.282290	-9 ± 0.34	1.33	361
Z17	0.000542 ± 3	0.282072 ± 86	0.282061	-2 ± 0.03	1.62	1063
Z18	0.000402 ± 3	0.282318 ± 83	0.282312	1 ± 0.01	1.28	780
Z28	0.000881 ± 12	0.282424 ± 65	0.282415	-1 ± 0.02	1.15	529
Z29	0.001322 ± 15	0.282396 ± 66	0.282384	-3 ± 0.06	1.21	485
Z48	0.001132 ± 17	0.282272 ± 92	0.282261	-7 ± 0.16	1.37	511
Z41	0.000752 ± 9	0.282156 ± 84	0.282149	-11 ± 0.22	1.52	512
Z61	0.000891 ± 5	0.281342 ± 79	0.281308	-7 ± 0.07	2.63	2000
CW-02A: Rio Bonito Formation (Paraguaçu Member)						
Z3	0.000681 ± 19	0.281057 ± 49	0.281022	-2 ± 0.05	3.00	2672
Z12	0.002257 ± 103	0.282353 ± 92	0.282313	4 ± 0.22	1.30	924
Z11	0.000550 ± 9	0.281491 ± 55	0.281470	-2 ± 0.04	2.41	1978
Z9	0.001955 ± 19	0.282296 ± 66	0.282276	-6 ± 0.10	1.37	555
Z8	0.000696 ± 5	0.282301 ± 64	0.282291	0 ± 0.01	1.32	760
Z17	0.000178 ± 6	0.281958 ± 55	0.281954	1 ± 0.04	1.76	1353
Z16	0.000587 ± 2	0.281432 ± 50	0.281410	-4 ± 0.03	2.49	1976
Z15	0.001924 ± 13	0.282291 ± 61	0.282272	-6 ± 0.11	1.37	524
Z21	0.001269 ± 59	0.281662 ± 52	0.281637	-17 ± 0.96	2.22	1037
Z19	0.001282 ± 19	0.282423 ± 63	0.282410	-1 ± 0.03	1.17	535
Z23	0.000745 ± 42	0.281089 ± 49	0.281051	0 ± 0.00	2.96	2699
Z30	0.001073 ± 5	0.281335 ± 61	0.281294	-7 ± 0.06	2.65	2032
Z24	0.000736 ± 25	0.282286 ± 53	0.282277	-3 ± 0.13	1.34	687
Z33	0.000357 ± 12	0.281077 ± 50	0.281059	-2 ± 0.07	2.94	2610
Z36	0.002080 ± 68	0.282095 ± 67	0.282074	-13 ± 0.60	1.66	537
Z27	0.001114 ± 9	0.282373 ± 65	0.282363	-4 ± 0.07	1.23	482
Z35	0.001094 ± 10	0.282253 ± 60	0.282242	-8 ± 0.18	1.40	517
Z43	0.001641 ± 22	0.281496 ± 63	0.281434	-3 ± 0.06	2.47	1968
Z52	0.000852 ± 26	0.281754 ± 87	0.281738	-15 ± 0.64	2.07	1001
Z54	0.001619 ± 25	0.281654 ± 72	0.281600	-2 ± 0.04	2.25	1779
Z49	0.000660 ± 34	0.281689 ± 69	0.281676	-16 ± 1.00	2.15	1029

Appendix B (*Continued*)

Sample/grain	$^{176}Lu/^{177}Hf$ (±2σ)	$^{176}Hf/^{177}Hf$ (±2σ)	$^{176}Hf/^{177}Hf(t)$	$\varepsilon_{Hf(t)}$ (±2σ)	T_{DM} (Ga)	Age (Ma)
CW-03: Rio Bonito Formation (Paraguaçu Member)						
Z02	0.000961 ± 83	0.282282 ± 31	0.282272	-6 ± 0.60	1.35	527
Z09	0.000961 ±109	0.281696 ± 34	0.281678	-17 ± 2.12	2.16	1008
Z12	0.001236 ± 48	0.281658 ± 45	0.281634	-17 ± 0.83	2.22	1045
Z60	0.000433 ± 9	0.281618 ± 30	0.281609	-18 ± 0.53	2.23	1042
Z57	0.001011 ± 12	0.281111 ± 50	0.281057	2 ± 0.03	2.95	2756
Z52	0.001401 ±121	0.281551 ± 56	0.281501	-3 ± 0.30	2.38	1866
Z49	0.000490 ± 9	0.281052 ± 42	0.281027	-2 ± 0.05	2.99	2638
Z24	0.001823 ±177	0.281748 ± 53	0.281713	-15 ± 1.69	2.13	1004
Z25	0.001900 ±107	0.281382 ± 58	0.281311	-7 ± 0.44	2.64	1984
Z26	0.000743 ± 80	0.281685 ± 56	0.281671	-17 ± 1.92	2.16	1012
Z44	0.001178 ± 16	0.282410 ± 55	0.282398	-2 ± 0.04	1.18	541
Z27	0.000682 ± 39	0.282044 ± 43	0.282034	-9 ± 0.58	1.67	790
Z39	0.001017 ± 49	0.282254 ± 48	0.282244	-7 ± 0.40	1.39	539
Z38	0.001209 ± 83	0.281507 ± 71	0.281465	-5 ± 0.40	2.43	1843
Z28	0.001170 ± 71	0.282384 ± 53	0.282373	-3 ± 0.22	1.22	508
Z31	0.001004 ± 77	0.281457 ± 57	0.281419	-3 ± 0.26	2.48	1994
Z33	0.000766 ± 65	0.281703 ± 28	0.281688	-16 ± 1.43	2.14	1027
Z35	0.001437 ± 90	0.282473 ± 71	0.282452	5 ± 0.37	1.10	768
Z36	0.001336 ±170	0.281340 ± 51	0.281288	-7 ± 0.86	2.66	2052
CW-04B: Rio Bonito Foramtion (Sideròpolis Member)						
Z02	0.001310 ± 78	0.282513 ± 98	0.282497	4 ± 0.30	1.04	650
Z12	0.000744 ± 24	0.281683 ± 82	0.281657	2 ± 0.07	2.16	1849
Z11	0.001011 ± 6	0.281565 ± 78	0.281527	0 ± 0.00	2.34	1952
Z17	0.000302 ± 56	0.282377 ± 65	0.282373	-1 ± 0.20	1.20	605
Z18	0.001245 ± 36	0.281625 ± 78	0.281583	-3 ± 0.09	2.27	1770
Z19	0.000827 ± 63	0.281742 ± 91	0.281726	-14 ± 1.37	2.09	1032
Z20	0.001101 ± 21	0.281589 ± 89	0.281550	-1 ± 0.03	2.31	1878
Z21	0.000812 ± 23	0.281513 ± 83	0.281484	-5 ± 0.15	2.40	1837
Z39	0.001213 ± 65	0.281402 ±173	0.281352	-2 ± 0.14	2.57	2131
Z40	0.000916 ± 14	0.282363 ± 75	0.282354	-3 ± 0.07	1.24	537
Z30	0.000490 ± 35	0.281071 ± 58	0.281046	-3 ± 0.19	2.96	2594
Z28	0.000987 ±115	0.282109 ± 56	0.282099	-12 ± 1.64	1.59	554
Z51	0.000989 ± 53	0.281027 ± 82	0.280978	-6 ± 0.32	3.06	2565
Z58	0.000580 ± 7	0.282127 ±101	0.282121	-12 ± 0.26	1.55	519
Z55	0.000955 ± 14	0.282171 ± 96	0.282162	-11 ± 0.25	1.51	506
Z59	0.001473 ± 24	0.281320 ±105	0.281307	-42 ± 1.06	2.70	484
CW-05: Rio Bonito Foramtion (Sideròpolis Member)						
Z01	0.001043 ±106	0.281478 ± 57	0.281441	-5 ± 0.53	2.46	1882

Appendix B (*Continued*)

Sample/grain	$^{176}Lu/^{177}Hf$ (±2σ)	$^{176}Hf/^{177}Hf$ (±2σ)	$^{176}Hf/^{177}Hf(t)$	$\varepsilon_{Hf(t)}$ (±2σ)	T_{DM} (Ga)	Age (Ma)
Z03	0.000705 ± 16	0.281701 ± 43	0.281688	-16 ± 0.53	2.13	1007
Z09	0.000345 ± 18	0.282090 ± 50	0.282087	-13 ± 0.81	1.59	512
Z11	0.000682 ± 11	0.280706 ± 50	0.280672	-16 ± 0.30	3.46	2586
Z23	0.000868 ± 51	0.282407 ± 45	0.282395	3 ± 0.21	1.18	759
Z21	0.000772 ± 41	0.281727 ± 37	0.281712	-15 ± 0.90	2.10	1017
Z18	0.000833 ± 77	0.281677 ± 36	0.281654	-7 ± 0.65	2.17	1477
Z48	0.001057 ± 90	0.281578 ± 71	0.281557	-21 ± 1.92	2.32	1012
Z41	0.001182 ± 71	0.282158 ± 49	0.282136	-1 ± 0.09	1.53	966
Z27	0.000762 ± 28	0.281533 ± 64	0.281506	-3 ± 0.11	2.36	1882
Z30	0.000786 ± 10	0.281472 ± 55	0.281444	-5 ± 0.08	2.45	1870
Z32	0.001406 ± 23	0.281509 ± 49	0.281458	-4 ± 0.09	2.44	1881
Z38	0.000572 ± 16	0.281072 ± 54	0.281043	0 ± 0.01	2.97	2700
Z35	0.001117 ± 69	0.282268 ± 57	0.282253	-3 ± 0.19	1.38	721
Z36	0.000785 ± 42	0.281057 ± 54	0.281017	-1 ± 0.06	3.00	2705
Z60	0.000765 ± 8	0.281764 ± 40	0.281748	-13 ± 0.21	2.05	1056
Z61	0.000992 ± 41	0.281800 ± 40	0.281784	-16 ± 0.78	2.02	860
CW-11C: Rio do Rasto Formation (Serrinha Member)						
Z2	0.000791 ± 15	0.280619 ± 66	0.280570	-5 ± 0.11	3.58	3222
Z5	0.000598 ± 43	0.282555 ± 92	0.282548	6 ± 0.51	0.97	648
Z6	0.001702 ± 70	0.282150 ± 145	0.282112	3 ± 0.17	1.56	1189
Z7	0.001419 ± 93	0.281468 ± 52	0.281417	-5 ± 0.53	2.49	1900
Z11	0.002121 ± 58	0.282422 ± 127	0.282411	-7 ± 0.37	1.20	274
Z10	0.001145 ± 102	0.282158 ± 97	0.282148	-12 ± 1.29	1.53	455
Z12	0.000649 ± 24	0.281993 ± 72	0.281979	-4 ± 0.18	1.74	1113
Z9	0.000720 ± 30	0.282332 ± 60	0.282318	7 ± 0.40	1.28	1042
Z15	0.000251 ± 31	0.282074 ± 180	0.282071	-13 ± 1.90	1.61	544
Z16	0.001939 ± 122	0.281507 ± 126	0.281434	-3 ± 0.19	2.47	1995
Z20	0.001215 ± 50	0.282541 ± 63	0.282526	6 ± 0.33	1.00	679
Z18	0.003260 ± 129	0.282374 ± 510	0.282357	-9 ± 0.49	1.30	272
Z23	0.004306 ± 340	0.282430 ± 163	0.282388	-3 ± 0.23	1.26	518
Z25	0.001007 ± 103	0.282267 ± 91	0.282255	-5 ± 0.56	1.38	616
Z26	0.001073 ± 79	0.281671 ± 5749	0.281662	-30 ± 3.35	2.20	453
Z51	0.001931 ± 65	0.282696 ± 733	0.282680	6 ± 0.28	0.80	440
Z50	0.001228 ± 81	0.280994 ± 113	0.280930	-4 ± 0.27	3.12	2714
Z47	0.003345 ± 138	0.282308 ± 152	0.282280	-8 ± 0.40	1.40	450
Z53	0.001201 ± 53	0.282574 ± 61	0.282566	-1 ± 0.03	0.95	322
Z56	0.001900 ± 212	0.282361 ± 45	0.282345	-6 ± 0.67	1.28	446
Z46	0.003556 ± 108	0.282050 ± 2549	0.282017	-16 ± 0.78	1.79	492
Z43	0.004381 ± 693	0.282218 ± 72	0.282193	-14 ± 2.4	1.58	297

Appendix B (*Continued*)

Sample/grain	$^{176}Lu/^{177}Hf$ (±2σ)	$^{176}Hf/^{177}Hf$ (±2σ)	$^{176}Hf/^{177}Hf(t)$	$\varepsilon_{Hf(t)}$ (±2σ)	T_{DM} (Ga)	Age (Ma)
CW-16A: Botucatu Formation						
Z03	0.000319 ± 2	0.282063 ± 61	0.282061	-15 ± 0.15	1.63	476
Z05	0.000090 ± 1	0.282339 ± 57	0.282337	-2 ± 0.03	1.25	613
Z06	0.000039 ± 1	0.282537 ± 63	0.282537	3 ± 0.07	0.98	526
Z08	0.001085 ± 72	0.282278 ± 61	0.282273	-12 ± 0.89	1.36	266
Z02	0.002277 ± 170	0.281215 ± 79	0.281107	-3 ± 0.23	2.90	2483
Z11	0.001085 ± 72	0.282278 ± 61	0.282268	-7 ± 0.54	1.36	499
Z19	0.000152 ± 1	0.282399 ± 47	0.282398	-1 ± 0.01	1.17	553
Z14	0.000669 ± 15	0.282433 ± 88	0.282427	-1 ± 0.04	1.14	505
Z15	0.000414 ± 5	0.282230 ± 82	0.282222	3 ± 0.08	1.40	1011
Z20	0.001279 ± 7	0.282388 ± 56	0.282375	-3 ± 0.03	1.22	530
Z21	0.000906 ± 19	0.281932 ± 91	0.281904	6 ± 0.13	1.83	1636
Z23	0.001241 ± 7	0.281426 ± 59	0.281378	-3 ± 0.03	2.54	2049
Z24	0.000440 ± 11	0.281203 ± 69	0.281187	-13 ± 0.37	2.78	1918
Z26	0.000369 ± 2	0.282223 ± 57	0.282215	4 ± 0.05	1.41	1071
Z27	0.000667 ± 6	0.282405 ± 59	0.282402	-8 ± 0.11	1.17	246
Z28	0.000427 ± 25	0.282387 ± 79	0.282378	9 ± 0.61	1.19	1054
Z37	0.000690 ± 1	0.282237 ± 76	0.282221	6 ± 0.05	1.41	1160
Z34	0.000790 ± 7	0.282351 ± 39	0.282342	-2 ± 0.04	1.25	593
Z39	0.001151 ± 1	0.282366 ± 76	0.282355	-4 ± 0.03	1.24	487
Z52	0.000054 ± 2	0.282365 ± 52	0.282365	-8 ± 0.42	1.21	326
Z54	0.000064 ± 1	0.282382 ± 61	0.282381	-3 ± 0.05	1.19	522
Z56	0.000807 ± 1	0.282458 ± 49	0.282449	2 ± 0.01	1.11	611
Z60	0.001379 ± 19	0.282221 ± 49	0.282206	-7 ± 0.14	1.45	597
CW-16B: Botucatu Formation						
Z2	0.000717 ± 10	0.281452 ± 49	0.281445	-37 ± 0.82	2.47	485
Z8	0.000808 ± 21	0.282133 ± 69	0.282125	-12 ± 0.39	1.55	525
Z7	0.000784 ± 35	0.282349 ± 94	0.282342	-4 ± 0.24	1.25	508
Z10	0.001221 ± 8	0.282428 ± 76	0.282404	9 ± 0.13	1.16	1022
Z12	0.000862 ± 6	0.282544 ± 68	0.282538	-1 ± 0.02	0.99	337
Z13	0.000821 ± 9	0.282419 ± 69	0.282416	-7 ± 0.18	1.16	255
Z15	0.001362 ± 20	0.282307 ± 44	0.282293	-5 ± 0.10	1.33	568
Z19	0.000202 ± 5	0.282491 ± 58	0.282489	3 ± 0.11	1.04	589
Z21	0.000080 ± 1	0.282200 ± 40	0.282199	-5 ± 0.07	1.43	685
Z25	0.000821 ± 11	0.282566 ± 48	0.282562	-2 ± 0.04	0.96	275
Z24	0.000877 ± 51	0.281265 ± 42	0.281232	-9 ± 0.58	2.73	2017
Z27	0.001637 ± 88	0.281501 ± 66	0.281442	-5 ± 0.30	2.46	1883
Z29	0.000971 ± 15	0.282077 ± 51	0.282065	-11 ± 0.24	1.64	655
Z33	0.000924 ± 15	0.281051 ± 43	0.281002	-1 ± 0.01	3.02	2743

Appendix B(*Continued*)

Sample/grain	$^{176}Lu/^{177}Hf$ (±2σ)	$^{176}Hf/^{177}Hf$ (±2σ)	$^{176}Hf/^{177}Hf(t)$	$\varepsilon_{Hf(t)}$ (±2σ)	T_{DM} (Ga)	Age (Ma)
Z35	0.001241 ± 53	0.282370 ± 57	0.282365	-10 ± 0.53	1.24	234
Z45	0.000066 ± 14	0.281965 ± 28	0.281964	-18 ± 3.94	1.75	480
Z48	0.001234 ± 53	0.282437 ± 50	0.282432	-7 ± 0.38	1.15	230
Z51	0.000722 ± 10	0.281376 ± 43	0.281348	-4 ± 0.07	2.57	2056
Z55	0.001273 ± 29	0.282363 ± 49	0.282351	-4 ± 0.13	1.25	500
Z59	0.000668 ± 10	0.282471 ± 36	0.282468	-6 ± 0.15	1.08	251

Appendix C: Sm-Nd whole-rock results for samples of Serra do Rio do Rasto by TIMS

Sample	Sm (ppm)	Nd (ppm)	$^{147}Sm/^{144}Nd$	$^{143}Nd/^{144}Nd$	$\varepsilon_{(t)}$	T_{DM}(Ga)
Itararé Gorup - Rio do Sul Formation						
CW-01A	9.891	50.749	0.1178	0.512115+/-3	-10.2	1.46
Guatá Gorup - Rio Bonito Formation						
CW-01B	7.01	34.292	0.1236	0.511991+/-7	-12.62	1.76
CW-02A	5.044	26.347	0.1157	0.511972+/-13	-12.99	1.65
CW-02B	2.131	12.975	0.0993	0.511929+/-11	-13.84	1.47
CW-03	4.163	24.441	0.103	0.511880+/-8	-14.79	1.59
CW-04A	6.403	38.102	0.1016	0.512101+/-10	-10.48	1.27
CW-04B	3.61	20.67	0.1056	0.511928+/-16	-13.85	1.56
CW-05	14.184	96.954	0.0884	0.512227+/-6	-8.02	0.99
Guatá Gorup - Palermo Formation						
CW-06	8.463	46.982	0.1089	0.512214+/-19	-8.28	1.2
Passa Dois Gorup - Irati Formation						
CW-07	7.017	35.183	0.1206	0.512136+/-21	-9.79	1.47
Passa Dois Gorup - Serra Alta Formation						
CW-09A	6.041	28.906	0.1263	0.512235+/-12	-7.86	1.4
CW-09BCO	3.428	17.787	0.1165	0.512240+/-13	-7.77	1.25
CW-09C	4.065	21.493	0.1143	0.512237+/-5	-7.82	1.23
CW-09DCO	4.653	24.209	0.1162	0.512267+/-4	-7.23	1.2
CW-09ECO	4.715	23.543	0.1211	0.512287+/-10	-6.84	1.24
CW-09F	3.704	19.371	0.1156	0.512180+/-13	-8.93	1.33
CW-09G	3.694	19.594	0.114	0.512192+/-15	-8.69	1.29
CW-09BASE	2.57	14.345	0.1083	0.512226+/-3	-8.03	1.18
CW-09SUL_PIR	5.039	25.386	0.12	0.512315+/-12	-6.29	1.18
CW-09FRAN	3.23	17.381	0.1123	0.512211+/-16	-8.34	1.24
CW0-09NIVEL	4.252	22.74	0.113	0.512234+/-18	-7.88	1.22
Passa Dois Gorup - Teresina Formation						
CW-10A	7.328	36.321	0.122	0.512222+/-15	-8.12	1.35
CW-10BCO	3.395	17.306	0.1186	0.512234+/-5	-7.88	1.29
Passa Dois Gorup - Rio do Rasto Formation						
CW-11A	5.108	27.013	0.1143	0.512221+/-14	-8.14	1.25
CW-11B	74.462	283.18	0.1589	0.512336+/-4	-5.9	1.95
CW-11C	35.383	202.916	0.1054	0.512273+/-7	-7.13	1.08
CW-13	10.812	56.737	0.1152	0.512252+/-5	-7.53	1.22
CW-14	5.067	26.355	0.1162	0.512239+/-12	-7.79	1.25
São Bento Gorup - Botucatu Formation						
CW-16A	0.604	3.143	0.1162	0.512053+/-3	-11.41	1.53
CW-16B	2.361	11.141	0.1281	0.512053+/-14	-11.42	1.75
CW-16C	5.833	26.852	0.1313	0.512261+/-22	-7.36	1.43

References

Aboarrage, A.M.; Lopes, R.C. 1986. Projeto a Borda Leste da Bacia do Paraná: integração geológica e avaliação econômica. DNPM/CPRM, Porto Alegre. 18 v.

Almeida F.F.M. 1978. Tectonic map of South America 1:5.000.000. Explanatory note, Brasilia, DNPM/CGMW/UNESCO, 23p.

Andersen, T.; Griffin, W.L.; Pearson, N.J. 2002. Crustal Evolution in the SW Part of the Baltic Shield: the Hf Isotope Evidence. *Journal of Petrology*, **43** 9: 1725-1747.

Andersen, T. 2005. Detrital zircons as tracers of sedimentary provenance: limiting conditions from statistics and numerical simulation. *Chemical Geology*, **216**: 249–270.

Anon. 2008. West Gondwana amalgamation based on detrital zircon ages from Neoproterozoic Ribeira and Dom Feliciano belts of South America and comparison with coeval sequences from SW Africa. **294**, 239–256.

Assine M. L., Zacharias A. Á. and Perinotto J. A. J. 2003 Paleocorrentes, paleogeografia e seqüências deposicionais da Formação Tatuí, centro-leste do estado de São Paulo. *Brazilian Journal of Geology* **33**, 33–40.

Augustsson, C.; Münker, C.; Bahlburg, H.; Fanning, C. M. 2006. Provenance of late Palaeozoic metasediments Provenance of the SW South American Gondwana margin: a combined U–Pb and Hf-isotope study of single detrital zircons. *Journal of the Geological Society*, **163**: 983-995.

Basei M., Frimmel H. E., Nutman A. P. and Preciozzi F. 2005. A connection between the Neoproterozoic Dom Feliciano Brazil/Uruguay and Gariep Namibia/South Africa orogenic belts–evidence from a reconnaissance reconnaissance provenance study *Precambrian Research,* **139**, 195–221.

Bowring, S. A.; Schmitz, M. D. 2003 High-Precision U-Pb Zircon Geochronology and the Stratigraphic Record. Reviews in Mineralogy and Geochemistry, **53**: 305-326.

Bühn B., Pimentel M. M., Matteini M. and Dantas E. L. 2009. High spatial resolution analysis of Pb and U isotopes for geochronology by laser ablation multi-collector inductively coupled plasma mass spectrometry LA-MC-ICP-MS. *Anais da Academia Brasileira de Ciências* **81**, 99–114.

Cury L. F. 2009. Geologia do Terreno Paranaguá. Tese de Doutorado, Instituto de Geociências, Universidade de São Paulo USP, 187 p.

Casquet, C.; Pankhurst, R.J.; Rapela, C.W.; Galindo, C.; Fanning, C.M.; Chiaradia, M.; Baldo, E.; González-Casado, J.M.; Dahlquist, J.A. 2008. The Mesoproterozoic Maz terrane in the Western Sierras Pampeanas, Argentina, equivalent to the Arequipa–Antofalla block of southern Peru? Implications for West Gondwana margin evolution. *Gondwana Research*. **13**, 163-175.

Casquet, C.; Fanning, C.M.; Galindo, C.; Pankhurst, R.J.; Rapela, C.W.; Torres, P. 2010. The Arequipa Massif of Peru: New SHRIMP and isotope constraints on a Paleoproterozoic inlier in the Grenvillian orogen. *Journal of South American Earth Sciences*. **29**, 128-142.

Casquet, C.; Rapela, C.W.; Pankhurst, R.J.; Baldo, E. G.; Galindo, C.; Fanning, C.M.; Dahlquist, J.A.; Saavedra, J. 2012. A history of Proterozoic terranes in southern South America: From Rodinia to Gondwana. *Geoscience Frontiers*. 3, 137-145.

Cawood, P. T. 2005. Terra Australis Orogen: Rodinia breakup and development of the Pacific and Iapetus margins of Gondwana during the Neoproterozoic and Paleozoic**.** Earth-Science Reviews, **69:** 249–279.

Condie, K.C., Beyer, E., Belousova, E., Griffin, W.L., O'Reilly, S.Y., 2005. U–Pb isotopic ages and Hf isotopic composition of single zircons — the search for juvenile Precambrian continental crust. *Precambrian Research* **139**, 42–100.

Condie, K.C., Belousova, E., Griffin, W.L., Sircombe, K.N., 2009. Granitoid events in space and time: constraints from igneous and detrital zircon age spectra. *Gondwana Research* **15**, 228–242.

Cordani, U.G.; Brito Neves, B.B.; Fuck, R.A.; Porto, R.; Thomaz Filho, A.; Cunha, F.M.B. 1984. Estudo preliminar de integração do pré-cambriano com os eventos tectônicos das bacias sedimentares brasileiras. Série Ciência-Técnica-Petróleo, Rio de Janeiro. **15**, 12-20.

Coutinho, J.M.V.; Hachiro, J.; Coimbra, A.M.; Santos, P.R. 1991. Ash-fall derived vitroclastic tuffaceous sediments in the Permian of the Paraná Basin and their provenance. In: Ulbrich, H. & Rocha-Campos, A.C. eds.. Gondwana Seven. São Paulo: Universidade de São Paulo, p. 147-160.

Coutinho, J.M.V., Hachiro, J., 2005. Distribution, mineralogy, petrography, provenance and significance of Permian ash-carrying deposits in the Paraná Basin. Revista do Instituto de Geociências 5, 29–39.

da Silva L. C., Hartmann L. A., McNaughton N. J. and Fletcher I. 2000 Zircon U-Pb SHRIMP dating of a Neoproterozoic overprint in Paleoproterozoic granitic-gneissic terranes, southern Brazil. *Am Mineral* **85**, 649–667.

De Wit M. J., Stankiewicz J. and Reeves C. 2008 Restoring Pan-African-Brasiliano connections: more Gondwana control, less Trans-Atlantic corruption. *Geological Society, London, Special Publications* **294**, 399–412.

Dodson W.H., Compston W., Williams I.S., Wilson J.F. 1988. A search for ancient detrital zircons in Zimbabwean sediments. *Journal of the Geological Society* **145**:977-983.

Eglington B. M., Thomas R. J., Armstrong R. A. and Walraven F. 2003. Zircon geochronology of the Oribi Gorge Suite, KwaZulu-Natal, South Africa: constraints on the timing of trans-current shearing in the Namaqua–Natal Belt. *Precambrian Research* **123**, 29–46.

Erwin D. H. 2001. *Extinction: End-Permian Mass Extinction*, John Wiley & Sons, Ltd, Chichester, UK.

Fanning C. M., Hervé F., Pankhurst R. J., Rapela C. W., Kleiman L. E., Yaxley G. M. and Castillo P. 2011. Lu–Hf isotope evidence for the provenance of Permian detritus in accretionary complexes of western Patagonia and the northern Antarctic Peninsula region. *Journal of South American Earth Sciences* **32**, 485–496.

Frimmel H. E., Tack L., Basei M. S. and Nutman A. P. 2006. Provenance and chemostratigraphy of the Neoproterozoic West Congolian Group in the Democratic Republic of Congo. *Journal of African Earth Sciences,* **46**: 221-239.

Frimmel H. E., Basei M. S. and GAUCHER C. 2011. Neoproterozoic geodynamic evolution of SW-Gondwana: a southern African perspective. *Int J Earth Sci Geol Rundsch* **100**, 323–354.

Gerdes, A.; Zeh, A. 2006. Combined U–Pb and Hf isotope LA-MC-ICP-MS analyses detrital zircons: Comparison with SHRIMP and new constraints for the provenance and age of an Armorican metasediment in Central Germany. *Earth and Planetary Science Letters* **249**, 47–61.

Gioia, S.M.C.L. & Pimentel, M.M. 2000. The Sm-Nd isotopic method in the Geochronology Laboratory of the University of Brasília. Anais da Academia Brasileira de Ciências 72: 219-245.

Hartmann L. A., Piñeyro D., Bossi J. and Leite J. 2000. Zircon U-Pb SHRIMP dating of Palaeoproterozoic Isla Mala granitic magmatism in the Rio de la Plata Craton, Uruguay. *Journal of South American Earth Sciences*, **13**: 105-113.

Heilbron M., Valeriano C. M., Tassinari C. C. G., Almeida J., Tupinamba M., Siga O. and Trouw R. 2008. Correlation of Neoproterozoic terranes between the Ribeira Belt, SE Brazil and its African counterpart: comparative tectonic evolution and open questions. *Geological Society, London, Special Publications* **294**, 211–237.

Hervé F., Fanning C. M., Calderón M. and Mpodozis C. 2014. Early Permian to Late Triassic batholiths of the Chilean Frontal Cordillera 28°–31°S: SHRIMP U–Pb zircon ages and Lu–Hf and O isotope systematics. *LITHOS* **184-187**, 436–446.
.

Isozaki, Y. 2003. Guadalupian–Lopingian boundary event in mid-Panthalassa: correlation of accreted deep-sea chert and mid-oceanic atoll carbonate. *Proceedings of the XVth International Congress on Carboniferous and Permian Stratigraphy*,111–124. Available at: http://ea.c.u-tokyo.ac.jp/earth/Members/Isozaki/07Neth.Acad.pdf.

Isozaki, Y., Kawahata, H. and Ota A. 2006. A unique carbon isotope record across the Guadalupian–Lopingian Middle–Upper Permian boundary in mid-oceanic paleo-atoll carbonates: The high-productivity "Kamura event" and its collapse in Panthalassa. *Global and Planetary Change* **55**, 21–38.

Isozaki, Y.; Kawahata H. and Minoshima K. 2007. The Capitanian Permian Kamura cooling event: The beginning of the Paleozoic–Mesozoic transition. *Palaeoworld* **16**, 16–30.

Isozaki, Y.; Isozaki, Y.; Shimizu N., Shimizu N., Yao J., Yao J., Ji Z., Ji Z., Matsuda T. and Matsuda T. 2007. End-Permian extinction and volcanism-induced environmental stress: The Permian–Triassic boundary interval of lower-slope facies at Chaotian, South China. *Palaeogeography, Palaeoclimatology, Palaeoecology* **252**, 218–238.

López-Gamundí O. 2006a. Permian plate margin volcanism and tuffs in adjacent basins of west Gondwana: Age constraints and common characteristics. *Journal of South American Earth Sciences* **22**, 227–238.

López-Gamundí O. 2006b. Permian plate margin volcanism and tuffs in adjacent basins of west Gondwana: Age constraints and common characteristics. *Journal of South American Earth Sciences* **22**, 227–238.

Matteini, M.; Dantas, E. L.; Pimentel, M. M. and Bühn, B. 2010. Combined U-Pb and Lu-Hf isotope analyses by laser ablation MC-ICP-MS: methodology and applications.

Milani, E.J.; França, A.B.; Schneider, R.L. 1994. Bacia do Paraná. Boletim de Geociências da PETROBRÁS, v. 8, n. 1, p. 69-82.

Milani E. J., França A. B. and Schneider R. L. 1994a. Bacia do Paraná. Boletim *de Geociências da PETROBRÁS*.

Milani E. J., França A. B. and Schneider R. L. 1994b. Bacia do Paraná. *Boletim de Geociências da Petrobras* **8**, 69–82.

Milani, E.J. 1997. Evolução Tectono-Estratigráfica da Bacia do Paraná e o seu relacionamento com a geodinânica fanerozóica do Gondwana Sul-Ocidental. Tese de Doutorado, Instituto de Geociências, Universidade Federal do Rio Grande do Sul, 255 p.

Milani E. J., Faccini U. F., Scherer C. M., Araújo L. M. and Cupertino J. A. 1998. Sequências e hierarquia estratigráfica da bacia do Paraná Ordoviciano ao Cretáceo, sul do Brasil. *Boletim IG-USP. Série Científica* **29**, 125–173.

Milani E. J. and Ramos V. A. 1998a. Orogenias paleozóicas no domínio sul-ocidental do

Gondwana e os ciclos de subsidência da Bacia do Paraná. *Revista Brasileira de Geociências*.

Milani E. J. and Ramos V. A. 1998b. Orogenias paleozóicas no domínio sul-ocidental do Gondwana e os ciclos de subsidência da Bacia do Paraná. *Revista Brasileira de Geociências*.

Milani, E. J.; Melo, J. H. G.; Souza, P. A.; Fernandes, L. A.; Almério Barros França, A. B. 2007. Bacia do Paraná. Geoci. Petrobras, Rio de Janeiro, v. 15, n. 2, p. 265-287.

Neves B. B. de B., Fuck R. A. and Pimentel M. M. 2014 The Brasiliano collage in South America: a review. *Brazilian Journal of Geology* **44**, 493–518.

Orlandi Filho,V.; Krebs, A.S.J.; Giffoni, L.E. 2006. Coluna White, Serra do Rio do Rastro, SC - Seção Geológica Clássica do Continente Gondwana no Brasil. In: Winge, M.; Schobbenhaus, C.; Berbert-Born, M.; Queiroz, E.T.; Campos, D.A.; Souza, C.R.G.; Fernandes, A.C.S. Edit. Sítios Geológicos e Paleontológicos do Brasil. Publicado na Internet em 22/12/2006 no endereço http://www.unb.br/ig/sigep/sitio024/sitio024.pdf

Patchett, P.J. & Tatsumoto, M. 1980. A routine high-precision method for Lu-Hf isotope geochemistry and chronology. Contrib. Mineral. Petrol., **76**: 263-268.

Patchett, P.J. & Tatsumoto, M. 1981. Lu/Hf in chondrites and definition of a chondritic hafnium growth curve. Lunar Planet. Sci., **12**: 822-824.

Patchett, P.J., Kouvo, O., Hedge, C. E., Tatsumoto, M. 1981. Evolution of continental crust and mantle heterogeneity. Contrib. Mineral. Petrol., **78**: 279-297.

Patchett, P.J. 1983. Importance of the Lu-Hf isotopic system in studies of planetary chronology and chemical evolution. Acta, **47**: 81-91.

Ramos Victor A 1984 Patagonia: a Paleozoic continent adrift? Actas. In Noveno Congreso Geologico Argentino. S. C. Bariloche. pp. 311–325.

Ramos, V.A. 1988. Late Proterozoic - Early Paleozoic of South America - a collisional history. *Episodes,* 11(3):168-174.

Ramos V. A. 2008 Patagonia: A paleozoic continent adrift? *Journal of South American*

Earth Sciences **26**, 235–251.

Ramos, V. A. 2010. The Grenville-age basement of the Andes. *Journal of South American Earth Sciences***, 29**, 77–91.

Ramos Victor A, Chemale F., Naipauer M. and Pazos P. J. 2014 A provenance study of the Paleozoic Ventania System Argentina: Transient complex sources from Western and Eastern Gondwana. *Gondwana Research* **26**, 719–740.

Richard, P.; Shimizu, N. & Allègre. CJ. 1976.^{143}Nd/^{146}Nd A Natural Tracer: An Application to Oceanic Basalts. *Earth Plan Sci Lett* **31:** 269-278.

Rocha-Campos A. C., Basei M. A., Nutman A. P., Kleiman L. E., Varela R., Llambías E. J., Canile F. M. and de C R da Rosa O. 2011. 30million years of Permian volcanism recorded in the Choiyoi igneous province W Argentina and their source for younger ash fall deposits in the Paraná Basin: SHRIMP U–Pb zircon geochronology evidence. *Gondwana Research* **19**, 509–523.

Rodrigues J. B., Pimentel M. M., Bühn B. and Matteini M. 2012. Provenance of the Vazante Group: New U–Pb, Sm–Nd, Lu–Hf isotopic data and implications for the tectonic evolution of the Neoproterozoic Brasília Belt. *Gondwana Research* **21**, 439–450.

Santos R. V., Souza P. A., Alvarenga C. J. S. de, Dantas E. L., Pimentel M. M., Oliveira C. G. and de Araújo L. M. 2006. Shrimp U–Pb zircon dating and palynology of bentonitic layers from the Permian Irati Formation, Paraná Basin, Brazil. *Gondwana Research* **9**, 456–463.

Schmitt R. S., Trouw R. and Van Schmus W. R. 2004. Late amalgamation in the central part of West Gondwana: new geochronological data and the characterization of a Cambrian collisional orogeny in the Ribeira Belt SE Brazil. *Precambrian Research* **133**, 29–61.

Schmitz M. D. and Bowring, S. A. 2004. Lower crustal granulite formation during Mesoproterozoic Namaqua-Natal collisional orogenesis, southern Africa. *South African Journal of Geology* **107**, 261–284.

Schmitt R. S., Trouw R. A. J., Medeiros S. R. and Dantas E. L. 2008. Age and geotectonic setting of Late Neoproterozoic juvenile mafic gneisses and associated paragneisses from the Ribeira belt SE Brazil based on geochemistry and Sm–Nd data — Implications on Gondwana assembly. *Gondwana Research* **13**, 502–515.

Schneider, R.L.; Mühlmann, H.; Tommasi, E.; Medeiros, R.A.; Daemon, R.F.; Nogueira, A.A. 1974. Revisão estratigráfica da Bacia do Paraná. In: Congresso brasileiro de Geologia, 28, Porto Alegre: SBG, v.1, p. 41-65.

Schneider, R.L.; Castro, J.C. 1975. Análise estratigráfica, sedimentológia e potencialidades petrolíferas da Formação Rio Bonito no sudeste da Bacia do Paraná. PETROBRAS/DEXPRO, Relatório Interno nº. 5011, 39p.

Sepkoski J. J. Jr 1984. JSTOR: Paleobiology, Vol. 10, No. 2 Spring, pp. 246-267. *Paleobiology*.

Sepkoski Jr., J.J., 1996. Patterns of Phanerozoic extinction: a perspective from global data bases. In: Walliser, O. (Ed.), Global Events and Event Stratigraphy. Springer, New York, pp. 35–51

Sircombe, K.N., 2000. Quantitative comparison of geochronological data using multivariate analysis: a provenance study example from Australia. Geochim. Cosmochim. Acta 64, 1593– 1619.

Stanley S. M. and Yang X. 1994. A Double Mass Extinction at the End of the Paleozoic Era. *Science* **266**, 1340–1344.

Turner B. R. 1999. Tectonostratigraphical development of the Upper Karooforeland basin: Orogenic unloading versus thermally-induced Gondwana rifting. *Journal of African Earth Sciences* **28**, 215–238.

Veevers, J. J.; Saeed, A.; Belousova, E. A.; Griffin, W. L. 2005. U–Pb ages and source composition by Hf-isotope and trace-element analysis of detrital zircons in Permian sandstone and modern sand from southwestern Australia and a review of the paleogeographical and denudational history of the Yilgarn Craton. *Earth-Science Reviews* **68**, 245–279.

Veevers J. J. and Saeed A. 2007. Central Antarctic provenance of Permian sandstones in Dronning Maud Land and the Karoo Basin: integration of U–Pb and T DM ages and host-rock affinity from detrital zircons. *Sedimentary Geology* **202**, 653–676.

Vermeesch, P., 2004. How many grains are needed for a provenance study? Earth Planet. Sci. Lett. **224**, 351– 441

White,I.C. 1908. Relatório final da Comissão de Estudos das Minas de Carvão de Pedra do Brasil. DNPM , Rio de Janeiro,Parte I, p.1-300 ; Parte II, p. 301-617. ed. Fac-similar de 1988.

Yao, J.; Shu, L.; Santosh, M. 2011. Detrital zircon U–Pb geochronology, Hf-isotopes and geochemistry—New clues for the Precambrian crustal evolution of Cathaysia Block, South China. *Gondwana Research*, **20**: 553–567.

Ziegler A. M. 1997. Permian world topography and climate. *In Martini, I. P., ed. Late glacial and postglacial environmental changes Pleistocene, Carboniferous-Permian, and Proterozoic. Oxford, Oxford University Press, p. .*, 111–146.

CAPÍTULO V

Pangea break-up and the significance of Recurrence cycles in Permian Ash Layers from the Irati Formation, Brazil

Lindaray Sousa da Costa[1, 2], Roberto Ventura Santos[1], Elton Luiz Dantas[1], Carlos Jose Sousa de Alvarenga[1]

[1]Universidade de Brasília, Instituto de Geociências, Laboratório de Geocronologia 70910-900 Brasília-DF, Brazil

[2]Corresponding author lindaraygeo@gmail.com

Abstract:

The intracratonic Paraná Basin is located on the eastern side of the South American Platform and is made of sedimentary and volcanic rocks that are grouped into six second order sequences: Rio Ivaí, Paraná, Gondwana I, Gondwana II, Gondwana III and Bauru. The Gondwana I sequence includes the Irati Formation (Passa Dois Group), in which are found volcanic ashes intercalated with organic-rich mudstones and dolostones. These rocks are well exposed at the Petrox-Six Quarry São Matheus do Sul (PR). The zircon U-Pb data from these ash layers indicate ages ranging between 287 and 267 Ma, with a main peak at 278 Ma. Lu-Hf data of these zircons indicate a crustal signature ε_{Hf} ranging between -7 and -3 and Mesoproterozoic 1.2 (Ga) and Neoproterozoic 0.8 (Ga) Hf (T_{DM}) model ages. The Nd isotope data reinforce the zircon data, indicating a main crustal component in the source area of these rocks ε_{Nd} = -11.6 to -3.3. The data indicate that the volcanic ash beds interlayered in the sedimentary rocks of the Irati Formation are related to the Choiyoi volcanic province that is approximately 2.000 km to the west.

1. Introduction

The Permian period is marked by large transformations in Earth's surface conditions. During this period, events related to global climate changes were associated with several episodes of intense volcanism and meteorite impacts that had major effects on Earth's biosphere (Erwin, 1990; Isozaki et al., 2007b; Sepkoski, 1996; 1984). For instance, available studies indicate that the Permo-Triassic boundary marks one of the most important mass extinction events in the Phanerozoic, during which it is estimated that approximately 90% of living species disappeared (Sepkoski, 1996; 1984, among others). The mechanism that triggered this environmental change is still not fully understood but is usually attributed to a global volcanic event (e.g., Campbell et al., 1992; Renne et al., 1995) or to the impact of a large extraterrestrial bolide (e.g., Becker et al., 2001; Kaiho et al., 2001; Retallack et al., 1998). In addition to the Permo-Triassic boundary, another decline in biodiversity seems also to have occurred at the Middle-Late Permian (Isozaki, 2003; Isozaki et al., 2007; Isozaki et al., 2004; Stanley and Yang, 1994), likely related to major felsic volcanism. This extinction event occurred at the end of a global cooling event known as Kamura (Isozaki et al., 2007a), which is characterized by high positive carbon isotope values.

The Permian is also known for extensive black shale sediments deposited in intracontinental rifting or passive margin environments, most of which are associated with tectonic episodes of supercontinental break-up and mantle plume events (Faure and Cole, 1999; Veevers and Saeed, 2007). At the same time, the development of subduction related magmatism linked with orogenetic belts could have led to an uplift of sea level that provoked incursions of marine transgressions over the continental shield (Stollhofen et al., 2000). In South America, the Permian geological record is characterized by a thick sequence of sediments deposited in an epicontinental basin (Milani and Ramos, 1998) that is contemporaneous with intense explosive volcanism generated during Arc magmatism in the Andes (López-Gamundí, 2006). These volcanic events are important stratigraphic and biostratigraphic markers because they allow absolute dating of geological events. Particularly important are those strong volcanic events in which the ash settles down within a large geographic area.

The Permo-Triassic geologic period was marked by intense worldwide volcanic activity (Kay et al., 1989; Milani e Ramos, 1998; López-Gamundí, 2006). In the Paraná Basin, the record of this volcanic activity has been documented by various studies (Coutinho et al., 1991; Maynard et al., 1996; Milani e Ramos, 1998; Coutinho e Hachiro, 2005; Santos et al., 2006; Rocha-Campos et al. 2007, 2011). In the Irati Formation, volcanic ashes were initially described by Maynard et al. (1996) and later dated at 278 ± 2.2 Ma by Santos et al. (2006). This age is consistent with the 270 ± 1 Ma age data of ashes from the Collingham Formation in South Africa (Stollhofen et al., 2000), as well as the paleostratigraphic data from Souza and Marques-Toigo (2005).

Volcanic ash layers of the Irati Formation are between 2 and 4 cm thick and consist of dark gray clay rich material that is intercalated with black shales and dolostones. Thirteen of these layers are well exposed in the Six-Petrobras quarry that is located near the city of São Matheus do Sul, South Brazil (Maynard et al., 1996). These layers are made of montmorilonite, illite, kaolinite, quartz and subordinate pyrite and are believed to have a ryolitic component (dos Anjos et al., 2006; dos Anjos, 2008). Similar deposits were also described in other parts of the basin, such as in Argentina (e.g., Calingasta–Uspallata, Paganzo, Sauce Grande Basins; López-Gamundi, 2006) and South Africa (e.g., Karoo Basin; Johnson, 1991; Stolhofen et al., 2000).

This paper aims to better constrain the age range of the Irati volcanic ashes and identify their possible source areas. The source of the ash layers is still not clear and has been related to different geological processes: i) Andean calc-alkaline arc magmatism that occurred on the southwestern portion of South America (Santos et al., 2006) and ii) volcanism related to intercontinental rifting that is associated with marine sedimentation and sea level rise (Stollofen, 2000, Veerves and Saeed, 2007). Among the thirteen layers of the Six-Petrobras quarry, five were selected to perform a detailed isotope geochemical Nd and Lu-Hf and geochronological zircon U-Pb dating survey, which were used for comparisons with known volcanic sources in Southwestern Gondwana. These new absolute U-Pb data of Permian ash layers from the Petrobras-Six quarry were also compared with data from Santos et al. (2006) and allowed an estimation of how long volcanic events lasted in that part of globe during the Permian.

2. Geological Settings

The Paraná basin is a large intracratonic basin located at the central-eastern part of the South-American Platform. It comprises a thick (ca. 5.000 m) and extensive sedimentary-magmatic sequence, which covers an area of approximately 1,500,000 km^2 of Brazil, Uruguay, Argentina and Paraguay. According to Milani et al. (1994) and Milani (1997), six supersequences are represented in this basin, ranging from Late Ordovician to Late Cretaceous (Fig. 1a): Rio Ivaí (Rio Ivaí Group of Ordovician-Silurian age), Paraná (Paraná Group of Devonian age), Gondwana I (Fig. 1b) (Itararé, Guatá e Passa Dois groups of Carboniferous-Permian age), Gondwana II (Triassic units), Gondwana III (São Bento Group of Jurassic-Cretaceous age) and Bauru (Cretaceous). The Rio Ivaí, Paraná and Gondwana I sequences comprise a transgressive-regressive cycle, whereas supersequence Gondwana II, Gondwana III and Bauru consist of continental deposits crosscut by igneous intrusions.

The Irati Formation is part of the Permian Passa Dois Group (Gondwana I Supersequence) and extends through most of the basin. It has an average thickness of 40 m (Mendes et al., 1966) and is well known for its oil-bearing rocks and fossils. This unit is divided into the lower Taquaral Member, comprising siltstones and gray claystones, and the upper Assistência Member, formed by organic-rich claystones intercalated with limestone lenses. Rocks of the Passa Dois Group are cut by Cretaceous basic intrusions, which represented an important heat source for the maturation of the organic matter in the claystones.

The PETROBRAS-Six represents one of the largest reserves of oil shale in the world. The ore is concentrated in two main horizons: i) a 6.4 m thick layer with 6.4% oil content that contains bentonic layers and ii) a 3.2 m thick layer with 9.1% oil content (Petrobras, 2005). Centimetric and continuous ash layers extending for hundreds of meters are well exposed in the mine quarry (Fig. 2) and allow a detailed sampling. These light gray-laminated layers are 2 to 4 cm thick and are intercalated with organic-rich sediments. Previous studies have interpreted these layers as the product of sporadic rhyolitic volcanism based on petrographic and geochemical data (Coutinho et al., 1988; Maynard et al., 1996). Based on geochemical and XRD diffraction data, Dos

Anjos (2008) concluded that both the ash layers and the adjacent sedimentary layers have a rhyolitic component.

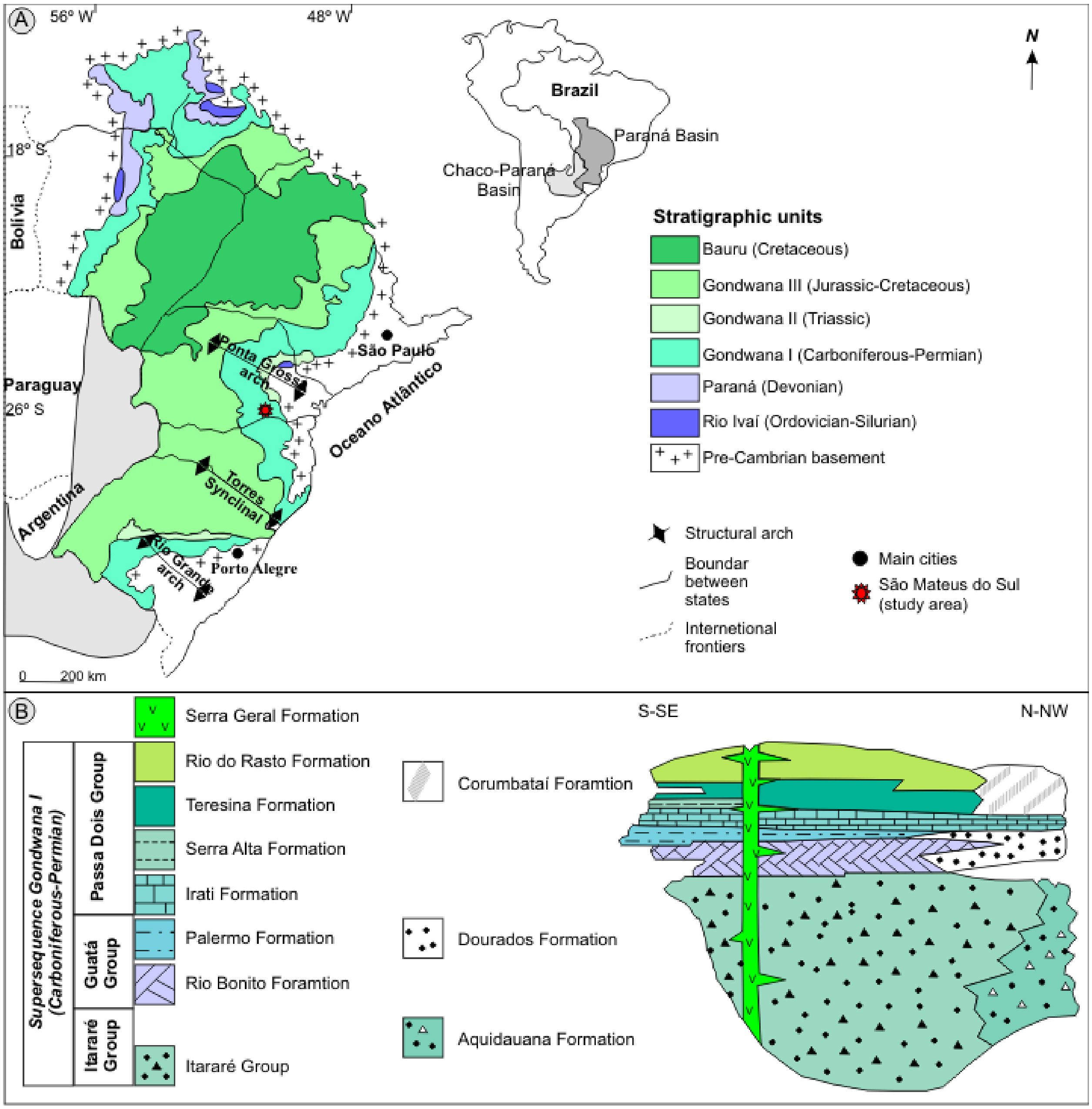

Fig. 1: a) Geologic map showing the distribution of stratigraphic units of the Paraná Basin. b) stratigraphic column of the Gondwana I Supersequence (modified of Mori *et al*., 2012).

3. Sampling and Methods

Ash layers were collected at the Six-Petrobras quarry, as shown in fig. 2. Samples of ash layers (SM-02, SM-04, SM-06, SM09, and SM-12) were collected across the succession and stored in plastic bags until processed in the lab.

All sample preparation and analyses were performed at the Geochronos Lab of the University of Brasília following Gioia and Pimentel (2000) for Sm-Nd, Bühn et al. (2009) for U-Pb zircon and Matteini el al. (2010) for Lu-Hf. The Sm-Nd analyses were carried out using a Thermo-Fisher 253 thermal ionization mass spectrometer (TIMS), and the U-Pb and Lu-Hf, in a Thermo-Fisher Neptune laser ablation multi-collector inductively coupled plasma mass spectrometer (LA-MC-ICP-MS).

Sample preparation U-Pb age determination involved grinding, sandblasting and separating the sample by magnetic susceptibility using isodynamic equipment. In this study, approximately 30 zircon grains from each concentrate were then chosen from under a binocular microscope and mounted in epoxy, together with reference zircons GJ-1. Later, the mounts were polished and observed under cathodoluminescence to observe their internal structures.

Zircon ages were obtained using LA-MC-ICP-MS, with ablation generated by moving the laser spot with a diameter of ~30 µm for 40 seconds. All data were processed using Isoplot/Ex (Ludwig, 2001) and software developed at the Geochronos Lab of University of Brasilia. The analytic processing consisted of reducing data showing points outside the regression line, very common Pb and high error. Then, a Concordia diagram (Wetherill, 1956) and a weighted average diagram (SM-06) were generated. In the latter case, it uses only the weighted average $^{206}Pb/^{238}U$ age, and avoids discordant data.

The measurement of Lu-Hf isotopes was performed on zircons previously analyzed by the laser ablation U-Pb method to determine the relationship among the Hf isotope ratios and age. The two spots analysed in each graing must be as close as possible in order to analyze portions of the zircon grain with the same isotopic characteristics (Matteini et al., 2010).

Zircons were selected based on the agreement factor of U-Pb ages (Conc. ≥ 90% e ≤ 110%). Fifty grains in the 5 ash layers were selected. Lu-Hf isotopic analysis was conducted using a spot ablation technique at the grain surface, with a diameter between 40 and 50 µm, for 40-50 seconds. The reference zircon GJ-1 was analyzed during the procedure for stabilization when reading data. The values $\varepsilon_{Hf(t)}$ combined with U-Pb age were calculated and plotted in binary diagrams that related the Hf isotopic variation to CHUR (Patchett e Tatsumoto et al. 1980; Patchett e Tatsumoto et al.1981; Patchett 1983). In the case of zircons older than 1 Ga, we used $^{207}Pb/^{206}Pb$ ratios, and in those younger than 1 Ga, we used $^{206}Pb/^{238}U$ ratios.

Sample dissolution for Sm and Nd isotopes was carried out using Teflon Savillex beakers or Parr-type Teflon bombs. Approximately 100 mg of each sample was spiked (^{149}Sm-^{150}Nd) and attacked with a heated mixture of concentrated HF and HNO3. After evaporation, HCl was added to each beaker. Once again, each sample was attacked with HCl 6N and prepared for chromatographic separation. Sm and Nd extraction was conducted following the technique of Richard et al. (1976) and Gioia and Pimentel (2000), in which the separation of the rare earth elements (REE) as a group using cation-exchange columns precedes reversed-phase chromatography for the separation of Sm and Nd using columns loaded with HDEHP (di-2-ethylhexeyl phosphoric acid) supported on Teflon powder. We also used the REE-Spec and Ln-Spec resins for REE and Sm-Nd separation. A mixed ^{149}Sm-^{150}Nd spike was used. Sm and Nd samples were loaded onto the Re evaporation filaments of a double filament assembly. Sm and Nd isotopic analyses were carried out using a Finningan MAT-262 mass spectrometer. Uncertainties on Sm/Nd and $^{143}Nd/^{144}Nd$ ratios are considered to be less than ± 0.1% (1σ) and 0.000001 (1σ), respectively, based on repeated analyses of international rock standards BCR-1 and BHVO-1. The $^{143}Nd/^{144}Nd$ ratios were normalized to a $^{146}Nd/^{144}Nd$ ratio of 0.7129. The Nd procedure blanks were smaller than 100 pg.

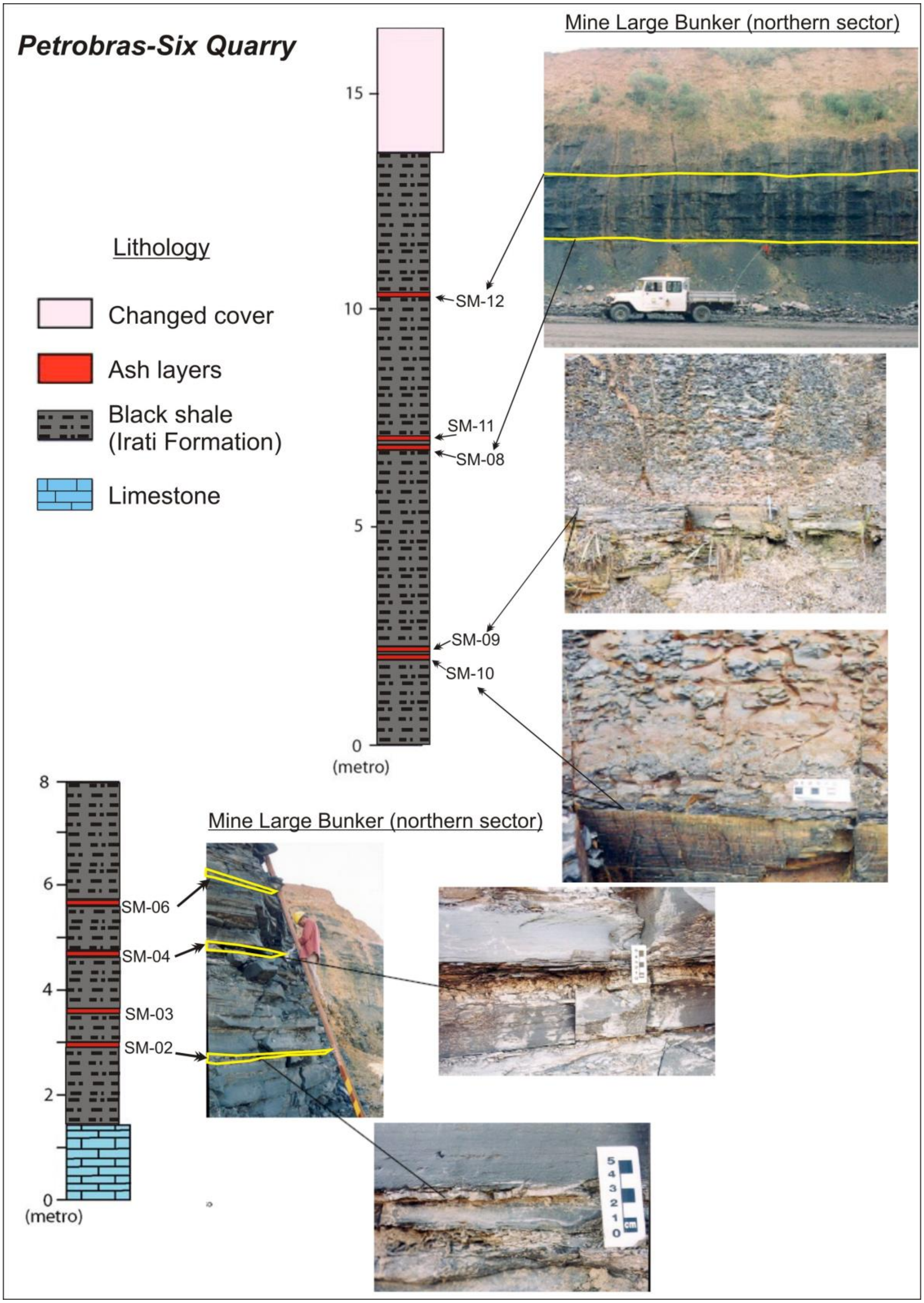

Fig. 2: Distribution of ash layers along the Irati Formation, exposed in the quarry PETROBRAS-Six, the city of São Mateus do Sul, Paraná (PR), Brazil.

4. Results

Cathodeluminescence images show that there are two main zircon populations in the analyzed samples (Fig. 3): i) a population of euhedral to subhedral grains that account for 80% of the zircon and are commonly zoned and have sizes varying between 50 to 200 µm ii) and a population of rounded and smaller grains that accounts for approximately 20% of the total grains.

The U-Pb data reveal that most zircons retrieved from the ash layers are Permian and have ages varying between 287 and 266 Ma (Appendix D), as shown in fig. 4, which presents the diagrams according to the stratigraphic position of the samples. Except for sample SM-02 (Fig. 4a), which has a zircon population that is 100% Permian, all other samples have a fraction of non-Permian grains that ranges between 19% and 45%. Most of these grains have ages varying between the Carboniferous and the Archaean. Concordia and weighted average (SM-06) diagrams, based on Permian zircons from each sample, exhibit the existence of 3 main volcanic events: 273-267 Ma, 279-278 Ma, and 287 Ma (Figs. 4a, 4b, 4c, 4d and 4e).

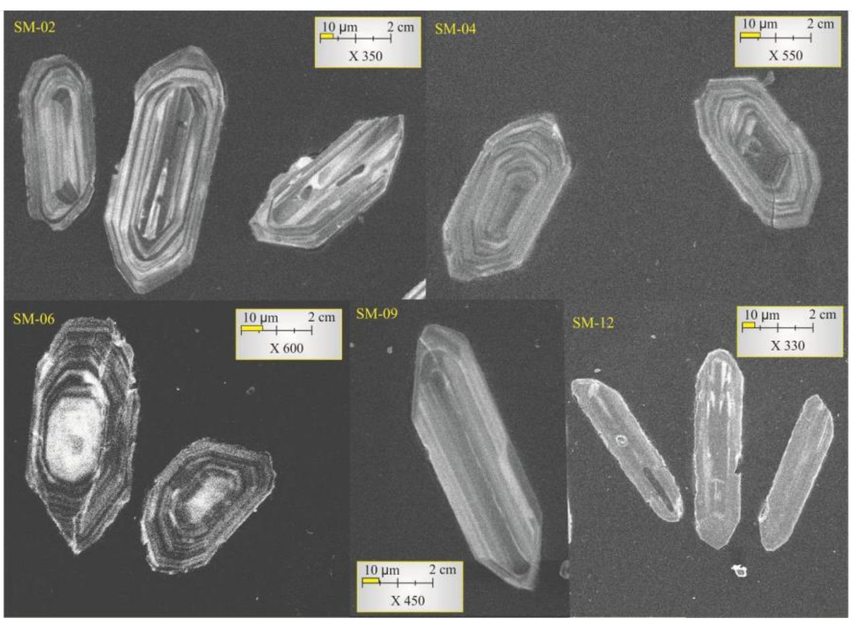

Fig. 3: Cathodoluminescence images showing the zircon grains of the ash layers that occur along the Irati Formation in PETROBRAS-Six.

The Lu-Hf data from each sample were obtained for a selected group of zircons (Figs. 5a, 5b, 5c, 5d and 5e) (Appendix E). Most ε_{Hf} values calculated for Permian zircons based on the weighted average ages fall near -7 and -3. Only sample SM-02 (Fig. 5a) has Permian zircons with ε_{Hf} values that are near zero or positive. These zircon grains present model ages ranging between 0.8 and 1.2 Ga. The Lu-Hf data of Precambrian zircons were obtained in samples SM-04 (Fig. 5b) and SM-12 (Fig. 5e). As shown in fig. 5, they have much more variable ε_{Hf} values and older model ages.

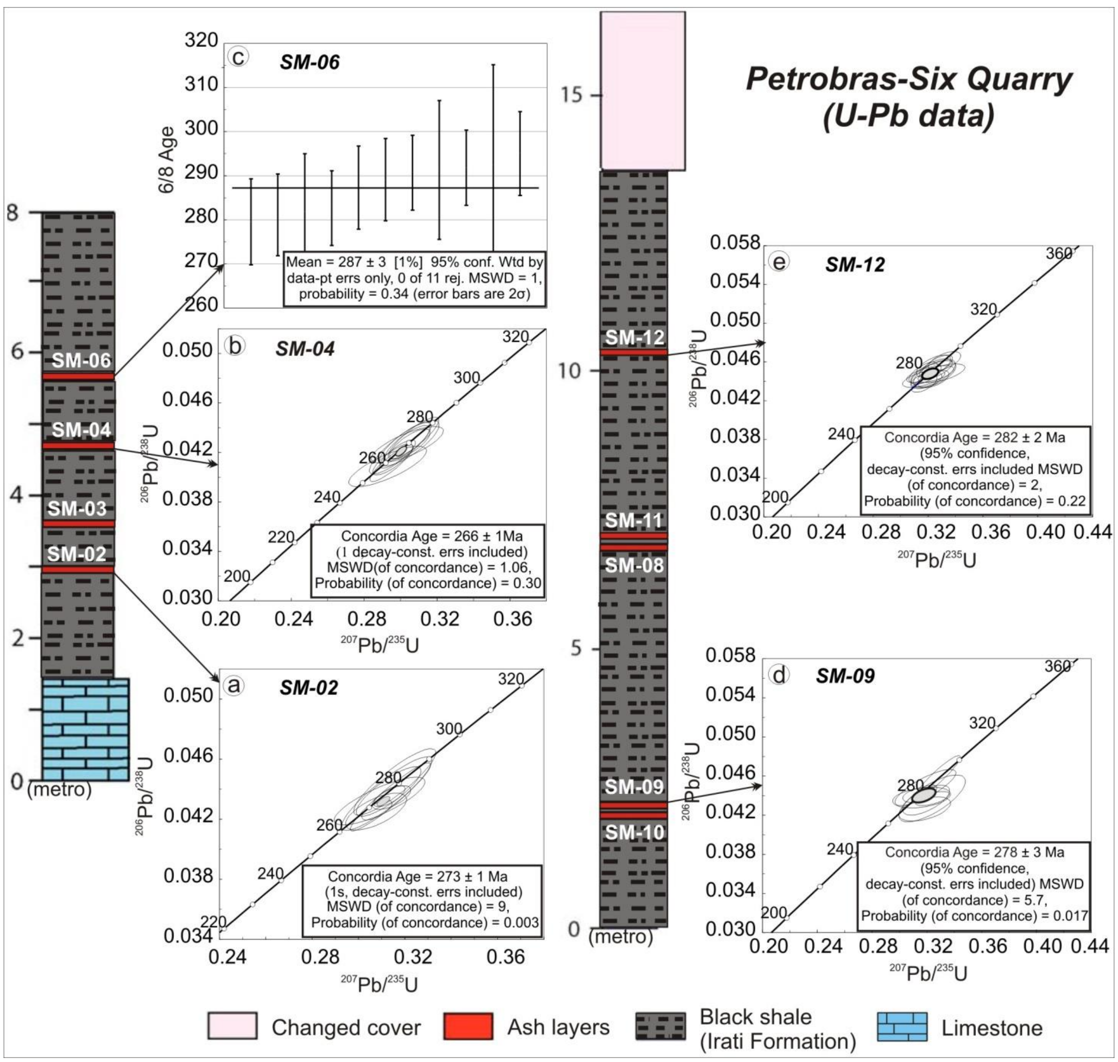

Fig. 4: Concordia diagram showing the U-Pb results obtained by LA-MC-ICP-MS for zircons of ash layer.

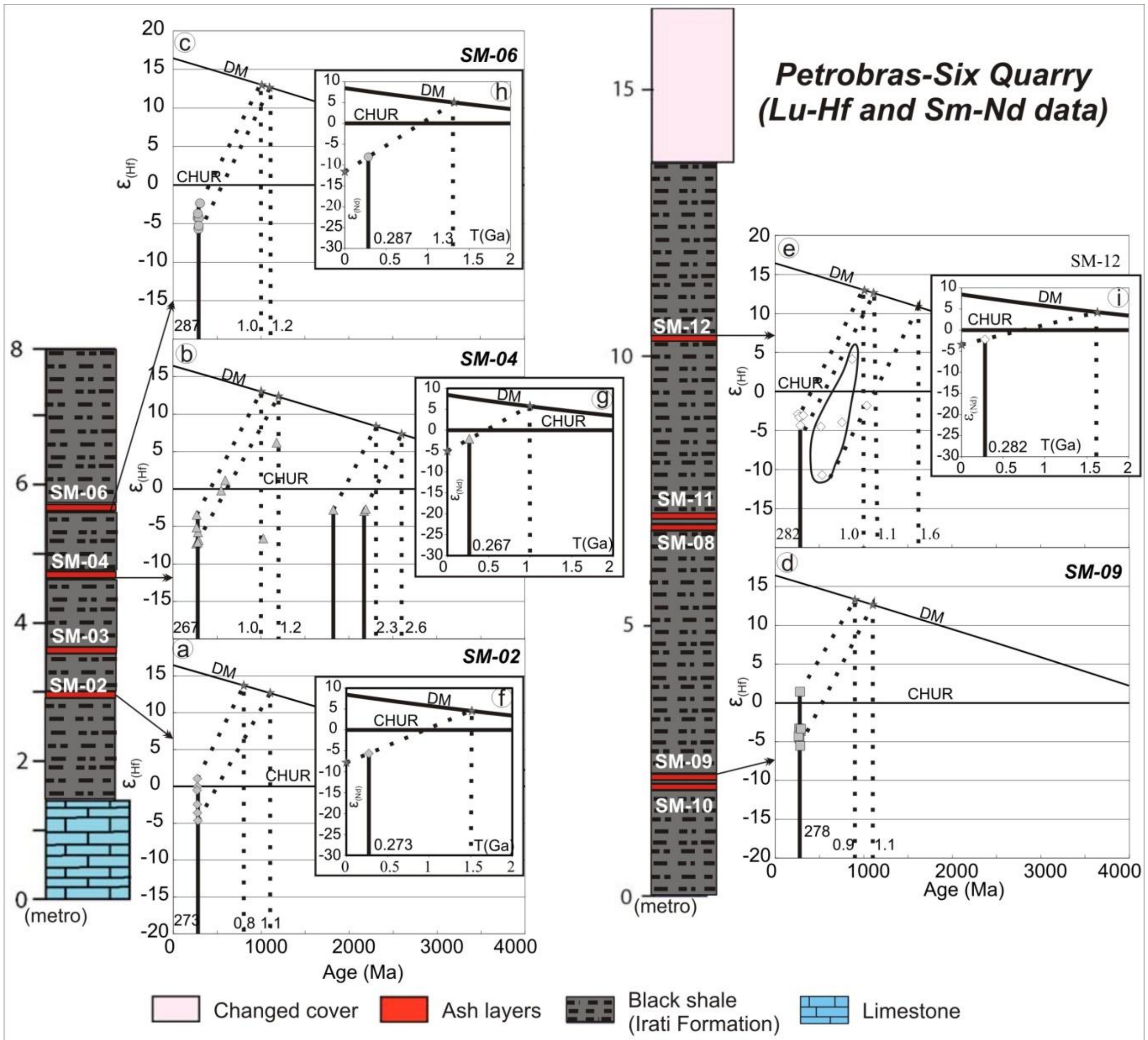

Fig. 5: Values $\varepsilon_{Hf(t)}$ combined with U-Pb age presente in diagrams a, b, c, d and e. Values $\varepsilon_{Nd(t)}$ *versus* T(Ga) are showing in f, g, h and i.

The whole-rock Sm-Nd data (Appendix F) of the ash layers are generally consistent with the Lu-Hf data and indicate a mixture of crustal and mantle sources (Figs. 5f, 5g, 5h and 5i). The Nd model ages calculated based on the weighted average ages vary between 1.0 Ga to 1.6 Ga, being older for sample SM-12 (Fig. 5i), which presents a larger population of Precambrian zircon grains. The calculated ε_{Nd} values are generally negative and vary between -3.3 and -11.6.

5. Discussion

Explosive volcanism may spread ashes over a very large area and, in many instances, even a globally (e.g., Campbell et al., 1992; Renne et al., 1995). These types of volcanic events are believed to have an important impact on the climate by promoting an abrupt change in average temperature over a short time interval. For instance, the last few decades were characterized by various volcanic events in western South America, as exemplified by those that happened in 2010-2011 in Chile and Argentina. The activity of the Puyehue–Cordón Caulle volcanic complex (Schipper et al., 2013), located in eastern Chile, delivered volcanic ash to the atmosphere that reached more than 15 km high and provoked a major impact on regional atmospheric conditions (Parejas et al., 2012). Because of the amount of dust particles delivered into the atmosphere, many airports were closed due to bad visibility. Available studies indicate that the volcanic ash spread all over the southern hemisphere and formed ash layers as far as 2,000 km from the source. Due to atmospheric circulation patterns, however, the most affected area was located to the east of the volcanic source (e.g., Argentina and Uruguay).

The Permian is also known to have had worldwide volcanic events with important impacts on biological communities and extinction (Isozaki, 2009; Stanley and Yang, 1994). For example, whereas the Permo-Triassic transition is marked by one of the largest biological extinction event of the Phanarezoic, the Middle-Late Permian G-LB, ca. 260 (Ma) is characterized by another less extensive biological extinction that was likely related to a cooling event known as Kamura (Isozaki, 2009; Isozaki et al., 2007b; Musashi et al., 2010). This cooling event was associated with extensive felsic volcanism that has the same age as the volcanic ash layers described herein.

The geochrological and isotope data presented here for the Six-Petrobras ash layers indicate that they have similar geochemical characteristics compared with the Choiyoi volcanism. Arguments in favor of Choiyoi volcanism as the main source of these ashes include the ash grain size, and the thickness of the layers, as well as their acid character, their lateral extension, and their similar age range (Coutinho et al., 1991; Coutinho e Hachiro, 2005; López-Gamundí, 2006; Rocha-Campos et al., 2006, 2011).

Based on SHRIMP geochronological data, Rocha-Campos et al. (2011) have identified 3 main volcanic pulses in Choiyoi with ages that range between 281.4 ± 2.5 Ma (early Permian), 264.7 ± 1.3 Ma (middle Permian) and 251.9 ± 2 Ma (Permian-Triássic transition). This 30 Ma age range is similar to that observed for the Permian zircons from the Petrobras-Six ash layers. Fig. 6, which compares the PETROBRAS-Six and Choiyoi zircon U-Pb data, show that the 2 older Choiyoi volcanic pulses compare favorably with our data. In particular, most zircons seem to be related to the 281 ± 2.5 Ma Choiyoi volcanic peak that corresponds to the Yacimiento Los Reyunos Formation.

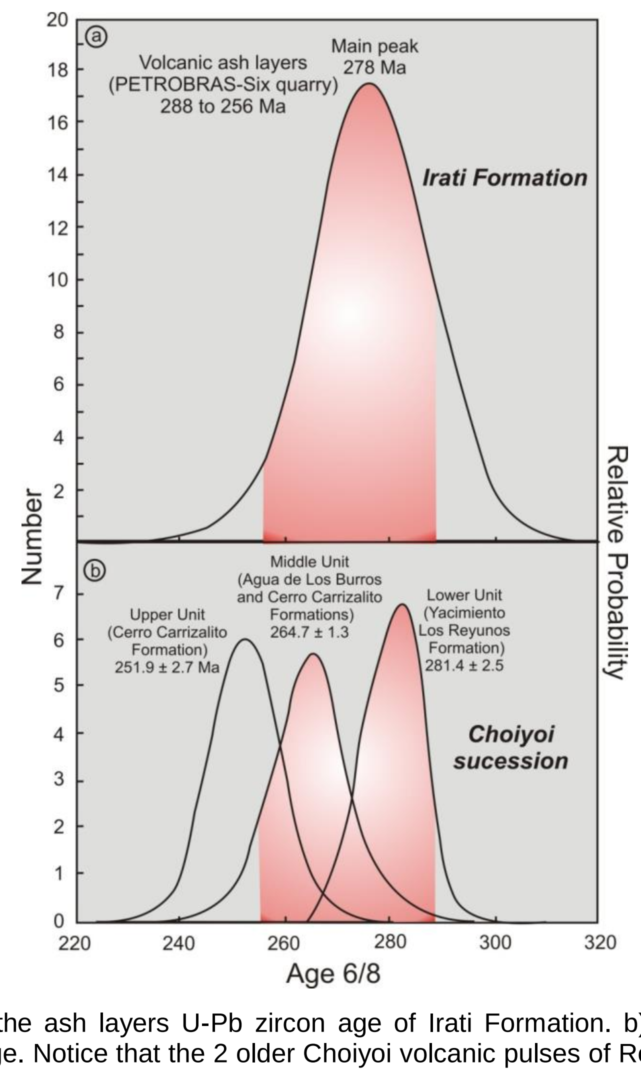

Fig. 6: a) Histogram of the ash layers U-Pb zircon age of Irati Formation. b) Irati Formation age (ash layers) *versus* Choiyoi age. Notice that the 2 older Choiyoi volcanic pulses of Rocha-Campos et al. (2011) superpose quite well to our data.

The relation of the PETROBRAS-SIX ashes to the Choiyoi volcanism is further reinforced by Lu-Hf isotope data. Fig. 7 compares the isotope data of Fanning et al. (2011) with the data of this study and shows that they have similar ε_{Hf} ranges. Whereas the Six-Petrobras samples have an ε_{Hf} ranging between 1.4 and -7.3, those from Choiyoi have an ε_{Hf} raging between 1.3 and -7.0. Similar to the U-Pb geochronological data, the Six-Petrobras data have a better match to 2 of the Choiyoi Peaks.

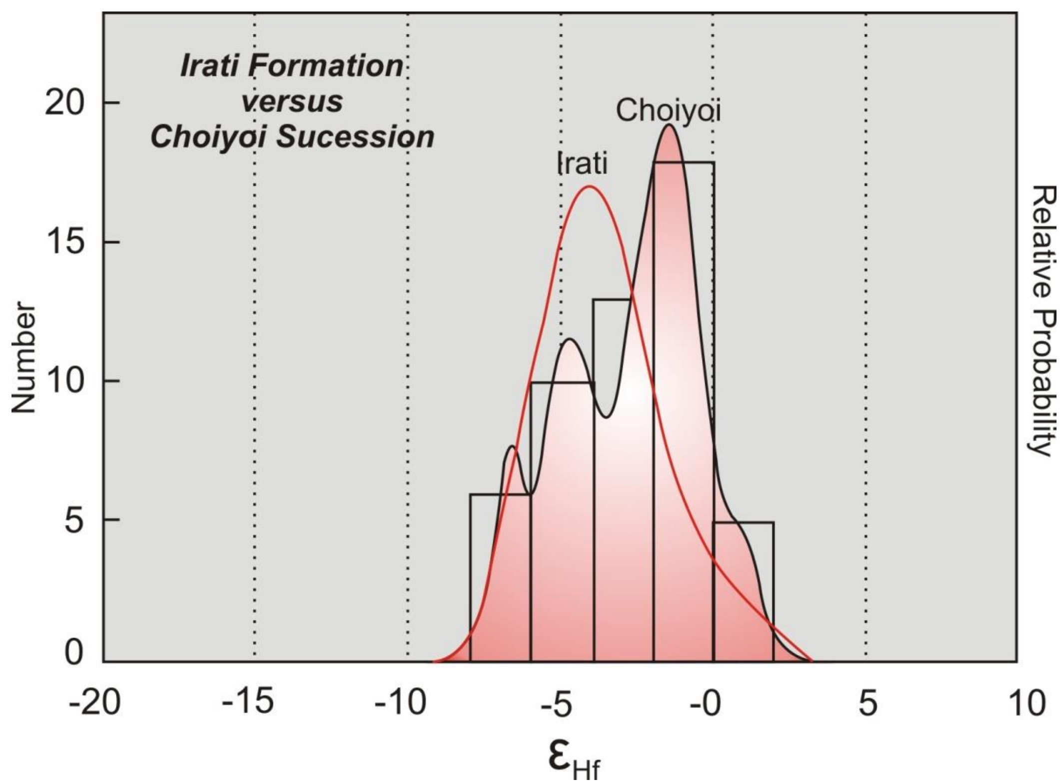

Fig. 7: Compares the isotope data of Fanning et al. (2011) with the data of this study and shows that they have a similar ε_{Hf} range.

The Choiyoi volcanism was likely related to an extense subduction zone that existed along Argentina, Chile, the Falklands and up to Antartica. This volcanism, which represents the youngest source of zircons found in the analyzed samples, may have traveled more than a thousand kilometers from its source (Fig. 8).

Available studies indicate that the Choiyoi volcanic event took place between 245 and 280 Ma, thus lasting approximately 30 Ma (Rocha-Campos et al., 2011). Other authors, however, argue that it could have initiated earlier, at 290 Ma (Bangert et al., 1999), thus indicating that it may have lasted even longer. The relationship between this volcanism and the granitic magmatism that extends between Chile and the Falklands (Hervé et al., 2006) is not clear, although they may have a similar age interval.

The U-Pb data presented here indicate that the Irati ash layers have zircon grains ranging between 266 and 288 Ma, which encompasses the younger zircon age peaks reported by Rocha-Campos et al. (2011) for the Choiyoi volcanics. The younger age, which was observed in sample SM004, also set a new minimum age of 266 ± 1 Ma for the Irati formation, which is approximately 12 Ma younger than that reported by Santos et al., (2006). These new minimum Irati age data, which will also impact the current biostratigraphic correlation between Gondwana areas, as discussed by Santos et al., (2006), are similar to the 270 Ma (Turner, 1999) and 264-268 Ma (Lanci et al., 2013) zircon ages for Karoo ash layers.

6. Conclusions

The zircon U-Pb data from the volcanic ash interlayered with sediment of the Irati Formation indicate ages ranging between 287 and 267 Ma, with a main peak at 278 Ma. The Lu-Hf data of these zircons indicate a crustal signature ε_{Hf} ranging between -7 and -3 and Mesoproterozoic 1.2 (Ga) and Neoproterozoic 0.8 (Ga) Hf (T_{DM}) model ages. The Nd isotope data reinforce the zircon data, indicating a main crustal component in the source area of these rocks ε_{Nd} = -11.6 to -3.3.

Based on these data, we conclude that the Irati ash layers are contemporaneous and have the same isotope signature as the volcanic rocks of the Choiyoi Province. They further show that the Irati recorded the last 15 Ma of this volcanic activity, which according to Rocha-Campos et al. (2014), lasted approximately 30 Ma. Finally, we propose that the Irati has an age of 266-267 Ma, not 178 Ma, as previously reported by Santos et al. (2006).

Fig. 8: Location map of Choiyoi Province. The figure also shows the occurrence area of the ash layers in the city of São Mateus do Sul (PR).

Appendix D: Summary U-Pb zircon results for ash layers Irati Formation by LA-MC-ICP-MS.

Sample/Grain	7/6 ratio	1s(%)	7/5 ratio	1s(%)	6/8 ratio	1s(%)	rho	7/6 age	1s(%)	7/5 age	1s(%)	6/8 age	1s(%)	Conc (%)
SM-02														
Z5	0.0516	0.96	0.2962	1.40	0.04160	1.02	0.71	269	22	263	3	263	3	98
Z12	0.0518	1.63	0.3018	1.79	0.04223	0.72	0.61	277	37	268	4	267	2	96
Z1	0.0522	2.17	0.3046	2.45	0.04230	1.13	0.45	295	49	270	6	267	3	91
Z10	0.0512	1.30	0.2998	1.47	0.04245	0.68	0.42	250	30	266	3	268	2	107
Z38	0.0513	1.27	0.3001	1.52	0.04246	0.84	0.52	253	29	266	4	268	2	106
Z30	0.0525	1.28	0.3076	1.74	0.04251	1.18	0.66	306	29	272	4	268	3	88
Z43	0.0524	0.59	0.3079	0.86	0.04261	0.63	0.68	303	13	273	2	269	2	89
Z11	0.0524	0.76	0.3097	1.01	0.04286	0.66	0.61	303	17	274	2	271	2	89
Z31	0.0522	2.32	0.3084	2.49	0.04289	0.92	0.59	292	52	273	6	271	2	93
Z14	0.0518	1.13	0.3064	1.36	0.04292	0.76	0.52	275	26	271	3	271	2	98
Z8	0.0520	1.81	0.3093	1.97	0.04310	0.80	0.62	287	41	274	5	272	2	95
Z19	0.0519	2.11	0.3091	2.59	0.04321	1.50	0.81	280	48	273	6	273	4	97
Z46	0.0517	1.96	0.3083	2.16	0.04328	0.90	0.64	270	45	273	5	273	2	101
Z36	0.0525	0.79	0.3143	1.08	0.04344	0.74	0.65	306	18	277	3	274	2	90
Z16	0.0523	0.73	0.3138	2.26	0.04349	2.13	0.95	300	17	277	5	274	6	91
Z7	0.0522	0.58	0.3133	0.88	0.04354	0.66	0.71	294	13	277	2	275	2	93
Z25	0.0518	1.13	0.3121	2.55	0.04370	2.28	0.89	277	26	276	6	276	6	100
Z39	0.0524	0.95	0.3158	1.22	0.04371	0.76	0.59	303	22	279	3	276	2	91
Z28	0.0518	0.98	0.3130	1.83	0.04384	1.54	0.84	275	22	276	4	277	4	100
Z42	0.0525	1.69	0.3174	1.81	0.04385	0.63	0.54	307	38	280	4	277	2	90
Z32	0.0519	0.69	0.3162	0.96	0.04422	0.66	0.64	280	16	279	2	279	2	100
Z34	0.0520	0.75	0.3172	0.97	0.04424	0.62	0.58	286	17	280	2	279	2	98
Z26	0.0515	1.06	0.3156	2.29	0.04448	2.03	0.88	262	24	279	6	281	6	107
Z22	0.0525	0.76	0.3228	1.28	0.04456	1.02	0.79	309	17	284	3	281	3	91
Z45	0.0516	0.66	0.3201	1.00	0.04500	0.75	0.72	268	15	282	2	284	2	106
Z44	0.0522	0.76	0.3241	1.03	0.04501	0.70	0.64	295	17	285	3	284	2	96
SM-04														
Z20	0.0520	2.48	0.2929	2.97	0.04087	1.63	0.78	285	57	261	7	258	4	91
Z21	0.0520	0.75	0.2951	1.65	0.04113	1.47	0.89	287	17	263	4	260	4	91
Z11	0.0518	0.87	0.2957	1.52	0.04144	1.24	0.81	275	20	263	4	262	3	95
Z6	0.0517	0.74	0.2983	1.34	0.04187	1.12	0.82	271	17	265	3	264	3	98
Z32	0.0514	1.14	0.2998	2.31	0.04234	2.01	0.87	257	26	266	5	267	5	104
Z31	0.0517	2.25	0.3037	2.66	0.04262	1.41	0.76	271	52	269	6	269	4	99
Z10	0.0518	0.93	0.3051	1.49	0.04269	1.16	0.77	278	21	270	4	270	3	97
Z37	0.0515	0.93	0.3036	1.65	0.04275	1.36	0.82	264	21	269	4	270	4	102
Z25	0.0517	1.32	0.3047	2.20	0.04276	1.76	0.80	271	30	270	5	270	5	99

Appendix D (*Continued*)

Sample/Grain	7/6 ratio	1s(%)	7/5 ratio	1s(%)	6/8 ratio	1s(%)	rho	7/6 age	1s(%)	7/5 age	1s(%)	6/8 age	1s(%)	Conc (%)
Z24	0.0516	0.93	0.3070	1.84	0.04316	1.59	0.86	268	21	272	4	272	4	102
Z14	0.0522	2.14	0.3116	2.43	0.04325	1.15	0.46	296	49	275	6	273	3	92
Z35	0.0512	2.87	0.3073	3.17	0.04357	1.36	0.67	248	66	272	8	275	4	111
Z36	0.0572	0.61	0.6984	1.59	0.08862	1.47	0.92	498	13	538	7	547	8	110
Z22	0.0590	1.26	0.7857	1.92	0.09656	1.45	0.75	568	27	589	9	594	8	105
Z30	0.0735	0.58	1.7330	1.46	0.17101	1.34	0.91	1028	12	1021	9	1018	13	99
Z26	0.0793	0.95	2.1448	1.63	0.19623	1.32	0.80	1179	19	1163	11	1155	14	98
Z9	0.1224	0.50	5.1401	1.45	0.30446	1.36	0.94	1992	9	1843	12	1713	20	86
Z7	0.1196	0.45	5.1396	1.26	0.31163	1.18	0.93	1950	8	1843	11	1749	18	90
Z05	0.1115	0.69	4.8830	1.53	0.31761	1.36	0.89	1824	12	1799	13	1778	21	97
Z17	0.1200	0.47	5.5168	1.43	0.33347	1.35	0.94	1956	8	1903	12	1855	22	95
Z8	0.2053	0.80	11.0834	3.76	0.39149	2.04	0.97	2869	13	2530	34	2130	66	74
Z12	0.1833	0.50	12.0603	1.18	0.47726	1.07	0.94	2683	8	2609	11	2515	22	94
SM-06														
Z11	0.0549	1.42	0.3227	1.53	0.04261	0.56	0.311	409	32	284	4	269	1	66
Z26	0.0603	1.71	0.3607	1.86	0.04335	0.74	0.366	616	36	313	5	274	2	44
Z7	0.0532	1.41	0.3248	1.55	0.04432	0.64	0.365	336	32	286	4	280	2	83
Z9	0.0567	2.11	0.3483	2.19	0.04458	0.60	0.234	479	46	303	6	281	2	59
Z38	0.0633	2.60	0.3898	2.73	0.04468	0.85	0.290	717	55	334	8	282	2	39
Z37	0.0577	1.97	0.3568	2.04	0.04482	0.54	0.218	520	43	310	5	283	1	54
Z10	0.0600	1.92	0.3768	2.01	0.04557	0.58	0.248	602	42	325	6	287	2	48
Z33	0.0568	1.39	0.3593	1.50	0.04587	0.57	0.324	484	30	312	4	289	2	60
Z25	0.0620	1.88	0.3944	1.95	0.04612	0.51	0.210	675	40	338	6	291	1	43
Z5	0.0601	1.72	0.3832	1.97	0.04623	0.95	0.461	608	37	329	6	291	3	48
Z14	0.0648	2.69	0.4136	2.74	0.04631	0.51	0.148	767	57	351	8	292	1	38
Z6	0.0560	1.69	0.3584	2.17	0.04639	1.37	0.619	454	38	311	6	292	4	64
Z13	0.0603	1.95	0.3896	2.02	0.04683	0.56	0.230	616	41	334	6	295	2	48
Z15	0.0666	2.86	0.4453	2.94	0.04847	0.69	0.210	827	59	374	9	305	2	37
Z35	0.0641	3.08	0.5430	3.12	0.06147	0.50	0.236	744	64	440	11	385	2	52
Z2	0.0592	1.10	0.5119	1.50	0.06272	1.02	0.662	574	24	420	5	392	4	68
Z24	0.0809	0.90	1.8479	1.22	0.16556	0.82	0.646	1220	18	1063	8	988	8	81
SM-09														
Z7	0.0546	1.93	0.3112	2.20	0.04130	1.05	0.459	398	43	275	5	261	3	66
Z37	0.0524	1.63	0.3075	2.63	0.04253	2.06	0.781	305	37	272	6	268	5	88
Z18	0.0541	2.11	0.3184	2.42	0.04265	1.19	0.478	377	47	281	6	269	3	71
Z49	0.0528	1.17	0.3125	1.38	0.04294	0.73	0.487	320	27	276	3	271	2	85
Z52	0.0543	1.04	0.3218	1.19	0.04301	0.58	0.422	382	23	283	3	271	2	71

Appendix D (*Continued*)

Sample/Grain	7/6 ratio	1s(%)	7/5 ratio	1s(%)	6/8 ratio	1s(%)	rho	7/6 age	1s(%)	7/5 age	1s(%)	6/8 age	1s(%)	Conc (%)
Z29	0.0532	1.66	0.3194	2.20	0.04355	1.43	0.643	337	37	281	5	275	4	81
Z46	0.0520	1.04	0.3133	1.28	0.04366	0.76	0.553	288	24	277	3	275	2	96
Z47	0.0538	1.41	0.3240	1.56	0.04371	0.67	0.603	361	31	285	4	276	2	76
Z33	0.0537	2.08	0.3238	3.06	0.04372	2.24	0.730	359	46	285	8	276	6	77
Z3	0.0523	2.55	0.3162	2.73	0.04381	0.98	0.342	300	58	279	7	276	3	92
Z1	0.0517	1.35	0.3142	1.53	0.04408	0.72	0.432	272	31	277	4	278	2	102
Z22	0.0534	1.25	0.3249	1.42	0.04415	0.68	0.433	345	28	286	4	278	2	81
Z34	0.0552	1.21	0.3365	2.49	0.04425	2.18	0.873	418	27	294	6	279	6	67
Z27	0.0508	1.88	0.3100	2.12	0.04427	0.98	0.679	231	43	274	5	279	3	121
Z40	0.0542	1.59	0.3315	2.15	0.04437	1.46	0.667	379	36	291	5	280	4	74
Z56	0.0522	0.75	0.3202	0.92	0.04451	0.53	0.500	293	17	282	2	281	1	96
Z39	0.0516	2.29	0.3190	2.85	0.04484	1.69	0.809	268	52	281	7	283	5	106
Z6	0.0529	1.30	0.3304	1.50	0.04531	0.76	0.469	324	30	290	4	286	2	88
Z2	0.0522	1.07	0.3267	1.28	0.04540	0.71	0.515	294	24	287	3	286	2	97
Z54	0.0522	0.70	0.3290	0.93	0.04575	0.62	0.608	292	16	289	2	288	2	99
Z38	0.0518	0.72	0.3282	2.03	0.04597	1.89	0.933	276	16	288	5	290	5	105
Z53	0.0537	1.07	0.4138	1.30	0.05583	0.73	0.521	360	24	352	4	350	2	97
Z23	0.0593	0.63	0.7102	0.96	0.08689	0.72	0.716	578	14	545	4	537	4	93
Z42	0.0600	0.61	0.8084	1.27	0.09766	1.11	0.870	605	13	602	6	601	6	99
Z14	0.0687	1.07	1.0572	1.99	0.11159	1.68	0.839	890	22	732	10	682	11	77
Z9	0.0729	1.67	1.2414	2.48	0.12349	1.84	0.737	1011	34	820	14	751	13	74
Z25	0.0736	0.70	1.5440	1.25	0.15208	1.04	0.818	1031	14	948	8	913	9	88
Z26	0.0735	0.67	1.5497	1.08	0.15286	0.84	0.756	1029	14	950	7	917	7	89
Z48	0.0746	0.58	1.6936	1.10	0.16470	0.94	0.837	1057	12	1006	7	983	9	93
SM-12														
Z37	0.0520	1.11	0.2991	1.94	0.04170	1.60	0.817	287	25	266	5	263	4	92
Z27	0.0526	2.04	0.3030	2.41	0.04180	1.28	0.760	311	46	269	6	264	3	85
Z28	0.0524	1.29	0.3060	1.62	0.04238	0.99	0.587	301	29	271	4	268	3	89
Z35	0.0513	2.07	0.3005	2.22	0.04251	0.79	0.555	252	48	267	5	268	2	106
Z23	0.0521	0.95	0.3103	1.35	0.04320	0.96	0.693	289	21	274	3	273	3	94
Z13	0.0530	1.17	0.3158	1.66	0.04322	1.19	0.700	328	26	279	4	273	3	83
Z45	0.0514	1.36	0.3083	1.77	0.04353	1.13	0.623	257	31	273	4	275	3	107
Z24	0.0523	2.24	0.3152	2.43	0.04371	0.95	0.611	298	51	278	6	276	3	92
Z43	0.0526	0.87	0.3173	1.18	0.04374	0.81	0.651	312	20	280	3	276	2	88
Z17	0.0505	1.76	0.3064	2.02	0.04402	0.99	0.472	217	41	271	5	278	3	128
Z25	0.0524	1.23	0.3187	1.46	0.04410	0.79	0.505	303	28	281	4	278	2	92
Z15	0.0531	1.16	0.3238	1.43	0.04424	0.84	0.557	332	26	285	4	279	2	84

Appendix D (*Continued*)

Sample/Grain	7/6 ratio	1s(%)	7/5 ratio	1s(%)	6/8 ratio	1s(%)	rho	7/6 age	1s(%)	7/5 age	1s(%)	6/8 age	1s(%)	Conc (%)
Z42	0.0519	1.81	0.3168	1.98	0.04427	0.82	0.610	281	41	279	5	279	2	100
Z11	0.0525	1.63	0.3239	2.08	0.04472	1.28	0.607	309	37	285	5	282	4	91
Z12	0.0521	2.02	0.3216	2.19	0.04473	0.83	0.589	292	46	283	5	282	2	97
Z30	0.0516	1.05	0.3185	1.43	0.04475	0.97	0.655	269	24	281	4	282	3	105
Z9	0.0525	1.43	0.3246	1.93	0.04483	1.30	0.662	308	32	285	5	283	4	92
Z39	0.0533	1.93	0.3298	2.12	0.04484	0.87	0.610	343	43	289	5	283	2	82
Z26	0.0511	0.94	0.3165	1.35	0.04493	0.97	0.696	244	22	279	3	283	3	116
Z49	0.0521	1.20	0.3257	1.51	0.04532	0.90	0.576	291	28	286	4	286	3	98
Z34	0.0516	1.21	0.3239	1.59	0.04556	1.02	0.625	266	28	285	4	287	3	108
Z14	0.0519	0.99	0.3266	1.39	0.04562	0.98	0.682	282	23	287	3	288	3	102
Z38	0.0523	1.16	0.3320	1.46	0.04608	0.88	0.577	297	26	291	4	290	2	98
Z46	0.0513	1.83	0.3281	2.04	0.04638	0.92	0.653	255	42	288	5	292	3	115
Z10	0.0543	1.54	0.3501	1.82	0.04678	0.97	0.512	382	34	305	5	295	3	77
Z20	0.0524	2.41	0.3492	2.61	0.04831	1.00	0.606	304	54	304	7	304	3	100
Z33	0.0565	1.13	0.3861	1.75	0.04958	1.34	0.756	471	25	331	5	312	4	66
Z19	0.0530	1.42	0.3713	1.90	0.05083	1.26	0.653	328	32	321	5	320	4	97
Z1	0.0580	2.39	0.6674	3.24	0.08342	2.20	0.674	531	52	519	13	517	11	97
Z41	0.0595	1.51	0.7071	2.54	0.08625	2.05	0.801	584	33	543	11	533	10	91
Z36	0.0628	1.02	0.8622	1.47	0.09950	1.06	0.705	703	22	631	7	611	6	87
Z18	0.0646	1.04	1.1100	1.88	0.12466	1.56	0.829	761	22	758	10	757	11	100

Appendix E: Lu-Hf isotope composition of zircon for ash layers Irati Formation by LA-MC-ICP-MS.

Sample	$^{176}Lu/^{177}Hf$ (±2σ)	$^{176}Hf/^{177}Hf$ (±2σ)	$^{176}Hf/^{177}Hf(t)$	$\varepsilon_{Hf(t)}$(±2σ)	$T_{DM(Ga)}$	Age (Ma)
SM-02						
Z14	0.0010 ±19	0.28261 ±49	0.28260	-1±0.013	0.9	271
Z19	0.00076 ±10	0.28255 ±46	0.28254	-2 ±0.07	1.0	273
Z25	0.00088 ±14	0.28251 ±62	0.28251	-4 ±0.14	1.0	276
Z26	0.00075 ±22	0.28248 ±66	0.28248	-5 ±0.23	1.1	281
Z28	0.00085 ±40	0.28261 ±66	0.28261	0±0.001	0.9	277
Z46	0.00067 ±16	0.28265 ±62	0.28264	1 ±0.03	0.8	273
SM-04						
Z2	0.00197 ±122	0.28242±42	0.282409	-7 ±0.6	1.2	291
Z6	0.00143 ±97	0.28242±29	0.282413	-7 ±0.6	1.2	264
Z10	0.00183 ±369	0.28253±172	0.282518	-3 ±0.7	1.0	270
Z18	0.00085 ±45	0.28245±45	0.282443	-6 ±0.4	1.1	285
Z29	0.00142 ±50	0.28241±34	0.282407	-7 ±0.4	1.2	281
Z25	0.00096 ±31	0.28247±50	0.282470	-5 ±0.3	1.1	270
Z22	0.00072 ±29	0.28245±56	0.282443	1 ±0.1	1.1	594
Z36	0.00261 ±140	0.28246±56	0.282434	0 ±0.0	1.2	547
Z30	0.00145 ±56	0.28198±74	0.281948	-7 ±0.3	1.8	1028
Z26	0.00164 ±36	0.28225±33	0.282212	6 ±0.2	1.4	1179
Z5	0.00113 ±36	0.28158±31	0.281543	-3 ±0.1	2.3	1824
Z4	0.00109 ±38	0.281356±38	0.281310	-3 ±0.1	2.6	2174
Z23	0.00148 ±32	0.28137±43	0.281305	-3 ±0.1	2.6	2194
SM-06						
Z4	0.00099 ±22	0.28245±207	0.282447	-6 ±0.2	1.1	287
Z5	0.00108 ±27	0.28246±48	0.282452	-5 ±0.2	1.1	291
Z6	0.00125 ±39	0.28249±58	0.282481	-4 ±0.2	1.1	292
Z7	0.00090 ± 41	0.28249±65	0.282488	-4 ±0.2	1.1	280
Z9	0.00088 ±19	0.28251±44	0.282503	-4 ±0.1	1.0	281
Z10	0.00105 ±26	0.28245±67	0.282444	-6 ±0.2	1.1	287
Z2	0.00152 ±53	0.28239±150	0.282382	-6 ±0.3	1.2	392
Z15	0.00100 ± 27	0.28238±126	0.282377	-8 ±0.3	1.2	305
Z31	0.00208 ± 57	0.28261± 81	0.282598	0 ±0.0	0.9	311
Z32	0.00085 ± 10	0.28253±54	0.282527	-2 ±0.0	1.0	304
Z35	0.00227 ± 47	0.28249±84	0.282471	-3 ±0.1	1.1	385
SM-09						
Z51	0.00082 ± 41	0.28252 ±34	0.282520	-3 ±0.2	1.0	272
Z56	0.00241 ± 47	0.28266 ±36	0.282649	1 ±0.0	0.9	281
Z54	0.00092 ± 17	0.28251 ±35	0.282501	-4 ±0.1	1.0	288
Z46	0.00106 ± 77	0.28249 ±55	0.282482	-5 ±0.4	1.1	275
Z43	0.00068 ± 9	0.28250 ±29	0.282497	-4 ±0.1	1.0	265
Z39	0.00075 ± 45	0.28245 ±50	0.282451	-6 ±0.4	1.1	283
Z38	0.00044 ± 29	0.28251 ±39	0.282509	-3 ±0.3	1.0	290
Z53	0.00238 ±110	0.28263 ±59	0.282615	2 ±0.1	0.9	350
Z23	0.00075 ± 52	0.28245 ±44	0.282438	0 ±0.0	1.1	537
Z48	0.00088 ± 38	0.28233 ±36	0.282316	7 ±0.4	1.3	1057
SM-12						
Z2	0.00105 ± 34	0.28255 ±43	0.282540	-3 ±0.1	1.0	259
Z14	0.00125 ± 53	0.28252 ±46	0.282512	-3 ±0.2	1.0	288
Z45	0.00119 ± 38	0.28253 ±53	0.282519	-3 ±0.1	1.0	275
Z49	0.00102 ± 56	0.28249 ±42	0.282483	-4 ±0.3	1.1	286
Z41	0.00269 ± 70	0.28217 ± 191	0.282146	-11 ±0.5	1.6	533
Z1	0.00043 ± 16	0.28234 ± 55	0.282332	-4 ±0.3	1.3	517
Z18	0.00103 ± 13	0.28221 ±164	0.282195	-4 ±0.1	1.5	757
Z19	0.00096 ± 7	0.28250 ±188	0.282498	-3 ±0.1	1.0	320
Z8	0.00145 ± 73	0.28237 ± 101	0.282351	4 ±0.3	1.2	871
Z47	0.00059 ± 17	0.28209 ±277	0.282077	-2 ±0.1	1.6	1037

Appendix F: Sm-Nd whole-rock results for samples of ash layers Irati Formation by TIMS.

Sample	Sm(ppm)	Nd(ppm)	$^{147}Sm/^{144}Nd$	$^{143}Nd/^{144}Nd$ (±2σ)	$\varepsilon_{Nd(t)}$	T_{DM} (Ga)
SM-02	3.163	14.284	0,1339	0,512243+/-13	-7,71	1,51
SM-04	7.265	39.951	0,1099	0,512380+/-16	-5,03	0,97
SM-06	1.470	8.988	0,0988	0,512043+/-20	-11,61	1,32
SM-12	3.416	12.838	0,1608	0,512467+/-9	-3,34	1,64

References

Bangert, B., Stollhofen, H., Lorenz, V., Armstrong, R.L., 1999. The geochronology and significance of ash-fall tuffs in the glacigenic, Carboniferous-Permian Dwyka Group of Namibia and South Africa. Journal of African Earth Sciences 29, 33–49.

Becker, L., Poreda, R.J., Hunt, A.G., Bunch, T.E., Rampino, M., 2001. Impact event at the Permian-Triassic boundary: evidence from extraterrestrial noble gases in fullerenes. Science 291, 1530–1533. doi:10.1126/science.291.5508.1530.

Campbell, I.H., Czamanske, G.K., Fedorenko, V.A., Hill, R.I., Stepanov, V., 1992. Synchronism of the Siberian Traps and the Permian-Triassic Boundary. Science 258, 1760–1763. doi:10.1126/science.258.5089.1760.

Coutinho, J.M.V.; Hachiro, J.; Coimbra, A.M.; Santos, P.R. 1991. Ash-fall derived vitroclastic tuffaceous sediments in the Permian of the Paraná Basin and their provenance. In: Ulbrich, H. & Rocha-Campos, A.C. eds.. Gondwana Seven. São Paulo: Universidade de São Paulo, p. 147-160.

Coutinho, J.M.V., Hachiro, J., 2005. Distribution, mineralogy, petrography, provenance and significance of Permian ash-carrying deposits in the Paraná Basin. Revista do Instituto de Geociências 5, 29–39.

dos Anjos, C.W.D Guimarães, E.M., Souza, P.A. 2006. Mineralogia e palinologia de níveis de folhelhos negros da Formação Irati Permiano nas porções norte e sul da Bacia do Paraná. Resumo expandido. XLIII Congresso Brasileiro de Geologia.

dos Anjos, C.W.D. 2008. Fatores condicionantes na gênese dos argilominerais dos folhelhos negros e pelitos associados da Formação Iratí no norte da Bacia do Paraná. Tese de Doutorado, Faculté des Sciences Fondamentales et Appliquées, Universidade de Poitiers, França, p124.

Erwin, D., 1990. The End-Permian Mass Extinction. Annual Review of Ecology and Systematics 21, 69–91. doi:10.1146/annurev.ecolsys.21.1.69

Faure, K., Cole, D., 1999. Geochemical evidence for lacustrine microbial blooms in the vast Permian Main Karoo, Paraná, Falkland Islands and Huab basins of southwestern Gondwana. Palaeogeography, Palaeoclimatology, Palaeoecology 152, 189–213.

Faure, G. and Mensing, T. 2005. Isotopes: Principles and Applications. 3rd Edition, ISBN-13: 978-0471384373, ISBN-10: 0471384372.

Fanning, C. M.; Hervé F., Pankhurst, R. J.; Rapela, C. W.; Kleimane, L. E., Yaxley, G. M.; Castillo, P. 2011. Lu-Hf isotope evidence for the provenance of Permian detritus in accretionary complexes of western Patagonia and the northern Antarctic Peninsula region. *Journal of South American Earth Sciences*, 32: 485-496.

Hervé, F., Faúndez, V., Brix, M., Fanning, M., 2006. Jurassic sedimentation of the Miers Bluff formation, Livingston Island, Antarctica: evidence from SHRIMP UePb ages of detrital and plutonic zircons. Antarctic Science 18, 229-238.

Hervé F., Fanning C. M., Calderón M. and Mpodozis C. 2014 Early Permian to Late Triassic batholiths of the Chilean Frontal Cordillera 28°–31°S: SHRIMP U–Pb zircon ages and Lu–Hf and O isotope systematics. *LITHOS* **184-187**, 436–446.

Isozaki, Y., 2003. Guadalupian–Lopingian boundary event in mid-Panthalassa: correlation of accreted deep-sea chert and mid-oceanic atoll carbonate. Proceedings of the XVth International Congress on Carboniferous and Permian Stratigraphy 111–124.

Isozaki, Yukio, Yao, J., Matsuda, T., SAKAI, H., Ji, Z., Shimizu, N., Kobayashi, N., KAWAHATA, H., NISHI, H., TAKANO, M., 2004. Stratigraphy of the Middle-Upper Permian and Lowermost Triassic at Chaotian, Sichuan, China. Proceedings of the Japan Academy, Series B 80, 10–16.

Isozaki, Y., Isozaki, Y., Shimizu, N., Shimizu, N., Yao, J., Yao, J., Ji, Z., Ji, Z., Matsuda, T., Matsuda, T., 2007. End-Permian extinction and volcanism-induced environmental stress: The Permian–Triassic boundary interval of lower-slope facies at Chaotian, South China. Palaeogeography, Palaeoclimatology, Palaeoecology 252, 218–238. doi:10.1016/j.palaeo.2006.11.051.

Isozaki, Y., Kawahata, H., Minoshima, K., 2007a. The Capitanian Permian) Kamura cooling event: The beginning of the Paleozoic–Mesozoic transition. Palaeoworld 16, 16–30. doi:10.1016/j.palwor.2007.05.011.

Isozaki, Y., Shimizu, N., Yao, J., Ji, Z., Matsuda, T., 2007b. End-Permian extinction and volcanism-induced environmental stress: The Permian–Triassic boundary interval of lower-slope facies at Chaotian, South China. Palaeogeography, Palaeoclimatology, Palaeoecology 252, 218–238. doi:10.1016/j.palaeo.2006.11.051.

Isozaki, Y., 2009. Integrated “plume winter” scenario for the double-phased extinction during the Paleozoic–Mesozoic transition: The G-LB and P-TB events from a

Panthalassan perspective. JOURNAL OF ASIAN EARTH SCIENCES 36, 459–480. doi:10.1016/j.jseaes.2009.05.006.

Johnson, M.R. 1991. Sandstone petrography, provenance and plate tectonic setting in Gondwana context of the southeastern Cape-Karoo Basin. *South African Journal*, Johannesburg **94**: 137-154.

Kaiho, K., Kajiwara, Y., Nakano, T., Miura, Y., Kawahata, H., Tazaki, K., Ueshima, M., Chen, Z., Shi, G.R., 2001. End-Permian catastrophe by a bolide impact: Evidence of a gigantic release of sulfur from the mantle. Geology 29, 815–818. doi:10.1130/0091-76132001)029<0815:EPCBAB>2.0.CO;2

Kay, S.M., Ramos, V.A., Mpodozis, C., Sruoga, P., 1989. Late Paleozoic to Jurassic silicic magmatism at the Gondwana margin: Analogy to the Middle Proterozoic in North America? Geology 17, 324–328.

Lanci, L., Tohver, E., Wilson, A., Flint, S., 2013. Upper Permian magnetic stratigraphy of the lower Beaufort Group, Karoo Basin. Earth and Planetary Science Letters 375, 123–134. doi:10.1016/j.epsl.2013.05.017

López-Gamundí, O., 2006. Permian plate margin volcanism and tuffs in adjacent basins of west Gondwana: Age constraints and common characteristics. Journal of South American Earth Sciences 22, 227–238. doi:10.1016/j.jsames.2006.09.012

Ludwig, K.R., 2001. Using Isoplot/Ex version 2.4. A Geochronological Toolkit for Microsoft: Berkeley Geochronology Center, Special Publications, vol. 1, p. 54.

Matteini, M.; Dantas, E. L.; Pimentel, M. M. and Bühn, B. 2010. Combined U-Pb and Lu-Hf isotope analyses by laser ablation MC-ICP-MS: methodology and applications.

Maynard J.B., Chocyk J.M, Gaines R.R., Krekeler M.P., Prokopenko M., Summers A.M., Huff W.D. 1996. Bentonites in the Late Permian Tatarian Irati Formation of Brazil: geochemistry and potential of stratigraphic correlation. In: Geological Society of America Annual Meeting, 28, Abstracts**,** p. 280.

Mendes, J.C.; Fulfaro, V.J.; Amaral, S.E.; Landim, P.M.B. 1966. A Formação Irati Permiano e fácies associadas. Boletim da Sociedade Brasileira de Geologia. v. 15, n. 3, p. 23-43.

Milani, E.J., França, A.B., Schneider, R.L., 1994. Bacia do Paraná. Boletim de Geociências da Petrobras 8, 69–82.

Milani, E.J., Ramos, V.A., 1998. Orogenias paleozóicas no domínio sul-ocidental do Gondwana e os ciclos de subsidência da Bacia do Paraná. Revista Brasileira de Geociências.

Milani, E.J. 1997. Evolução Tectono-Estratigráfica da Bacia do Paraná e o seu relacionamento com a geodinânica fanerozóica do Gondwana Sul-Ocidental. Tese de Doutorado, Instituto de Geociências, Universidade Federal do Rio Grande do Sul, 255 p.

Musashi, M., Isozaki, Y., Kawahata, H., 2010. An Early–Middle Guadalupian Permian) isotopic record from a mid-oceanic carbonate buildup: Akiyoshi Limestone, Japan. Global and Planetary Change 73, 114–122. doi:10.1016/j.gloplacha.2010.03.013

Parejas, C.S., Lara, L.E., Bertin, D., 2012. The 2011-2012 eruption of Cordón Caulle volcano Southern Andes): Evolution, crisis management and current hazards. Geophysical Research Abstracts Vol. 14, EGU2012-9382-2, EGU General Assembly 2012.

Patchett, P.J. & Tatsumoto, M. 1980. A routine high-precision method for Lu-Hf isotope geochemistry and chronology. Contrib. Mineral. Petrol., **76**: 263-268.

Patchett, P.J. & Tatsumoto, M. 1981. Lu/Hf in chondrites and definition of a chondritic hafnium growth curve. Lunar Planet. Sci., **12**: 822-824.

Patchett, P.J. 1983. Importance of the Lu-Hf isotopic system in studies of planetary chronology and chemical evolution. Acta, **47**: 81-91.

Renne, P.R., Black, M.T., Zichao, Z., Richards, M.A., Basu, A.R., 1995. Synchrony and Causal Relations Between Permian-Triassic Boundary Crises and Siberian Flood Volcanism. Science 269, 1413–1416. doi:10.1126/science.269.5229.1413

Retallack, G.J., Seyedolali, A., Krull, E.S., Holser, W.T., Ambers, C.P., Kyte, F.T., 1998. Search for evidence of impact at the Permian-Triassic boundary in Antarctica and Australia. Geology 26, 979–982. doi:10.1130/0091-76131998)026<0979:SFEOIA>2.3.CO;2

Richard, P.; Shimizu, N. & Allègre. CJ. 1976.^{143}Nd/^{146}Nd A Natural Tracer: An Application to Oceanic Basalts. *Earth Plan Sci Lett* **31:** 269-278.

Rocha-Campos, A.C., Basei, M.A.S., Nutman, A., dos Santos, P.R., 2007. SHRIMP U–Pb ages of the late Paleozoic sedimentary sequence, Paraná Basin, Brazil. 40 Simpósio sobre cronestratigrafia da Bacia do Paraná, XX Congresso Brasileiro de Paleontologia, Sociedade Brasileira de Paleontologia, Búzios: Boletim de Resumos, vol. 33.

Rocha-Campos, A.C., Basei, M.A., Nutman, A.P., Kleiman, L.E., Varela, R., Llambías, E.J., Canile, F.M., da Rosa, O. de C.R., 2011. 30million years of Permian volcanism recorded in the Choiyoi igneous province W Argentina) and their source for younger ash fall deposits in the Paraná Basin: SHRIMP U–Pb zircon geochronology evidence. Gondwana Research 19, 509–523. doi:10.1016/j.gr.2010.07.003

Santos, R.V., Souza, P.A., Alvarenga, C.J.S. de, Dantas, E.L., Pimentel, M.M., Oliveira, C.G., de Araújo, L.M., 2006. Shrimp U–Pb zircon dating and palynology of bentonitic layers from the Permian Irati Formation, Paraná Basin, Brazil. Gondwana Research 9, 456–463. doi:10.1016/j.gr.2005.12.001.

Schipper, C.I., Castro, J.M., Tuffen, H., James, M.R., How, P., 2013. Shallow vent architecture during hybrid explosive–effusive activity at Cordón Caulle Chile, 2011–12): Evidence from direct observations and pyroclast textures. Journal of Volcanology and Geothermal Research 262, 25–37. doi:10.1016/j.jvolgeores.2013.06.005

Sepkoski, J.J., Jr, 1984. JSTOR: Paleobiology, Vol. 10, No. 2 Spring, 1984), pp. 246-267. Paleobiology. doi:10.2307/2400399

Stanley, S.M., Yang, X., 1994. A Double Mass Extinction at the End of the Paleozoic Era. Science 266, 1340–1344. doi:10.1126/science.266.5189.1340

Stollhofen, H., Stanistreet, I.G., Bangert, B., Grill, H., 2000. Tuffs, tectonism and glacially related sea-level changes, Carboniferous–Permian, southern Namibia. Palaeogeography, Palaeoclimatology, Palaeoecology 161, 127–150.

Souza, P. A.; Marques-Toigo, M. Progress on the palynostratigraphy of the Permian strata in Rio Grande do Sul State, Paraná Basin, Brazil. Anais da Academia Brasileira de Ciências, Rio de Janeiro, v. 77, p. 353-365, 2005.

Turner, B.R., 1999. Tectonostratigraphical development of the Upper Karooforeland basin: Orogenic unloading versus thermally-induced Gondwana rifting. Journal of African Earth Sciences 28, 215–238. doi:10.1016/S0899-536299)00025-1

Wetherill, G. W. 1956. Discordant uaranium-lead ages. Trans. Am. Geophys. Union, 37: 320-326.

White,I.C. 1908. Relatório final da Comissão de Estudos das Minas de Carvão de Pedra do Brasil. DNPM, Rio de Janeiro, Parte I, p.1-300; Parte II, p. 301-617. ed. Fac-similar de 1988.

Veevers J. J. and Saeed A. 2007 Central Antarctic provenance of Permian sandstones in Dronning Maud Land and the Karoo Basin: integration of U–Pb and T DM ages and host-rock affinity from detrital zircons. *Sedimentary Geology* **202**, 653–676.

Capítulo VI

6.1. Considerações Finais e Conclusões

O Permiano foi palco de grandes transformações na história do planeta, com destaque para um dos principais registros de extinção biológica no Fanerozóico. Ao contrário da transição Cretéceo-Terciário, na qual o evento de extinção tem sido atribuído a impactos de bólides (Koeberl and MacLeod, 2002), os motivos que levaram à extinção na transição Permo-Triássica ainda não são claros (Erwin, 2001; Koeberl and MacLeod, 2002; Isozaki *et al*., 2007b). Estima-se que 90% da biodiversidade marinha tenha desaparecido nessa transição (Sepkoski, 1986;1996) e que o evento de extinção se deu em mais de uma etapa (Stanley and Yang, 1994), sendo uma no Permiano Médio e outra na transição Permo-Triássica propriamente dita. Estudos mais recentes apontam que o Permiano Médio foi caracterizado por uma diminuição global na temperatura provocado possivelmente por vulcanismo félsico explosivo (Isozaki *et al*., 2006; Isozaki *et al.*, 2007a; Isozaki *et al*., 2007c; Isozaki, 2009a).

Um dos pontos em aberto com relação às transformações ocorridas durante o Permiano, refere-se ao papel dos processos tectônicos como indutores das mudanças climáticas. Durante esse período, toda a porção sul e sudoeste de Gondwana passou por profundas mudanças graças à formação de uma extensa cadeia de montanha relacionada à Orogênese Gondwanides (Turner, 1999; López-Gamundí, 2006; Milani e De Wit, 2008; Ramos, 2008). Com base em reconstruções paleogeografias, essa zona de convergência teria quase 18 mil quilômetros de extensão, tendo deixado seus registros diretos na América do Sul, África, Antártica e Austrália. Um dos pontos a serem avaliados com relação aos resultados do presente estudo é o registro indireto dessa zona de convergência, entendendo por esse tipo de registro a extensão da dispersão de cinzas decorrentes do vulcanismo explosivo associado a essa extensa zona de subducção.

Esta tese abordou a evolução do Permiano da Bacia do Paraná, sudeste do Brasil, e envolve o estudo de duas áreas representativas da ocorrência de rochas desse período. A primeira aborda a proveniência dos sedimentos ao longo da Coluna White, que constitui uma seção clássica do Permiano da Bacia do Paraná ao longo da Serra do Rio do Rasto, Estado de Santa Catarina. Estudos isotópicos pelos métodos Sm-Nd em rocha total e U-Pb e Lu-Hf em zircões detríticos revelaram que a história geológica entre o Permiano Inferior e Médio (Grupo Guatá) difere de forma significativa da história geológica entre o Permiano Médio e Superior (Grupo Passa Dois). Os resultados indicam que os sedimentos da base foram derivados de fontes dominantemente Paleoproterozóicas, Mesoproterozóicas e Neoproterozóicas, enquanto os sedimentos do topo são constituídos por fontes dominantemente Neoproterozóicas e Paleozóicas. A presença de zircões Paleozóicos associados aos sedimentos do Grupo Passo Dois sugere a passagem do Permiano Inferior-Médio para o Permiano Médio-Superior foi acompanhada pela inversão tectônica da bacia, que teria passado de condições dominantemente cratônicas para uma bacia com características do tipo *foreland*. Embora a discussão sobre a natureza *foreland* da Bacia do Paraná esteja além do escopo do presente estudo, cabe destacar que a mudança de fonte observada indica o quanto a mesma foi sujeita aos reflexos da orogenia que afetou toda a borda sul e sudoeste de Gondwana. Assim, a paleogeografia do Permiano da parte sul do Brasil foi acompanhada pela exumação de uma grande cadeia de montanha, que além de suprir sedimentos, afetou significativamente a taxa de subsidência da Bacia do Paraná, conforme já havia sido proposto por outros autores (Milani, 1997; Milani e Ramos, 1998).

A segunda contribuição desse estudos abordou a relação entre o vulcanismos Choioy e a presença de cinzas vulcânicas permianas na Mina PetroSix, Estado do Paraná. Um dos níveis de cinza dessa mina foi datado por Santos *et al*. (2006), que reportou uma idade de 278 Ma em zircões aciculares e prismáticos. No presente estudo, foram datadas outras cinco camadas de cinzas vulcânicas pelo método U-Pb e apresentados novos dados de Lu-Hf em zircões e Sm-Nd em rocha total. Os resultados indicam um intervalo de mais de 15 Ma de anos durante o qual o vulcanismo esteve ativo, sendo que o pico principal do vulcanismo ocorreu em 278 Ma. Demonstrou-se ainda a forte compatibilidade em idade e geoquímica com as rochas volcânicas Choiyoi, tomando-se por base os estudos de Rocha-Campos *et al*., (2011). Em conjunto, esses estudos revelam a importância do Permiano da Bacia do Paraná para se entender os modelos de evolução global durante esse período. Assim, foram discutidas as correlações entre os eventos vulcânicos registrados no Irati e eventos semelhantes registrados em outras bacias, como do Karoo, na Antártica e outras partes do planeta (Isozaki, 2009b), deixando-se em aberto a possibilidade de esse vulcanismo ter afetado as condições climáticas globais do planeta.

CAPÍTULO VII

7.1. Referências Bibliográficas

Aborrage, A.M.; Lopes, R.C. 1986. Projeto a Borda Leste da Bacia do Paraná: integração geológica e avaliação econômica. DNPM/CPRM, Porto Alegre. 18 v.

Almeida F.F.M. 1978. Tectonic map of South America 1:5.000.000. Explanatory note, Brasilia, DNPM/CGMW/UNESCO, 23p.

Andersen, T.; Griffin, W.L.; Pearson, N.J. 2002. Crustal Evolution in the SW Part of the Baltic Shield: the Hf Isotope Evidence. Journal of Petrology, 43 9: 1725-1747.

Andersen, T. 2005. Detrital zircons as tracers of sedimentary provenance: limiting conditions from statistics and numerical simulation. Chemical Geology, 216: 249–270.

Anon. 2008. West Gondwana amalgamation based on detrital zircon ages from Neoproterozoic Ribeira and Dom Feliciano belts of South America and comparison with coeval sequences from SW Africa., 294, 239–256. Available at: http://sp.lyellcollection.org/content/294/1/239.full.

Araújo, L.M. 2001. Análise da Expressão Estratigráfica dos Parâmetros de Geoquímica Orgânica e Inorgânica nas Sequências Deposicionais do Irati. Tese de Doutorado em Geociências, Instituto de Geociências, Universidade Federal do Rio Grande do Sul, 307 p.

Assine M. L., Zacharias A. Á. and Perinotto J. A. J. 2003. Paleocorrentes, paleogeografia e seqüências deposicionais da Formação Tatuí, centro-leste do estado de São Paulo. Brazilian Journal of Geology 33, 33–40.

Augustsson, C.; Münker, C.; Bahlburg, H.; Fanning, C. M. 2006. Provenance of late Palaeozoic metasediments Provenance of the SW South American Gondwana margin: a combined U–Pb and Hf-isotope study of single detrital zircons. Journal of the Geological Society, 163: 983-995.

Barbosa, O. & Gomes, F.A. 1958. Pesquisa de Petróleo na Bacia do Rio Corumbataí, Estado de São Paulo. Divisão de Geologia e Mineralogia do DNPM, Boletim 171, 40p.

Basei M., Frimmel H. E., Nutman A. P. and Preciozzi F. 2005. A connection between the Neoproterozoic Dom Feliciano Brazil/Uruguay and Gariep Namibia/South Africa orogenic belts–evidence from a reconnaissance reconnaissance provenance study Precambrian Research, 139, 195–221.

Bangert, B., Stollhofen, H., Lorenz, V., Armstrong, R.L., 1999. The geochronology and significance of ash-fall tuffs in the glacigenic, Carboniferous-Permian Dwyka Group of Namibia and South Africa. Journal of African Earth Sciences 29, 33–49.

Becker, L., Poreda, R.J., Hunt, A.G., Bunch, T.E., Rampino, M., 2001. Impact event at the Permian-Triassic boundary: evidence from extraterrestrial noble gases in fullerenes. Science 291, 1530–1533. doi:10.1126/science.291.5508.1530

Bowring, S. A.; Schmitz, M. D. 2003 High-Precision U-Pb Zircon Geochronology and the Stratigraphic Record. Reviews in Mineralogy and Geochemistry, 53: 305-326.

Bühn B., Pimentel M. M., Matteini M. and Dantas E. L. 2009. High spatial resolution analysis of Pb and U isotopes for geochronology by laser ablation multi-collector inductively coupled plasma mass spectrometry LA-MC-ICP-MS. Anais da Academia Brasileira de Ciências. 81, 99–114.

Campbell, I.H., Czamanske, G.K., Fedorenko, V.A., Hill, R.I., Stepanov, V., 1992. Synchronism of the Siberian Traps and the Permian-Triassic Boundary. Science 258, 1760–1763. doi:10.1126/science.258.5089.1760

Casquet, C.; Pankhurst, R.J.; Rapela, C.W.; Galindo, C.; Fanning, C.M.; Chiaradia, M.; Baldo, E.; González-Casado, J.M.; Dahlquist, J.A. 2008. The Mesoproterozoic Maz terrane in the Western Sierras Pampeanas, Argentina, equivalent to the Arequipa–Antofalla block of southern Peru? Implications for West Gondwana margin evolution. Gondwana Research. 13, 163-175.

Casquet, C.; Fanning, C.M.; Galindo, C.; Pankhurst, R.J.; Rapela, C.W.; Torres, P. 2010. The Arequipa Massif of Peru: New SHRIMP and isotope constraints on a Paleoproterozoic inlier in the Grenvillian orogen. Journal of South American Earth Sciences. 29, 128-142.

Casquet, C.; Rapela, C.W.; Pankhurst, R.J.; Baldo, E. G.; Galindo, C.; Fanning, C.M.; Dahlquist, J.A.; Saavedra, J. 2012. A history of Proterozoic terranes in southern South America: From Rodinia to Gondwana. Geoscience Frontiers. 3, 137-145.

Cawood, P. T. 2005. Terra Australis Orogen: Rodinia breakup and development of the Pacific and Iapetus margins of Gondwana during the Neoproterozoic and Paleozoic. Earth-Science Reviews, 69: 249–279.

Condie, K.C., Belousova, E., Griffin, W.L., Sircombe, K.N., 2009. Granitoid events in space and time: constraints from igneous and detrital zircon age spectra. Gondwana Research 15, 228–242.

Condie, K.C., Beyer, E., Belousova, E., Griffin, W.L., O'Reilly, S.Y., 2005. U–Pb isotopic ages and Hf isotopic composition of single zircons — the search for juvenile Precambrian continental crust. Precambrian Research 139, 42–100.

Cordani, U.G.; Brito Neves, B.B.; Fuck, R.A.; Porto, R.; Thomaz Filho, A.; Cunha, F.M.B. 1984. Estudo preliminar de integração do pré-cambriano com os eventos tectônicos das bacias sedimentares brasileiras. Série Ciência-Técnica-Petróleo, Rio de Janeiro. 15, 12-20.

Coutinho, J.M.V.; Hachiro, J.; Coimbra, A.M.; Santos, P.R. 1991. Ash-fall derived vitroclastic tuffaceous sediments in the Permian of the Paraná Basin and their provenance. In: Ulbrich, H. & Rocha-Campos, A.C. eds.. Gondwana Seven. São Paulo: Universidade de São Paulo, p. 147-160.

Coutinho, J.M.V., Hachiro, J., 2005. Distribution, mineralogy, petrography, provenance and significance of Permian ash-carrying deposits in the Paraná Basin. Revista do Instituto de Geociências 5, 29–39.

Cury L. F. 2009. Geologia do Terreno Paranaguá. Tese de Doutorado, Instituto de Geociências, Universidade de São Paulo USP, 187 p.

da Silva L. C., Hartmann L. A., McNaughton N. J. and Fletcher I. 2000 Zircon U-Pb SHRIMP dating of a Neoproterozoic overprint in Paleoproterozoic granitic-gneissic terranes, southern Brazil. Am Mineral 85, 649–667.

Daemon, R.F. ; Quadros, L.P. 1969. Bioestratigrafia e Palinologia do Paleozóico Superior da Bacia do Paraná. PETROBRÁS/DESUL, Ponta Grossa, 1 v. Relatório Interno nº 384.

De Wit M. J., Stankiewicz J. and Reeves C. 2008 Restoring Pan-African-Brasiliano connections: more Gondwana control, less Trans-Atlantic corruption. Geological Society, London, Special Publications 294, 399–412.

DePaolo, D. J. and Wasserburg, G. J. 1976. Inferences about magma sources and mantle structure from variations of 143Nd/144Nd. Geophys. Res. Lett. 3, 743–6.

DePaolo, D. J. 1981. Neodymium isotopes in the Colorado Front Range and crust – mantle evolution in the Proterozoic. Nature 291, 193–7.

DePaolo, D.J. 1988. Neodymium isotope geochemistry – an introduction. Berlim, SpringerVerlag. 187p.

Dickin, A. P. 2005. Radiogenic Isotop Geology. School of Geography and Earth Sciences McMaster University, Hamilton, Ontario, 492 p.

Dodson W.H., Compston W., Williams I.S., Wilson J.F. 1988. A search for ancient detrital zircons in Zimbabwean sediments. Journal of the Geological Society 145:977-983.

dos Anjos, C.W.D Guimarães, E.M., Souza, P.A. 2006. Mineralogia e palinologia de níveis de folhelhos negros da Formação Irati Permiano nas porções norte e sul da Bacia do Paraná. Resumo expandido. XLIII Congresso Brasileiro de Geologia.

dos Anjos, C.W.D. 2008. Fatores condicionantes na gênese dos argilominerais dos folhelhos negros e pelitos associados da Formação Iratí no norte da Bacia do Paraná. Tese de Doutorado, Faculté des Sciences Fondamentales et Appliquées, Universidade de Poitiers, França, p124.

Eglington B. M., Thomas R. J., Armstrong R. A. and Walraven F. 2003 Zircon geochronology of the Oribi Gorge Suite, KwaZulu-Natal, South Africa: constraints on the timing of trans-current shearing in the Namaqua–Natal Belt. Precambrian Research 123, 29–46.

Eyles, C. H.; Eyles, N.; França, A. B. Glaciation and tectonics in an active intracratonic basin: the Late Palaeozoic Itararé Group, Paraná Basin, Brazil. Sedimentology, Oxford, v. 40, p. 1-25. 1993.

Erwin, D., 1990. The End-Permian Mass Extinction. Annual Review of Ecology and Systematics 21, 69–91.

Erwin D. H. 2001 Extinction: End-Permian Mass Extinction, John Wiley & Sons, Ltd, Chichester, UK.

Fanning, C. M.; Hervé F., Pankhurst, R. J.;, Rapela, C. W.; Kleimane, L. E., Yaxley, G. M.; Castillo, P. 2011. Lu-Hf isotope evidence for the provenance of Permian detritus in accretionary complexes of western Patagonia and the northern Antarctic Peninsula region. Journal of South American Earth Sciences, 32: 485-496.

Faure, K., Cole, D., 1999. Geochemical evidence for lacustrine microbial blooms in the vast Permian Main Karoo, Paraná, Falkland Islands and Huab basins of southwestern Gondwana. Palaeogeography, Palaeoclimatology, Palaeoecology 152, 189–213.

Faure, G. and Mensing, T. 2005. Isotopes: Principles and Applications. 3rd Edition, ISBN-13: 978-0471384373, ISBN-10: 0471384372.

Fedo, C. M.; Sircombe, K. N.; Rainbird, R. H. 2003. Detrital Zircon Analysis of the Sedimentary Record. Reviews in Mineralogy and Geochemistry 53, 277-303.

Formoso, M.L.L., Calarge, L.M., Garcia, A.J.V., Alves, D.B., Gomes, M.B., Misusaki, A.M.,1997. Permian tonsteins from the Paraná Basin, Rio Grande do Sul, Brazil. 11th Clay Conference, Otawa: Proceedings, pp. 613–621.

França, A. B. & Potter, P. E. 1988. Estratigrafia, ambiente deposicional e análise de reservatório do Grupo Itararé (Permo-Carbonífero), Bacia do Paraná. Boletim de Geociências da PETROBRÁS, v.2, p. 147-191.

Frimmel H. E., Tack L., Basei M. S. and Nutman A. P. 2006. Provenance and chemostratigraphy of the Neoproterozoic West Congolian Group in the Democratic Republic of Congo. Journal of African Earth Sciences, 46: 221-239.

Frimmel H. E., Basei M. S. and Gaucher C. 2011. Neoproterozoic geodynamic evolution of SW-Gondwana: a southern African perspective. Int J Earth Sci Geol Rundsch 100, 323–354.

Fulfaro, V. J.; Perinotto, J. A. J.; Barcelos, J. H. 1991. Formação Tietê: o pós-glacial no Estado de São Paulo. In: Simpósio de Geologia do Sudeste, 2., 1991, São Paulo. Atas. São Paulo: Sociedade Brasileira de Geologia, 1991. p. 397-404.

Gerdes, A.; Zeh, A. 2006. Combined U–Pb and Hf isotope LA-MC-ICP-MS analyses detrital zircons: Comparison with SHRIMP and new constraints for the provenance and age of an Armorican metasediment in Central Germany. Earth and Planetary Science Letters 249, 47–61.

Gioia, S.M.C.L. & Pimentel, M.M. 2000. The Sm-Nd isotopic method in the Geochronology Laboratory of the University of Brasília. Anais da Academia Brasileira de Ciências 72: 219-245.

Gordon JR., M. 1947. Classificação das formações gondwânicas do Paraná, Santa Catarina e Rio Grande do Sul. Notas Preliminares e Estudos da Divisão de Geologia e Mineralogia, DNPM, n. 38. In: Seventh Gondwana Symposium, São Paulo, Brasil, Julho, 1988. Brasília: DNPM, p. 67-86.

Griffin, W.L., Belousova, E.A., Shee, S.R., Pearson, N.J., O'Reilly, S.Y., 2004. Archaean crustal evolution in the northern Yilgarn Craton: UPb and Hf-isotope evidence from detrital zircons. Precambrian Res. 131, 231– 282.

Hartmann L. A., Piñeyro D., Bossi J. and Leite J. 2000 Zircon U-Pb SHRIMP dating of Palaeoproterozoic Isla Mala granitic magmatism in the Rio de la Plata Craton, Uruguay. Journal of South American Earth Sciences, 13: 105-113.

Heilbron M., Valeriano C. M., Tassinari C. C. G., Almeida J., Tupinamba M., Siga O. and Trouw R. 2008. Correlation of Neoproterozoic terranes between the Ribeira Belt, SE Brazil and its African counterpart: comparative tectonic evolution and open questions. Geological Society, London, Special Publications 294, 211–237.

Hervé, F., Faúndez, V., Brix, M., Fanning, M., 2006. Jurassic sedimentation of the Miers Bluff formation, Livingston Island, Antarctica: evidence from SHRIMP UePb ages of detrital and plutonic zircons. Antarctic Science 18, 229-238.

Hervé F., Fanning C. M., Calderón M. and Mpodozis C. 2014 Early Permian to Late Triassic batholiths of the Chilean Frontal Cordillera 28°–31°S: SHRIMP U–Pb zircon ages and Lu–Hf and O isotope systematics. LITHOS 184-187, 436–446.

Isozaki, Y. 2003 Guadalupian–Lopingian boundary event in mid-Panthalassa: correlation of accreted deep-sea chert and mid-oceanic atoll carbonate. Proceedings of the XVth International Congress on Carboniferous and Permian Stratigraphy, 111–124. Available at: http://ea.c.u-tokyo.ac.jp/earth/Members/Isozaki/07Neth.Acad.pdf.

Isozaki, Y.; Kawahata H.; Ota A. 2006 A unique carbon isotope record across the Guadalupian–Lopingian Middle–Upper Permian boundary in mid-oceanic paleo-atoll carbonates: The high-productivity “Kamura event” and its collapse in Panthalassa. Global and Planetary Change 55, 21–38.

Isozaki, Y.; Isozaki, Y.; Shimizu N., Shimizu N., Yao J., Yao J., Ji Z., Ji Z., Matsuda T. and Matsuda T. 2007 End-Permian extinction and volcanism-induced environmental stress: The Permian–Triassic boundary interval of lower-slope facies at Chaotian, South China. Palaeogeography, Palaeoclimatology, Palaeoecology 252, 218–238.

Isozaki, Y., Kawahata H.; Minoshima K. 2007 The Capitanian Permian Kamura cooling event: The beginning of the Paleozoic–Mesozoic transition. Palaeoworld 16, 16–30.

Isozaki, Y., Kawahata, H., Minoshima, K., 2007a. The Capitanian Permian Kamura cooling event: The beginning of the Paleozoic–Mesozoic transition. Palaeoworld 16, 16–30. doi:10.1016/j.palwor.2007.05.011.

Johnson, M.R. 1991. Sandstone petrography, provenance and plate tectonic setting in Gondwana context of the southeastern Cape-Karoo Basin. South African Journal, Johannesburg 94: 137-154.

Kaiho, K., Kajiwara, Y., Nakano, T., Miura, Y., Kawahata, H., Tazaki, K., Ueshima, M., Chen, Z., Shi, G.R., 2001. End-Permian catastrophe by a bolide impact: Evidence of a gigantic release of sulfur from the mantle. Geology 29, 815–818. doi:10.1130/0091-76132001)029<0815:EPCBAB>2.0.CO;2

Kay, S.M., Ramos, V.A., Mpodozis, C., Sruoga, P., 1989. Late Paleozoic to Jurassic silicic magmatism at the Gondwana margin: Analogy to the Middle Proterozoic in North America? Geology 17, 324–328.

Kemp, A.I.S., Wormald, R.J., Price, R.C., 2005. Hf isotopes in zircon reveal contrasting sources and crystallisation histories for alkaline to peralkaline granites of Temora, Southeastern Australia. Geology 33, 797–800.

Kemp, A.I.S., Hawkesworth, C.J., Paterson, B.A., Kinny, P., 2006. Episodic growth of the Gondwana Supercontinent from hafnium and oxygen isotopes in zircon. Nature 439, 580–583.

Kleiman, L. E., Japas, M. S. 2009. The Choiyoi volcanic province at 34°S–36°S San Rafael, Mendoza, Argentina: Implications for the Late Palaeozoic evolution of the southwestern margin of Gondwana. Tectonophysics, 473: 283–299.

Koeberl, C. and MacLeod K. G. 2002. Catastrophic Events and Mass Extinctions: Impacts and Beyond. Special papers (Geological Society of America): 356. ISBN 1-8137-2356-6.

Kooijman, E.; Berndt, J.; Mezger, K. 2012. U-Pb dating of zircon by laser ablation ICP-MS: recent improvements and new insights. Eur. J. Mineral. 24, 5–21.

Košler, J.; Fonneland, H.; Sylvester, P.; Tubrett, M.; Rolf-Birger Pedersen. 2002. U–Pb dating of detrital zircons for sediment provenance studies—a comparison of laser ablation ICPMS and SIMS techniques. Chemical Geology 182: 605–618.

Lanci, L., Tohver, E., Wilson, A., Flint, S., 2013. Upper Permian magnetic stratigraphy of the lower Beaufort Group, Karoo Basin. Earth and Planetary Science Letters 375, 123–134. doi:10.1016/j.epsl.2013.05.017

Lopes, R.C.; Lavina, E.L.; Signorelli, N. 1986. Fácies sedimentares e evolução paleoambiental do Super-grupo Tubarão na Borda Leste da Bacia do Paraná; uma seção regional nos estados do Rio Grande do Sul e Santa Catarina. In: Cong. Bras. Geol. 34, A-nais,. v.1, pp.206-218.

López-Gamundi, O.R., 2006. Permian plate margin volcanism and tuffs in adjacent basins of west Gondwana: age constrains and common characteristics. Journal of South American Earth Sciences, 22, 227–238.

López-Gamundí O. 2006a Permian plate margin volcanism and tuffs in adjacent basins of west Gondwana: Age constraints and common characteristics. Journal of South American Earth Sciences 22, 227–238.

López-Gamundí O. 2006b Permian plate margin volcanism and tuffs in adjacent basins of west Gondwana: Age constraints and common characteristics. Journal of South American Earth Sciences 22, 227–238.

Ludwig, K.R., 2001. Using Isoplot/Ex version 2.4. A Geochronological Toolkit for Microsoft: Berkeley Geochronology Center, Special Publications, vol. 1, p. 54.

Mac Gregor, JH. 1908. Mesosaurus Brasiliensis nov. sp. do Permiano do Brasil. In: Relatório da Comissão de Estudos das Minas de Carvão de Pedra do Brasil, por I. C. White. DNPM, Brasília, Edição Fac-Similar 1988. pp.301-336.

Maynard J.B., Chocyk J.M, Gaines R.R., Krekeler M.P., Prokopenko M., Summers A.M., Huff W.D. 1996. Bentonites in the Late Permian Tatarian Irati Formation of Brazil: geochemistry and potential of stratigraphic correlation. In: Geological Society of America Annual Meeting, 28, Abstracts, p. 280.

Mendes, J.C.; Fulfaro, V.J.; Amaral, S.E.; Landim, P.M.B. 1966. A Formação Irati Permiano e fácies associadas. Boletim da Sociedade Brasileira de Geologia. v. 15, n. 3, p. 23-43.

Milani, E.J.; França, A.B.; Schneider, R.L. 1994. Bacia do Paraná. Boletim de Geociências da PETROBRÁS, v. 8, n. 1, p. 69-82.

Milani E. J., França A. B. and Schneider R. L. 1994a Bacia do Paraná. Boletim de Geociências da PETROBRÁS.

Milani E. J., França A. B. and Schneider R. L. 1994b Bacia do Paraná. Boletim de Geociências da Petrobras 8, 69–82.

Milani, E.J. 1997. Evolução Tectono-Estratigráfica da Bacia do Paraná e o seu relacionamento com a geodinânica fanerozóica do Gondwana Sul-Ocidental. Tese de Doutorado, Instituto de Geociências, Universidade Federal do Rio Grande do Sul, 255 p.

Milani E. J., Faccini U. F., Scherer C. M., Araújo L. M. and Cupertino J. A. 1998 Sequências e hierarquia estratigráfica da bacia do Paraná Ordoviciano ao Cretáceo, sul do Brasil. Boletim IG-USP. Série Científica 29, 125–173.

Milani, E.J., Ramos, V.A., 1998. Orogenias paleozóicas no domínio sul-ocidental do Gondwana e os ciclos de subsidência da Bacia do Paraná. Revista Brasileira de Geociências.

Milani E. J. e Ramos V. A. 1998a Orogenias paleozóicas no domínio sul-ocidental do Gondwana e os ciclos de subsidência da Bacia do Paraná. Revista Brasileira de Geociências.

Milani E. J. e Ramos V. A. 1998b Orogenias paleozóicas no domínio sul-ocidental do Gondwana e os ciclos de subsidência da Bacia do Paraná. Revista Brasileira de Geociências.

Milani, E. J.; Melo, J. H. G.; Souza, P. A.; Fernandes, L. A.; Almério Barros França, A. B. 2007. Bacia do Paraná. Geoci. Petrobras, Rio de Janeiro, v. 15, n. 2, p. 265-287.

Matteini, M.; Dantas, E. L.; Pimentel, M. M. and Bühn, B. 2010. Combined U-Pb and Lu-Hf isotope analyses by laser ablation MC-ICP-MS: methodology and applications.

Mundil, R., Ludwig, K.R., Metcalfe, I., Renne, P., 2004. Age and timing of the Permian mass extinctions: U/Pb dating of closedsystem zircons. Science 305, 1760–1763.

Nebel, O.; Nebel-Jacobsen, Y.; Mezger, K.; Berndt, J. 2007. Initial Hf isotope compositions in magmatic zircon from early Proterozoic rocks from the Gawler Craton, Australia: A test for zircon model ages. Chemical Geology 241: 23–37.

Neves B. B. de B., Fuck R. A. and Pimentel M. M. 2014 The Brasiliano collage in South America: a review. Brazilian Journal of Geology 44, 493–518.

Orlandi Filho,V.; Krebs, A.S.J.; Giffoni, L.E. 2006. Coluna White, Serra do Rio do Rastro, SC - Seção Geológica Clássica do Continente Gondwana no Brasil. In: Winge, M.; Schobbenhaus, C.; Berbert-Born, M.; Queiroz, E.T.; Campos, D.A.; Souza, C.R.G.; Fernandes, A.C.S. Edit. Sítios Geológicos e Paleontológicos do Brasil. Publicado na Internet em 22/12/2006 no endereço http://www.unb.br/ig/sigep/sitio024/sitio024.pdf

Parejas, C.S., Lara, L.E., Bertin, D., 2012. The 2011-2012 eruption of Cordón Caulle volcano Southern Andes): Evolution, crisis management and current hazards. Geophysical Research Abstracts Vol. 14, EGU2012-9382-2, EGU General Assembly 2012.

Patchett, P.J. & Tatsumoto, M. 1980. A routine high-precision method for Lu-Hf isotope geochemistry and chronology. Contrib. Mineral. Petrol., 76: 263-268.

Patchett, P.J. & Tatsumoto, M. 1981. Lu/Hf in chondrites and definition of a chondritic hafnium growth curve. Lunar Planet. Sci., 12: 822-824.

Patchett, P.J., Kouvo, O., Hedge, C. E., Tatsumoto, M. 1981. Evolution of continental crust and mantle heterogeneity. Contrib. Mineral. Petrol., 78: 279-297.

Patchett, P.J. 1983. Importance of the Lu-Hf isotopic system in studies of planetary chronology and chemical evolution. Acta, 47: 81-91.

Ramos, V. A. 1984 Patagonia: a Paleozoic continent adrift? Actas. In Noveno Congreso Geologico Argentino. S. C. Bariloche. pp. 311–325.

Ramos, V.A. 1988. Late Proterozoic - Early Paleozoic of South America - a collisional history. Episodes, 11(3):168-174.

Ramos, V. A. 2008 Patagonia: A paleozoic continent adrift? Journal of South American Earth Sciences 26, 235–251.

Ramos, V. A. 2010. The Grenville-age basement of the Andes. Journal of South American Earth Sciences 29, 77–91.

Ramos, V. A.; Vujovich, G.; Martino, R.; Otamendi, J. 2010. Pampia: A large cratonic block missing in the Rodinia supercontinent. Journal of Geodynamics 50, 243–255.

Ramos, V. A.; Chemale F., Naipauer M. and Pazos P. J. 2014. A provenance study of the Paleozoic Ventania System Argentina: Transient complex sources from Western and Eastern Gondwana. Gondwana Research 26, 719–740.

Retallack, G.J., Seyedolali, A., Krull, E.S., Holser, W.T., Ambers, C.P., Kyte, F.T., 1998. Search for evidence of impact at the Permian-Triassic boundary in Antarctica and Australia. Geology 26, 979–982. doi:10.1130/0091-76131998)026<0979:SFEOIA>2.3.CO;2

Renne, P.R., Black, M.T., Zichao, Z., Richards, M.A., Basu, A.R., 1995. Synchrony and Causal Relations Between Permian-Triassic Boundary Crises and Siberian Flood Volcanism. Science 269, 1413–1416. doi:10.1126/science.269.5229.1413

Richard, P.; Shimizu, N. & Allègre. CJ. 1976.^{143}Nd/^{146}Nd A Natural Tracer: An Application to Oceanic Basalts. Earth Plan Sci Lett 31: 269-278.

Rocha-Campos, A.C., Basei, M.A.S., Nutman, A., dos Santos, P.R., 2007. SHRIMP U–Pb ages of the late Paleozoic sedimentary sequence, Paraná Basin, Brazil. 40 Simpósio sobre cronestratigrafia da Bacia do Paraná, XX Congresso Brasileiro de Paleontologia, Sociedade Brasileira de Paleontologia, Búzios: Boletim de Resumos, vol. 33.

Rocha-Campos, A.C., Basei, M.A.S., Nutman, A.P., dos Santos, P.R., 2006. SHRIMP U–Pb zircon geochrological calibration of the late Paleozoic Supersequence, Paraná Basin, Brazil. V South American Symposium on Isotope Geology, Punta del Este: Short Papers, pp. 298–301.

Rocha-Campos A. C., Basei M. A., Nutman A. P., Kleiman L. E., Varela R., Llambías E. J., Canile F. M. and de C R da Rosa O. 2011. 30million years of Permian volcanism recorded in the Choiyoi igneous province W Argentina and their source for younger ash fall deposits in the Paraná Basin: SHRIMP U–Pb zircon geochronology evidence. Gondwana Research 19, 509–523.

Rodrigues J. B., Pimentel M. M., Bühn B. and Matteini M. 2012 Provenance of the Vazante Group: New U–Pb, Sm–Nd, Lu–Hf isotopic data and implications for the tectonic evolution of the Neoproterozoic Brasília Belt. Gondwana Research 21, 439–450.

Santos Neto, E.V. 1993. Caracterização Geoquímica e Paleoambiente Deposicional da Sequência Carbonato-Pelítica Superior do Membro Assistência, Formação Irati no Estado de São Paulo, Bacia do Paraná. Dissertação de Mestrado, Instituto de Geociências, Universidade Federal do Rio de Janeiro, 203 p.

Santos, R.V., Sousa, P.A., Alvarenga, C.J.S., Dantas, E.L., Pimentel, M.M., Oliveira, C.G., Araújo, L.M. 2006. SHRIMP U-Pb Zircon dating and palinology of bentonitic layers from the Permian Irati Formation: Stratigraphic implications for southwestern gondwana. Gondwana research, 9:456-463.

Schipper, C.I., Castro, J.M., Tuffen, H., James, M.R., How, P., 2013. Shallow vent architecture during hybrid explosive–effusive activity at Cordón Caulle Chile, 2011–12): Evidence from direct observations and pyroclast textures. Journal of Volcanology and Geothermal Research 262, 25–37. doi:10.1016/j.jvolgeores.2013.06.005.

Schmitz M. D. and Bowring S. A. 2004 Lower crustal granulite formation during Mesoproterozoic Namaqua-Natal collisional orogenesis, southern Africa. South African Journal of Geology 107, 261–284.

Schmitt R. S., Trouw R. and Van Schmus W. R. 2004 Late amalgamation in the central part of West Gondwana: new geochronological data and the characterization of a Cambrian collisional orogeny in the Ribeira Belt SE Brazil. Precambrian Research 133, 29–61.

Schmitt R. S., Trouw R. A. J., Medeiros S. R. and Dantas E. L. 2008. Age and geotectonic setting of Late Neoproterozoic juvenile mafic gneisses and associated paragneisses from the Ribeira belt SE Brazil based on geochemistry and Sm–Nd data — Implications on Gondwana assembly. Gondwana Research 13, 502–515.

Schneider, R.L.; Castro, J.C. 1975. Análise estratigráfica, sedimentológia e potencialidades petrolíferas da Formação Rio Bonito no sudeste da Bacia do Paraná. PETROBRAS/DEXPRO, Relatório Interno nº. 5011, 39p.

Schneider, R.L.; Mühlmann, H.; Tommasi, E.; Medeiros, R.A.; Daemon, R.F.; Nogueira, A.A. 1974. Revisão estratigráfica da Bacia do Paraná. In: Congresso brasileiro de Geologia, 28, Porto Alegre: SBG, v.1, p. 41-65.

Sepkoski J. J. Jr 1984. JSTOR: Paleobiology, Vol. 10, No. 2 Spring, 1984, pp. 246-267. Paleobiology.

Sepkoski Jr., J.J., 1996. Patterns of Phanerozoic extinction: a perspective from global data bases. In: Walliser, O. (Ed.), Global Events and Event Stratigraphy. Springer, New York, pp. 35–51.

Sguigna, A. P.; Larabee, A. j.; Waddington, J. C. 1982. The half-life of ^{176}Lu by ϒ- ϒ coincidence measurement. Can. J. Phys., 60: 361-364.

Sircombe, K.N., 2000. Quantitative comparison of geochronological data using multivariate analysis: a provenance study example from Australia. Geochim. Cosmochim. Acta 64, 1593– 1619.

Stanley S. M. and Yang X. 1994 A Double Mass Extinction at the End of the Paleozoic Era. Science 266, 1340–1344.

Stollhofen, H., Stanistreet, I.G., Bangert, B., Grill, H., 2000. Tuffs, tectonism and glacially related sea-level changes, Carboniferous–Permian, southern Namibia. Palaeogeography, Palaeoclimatology, Palaeoecology 161, 127–150.

Souza, P. A.; Marques-Toigo, M. Progress on the palynostratigraphy of the Permian strata in Rio Grande do Sul State, Paraná Basin, Brazil. Anais da Academia Brasileira de Ciências, Rio de Janeiro, v. 77, p. 353-365, 2005.

Tera, F. and Wasserburg, G. J. 1972. U-Th-Pb systematics in three Apollo 14 basalts and problem of initial Pb in lunar rocks. Earth Planet. Sci. Lett., 14: 281-304.

Turner B. R. 1999 Tectonostratigraphical development of the Upper Karooforeland basin: Orogenic unloading versus thermally-induced Gondwana rifting. Journal of African Earth Sciences 28, 215–238.

Vail, P, R.; Mitchum, R. M.; Thompson, S. 1977. Seismic stratigraphy and global changes of sea level, part 3: relative changes of sea level from coastal onlap. In: Payton, C. E. ed.. Seismic stratigraphy – applications to hydrocarbon explration. Tulsa: American Association of Petroleum Geologists, p. 63-81 Memoir 26.

Veevers, J. J.; Saeed, A.; Belousova, E. A.; Griffin, W. L. 2005. U–Pb ages and source composition by Hf-isotope and trace-element analysis of detrital zircons in Permian sandstone and modern sand from southwestern Australia and a review of the paleogeographical and denudational history of the Yilgarn Craton. Earth-Science Reviews 68, 245–279.

Veevers J. J. and Saeed A. 2007 Central Antarctic provenance of Permian sandstones in Dronning Maud Land and the Karoo Basin: integration of U–Pb and T DM ages and host-rock affinity from detrital zircons. Sedimentary Geology 202, 653–676.

Vermeesch, P., 2004. How many grains are needed for a provenance study? Earth Planet. Sci. Lett. 224, 351– 441.

Wetherill, G. W. 1956. Discordant uaranium-lead ages. Trans. Am. Geophys. Union, 37: 320-326.

White,I.C. 1908. Relatório final da Comissão de Estudos das Minas de Carvão de Pedra do Brasil. DNPM, Rio de Janeiro, Parte I, p.1-300; Parte II, p. 301-617. ed. Fac-similar de 1988.

Yang, J. H.; Wu, F. Y.; Wilde, S.A., Xie, L. W.; Yang, Y. H.; Liu, X. M. 2007. Tracing magma mixing in granite genesis: in situ U–Pb dating and Hf-isotope analysis of zircons. Contributions to Mineralogy and Petrology 153, 177–190.

Yao, J.; Shu, L.; Santosh, M. 2011. Detrital zircon U–Pb geochronology, Hf-isotopes and geochemistry—New clues for the Precambrian crustal evolution of Cathaysia Block, South China. Gondwana Research 20, 553–567.

Ziegler A. M. 1997. Permian world topography and climate. In Martini, I. P., ed. Late glacial and postglacial environmental changes Pleistocene, Carboniferous-Permian, and Proterozoic. Oxford, Oxford University Press, p., 111–146.